TU Clausthal

Schriftenreihe des Instituts für
Geotechnik und Markscheidewesen

Seyedeh Roghayeh Mousavi

Dempster- Shafer Theory and modified rules to determine uncertainty in mineral prospection

IGMC

SCHRIFTENREIHE

GEOTECHNIK UND MARKSCHEIDEWESEN

Seyedeh Roghayeh Mousavi

Dempster-Shafer Theory and modified rules to determine uncertainty in mineral prospection

Herausgegeben vom
Institut für Geotechnik und Markscheidewesen der TU Clausthal
Erzstraße 18, D-38678 Clausthal-Zellerfeld, Telefon: 05323 / 72-2294

Seyedeh Roghayeh Mousavi aus dem Iran: Dempster-Shafer Theory and modified rules to determine uncertainty in mineral prospection In: Wissenschaftliche Schriftenreihe Geotechnik und Markscheidewesen.

Vollständiger Abdruck der von der Fakultät für Energie- und Wirtschaftswissenschaften der Technischen Universität Clausthal zur Erlangung des akademischen Grads eines Doktor-Ingenieurs (Dr.-Ing.) genehmigten Dissertation. Tag der mündlichen Prüfung war der 16. Dezember 2011.

Vorsitzender der
Promotionskommission: Univ.-Prof. Dr. rer. nat. H.-J. Gursky
Hauptberichterstatter: Univ.-Prof. Dr.-Ing. Wolfgang Busch
Berichterstatter: Univ.-Prof. Dr.-Ing. habil. Hossein Tudeshki

Der Druck dieses Hefts wurde aus Haushaltsmitteln des Instituts für Geotechnik und Markscheidewesen der Technischen Universität Clausthal finanziert.

Verantwortlich für die Herausgabe der Schriftenreihe: Univ.-Prof. Dr.-Ing. W. Busch

Bezugsnachweis: TU Clausthal
Institut für Geotechnik und Markscheidewesen
Erzstraße 18
38678 Clausthal-Zellerfeld

Kontakt: Tel.: 05323 / 72-2294
Fax: 05323 / 72-2479

E-Mail: IGMC@tu-clausthal.de

My Parent

Abstract

In this thesis mathematical methods and GIS techniques are applied to determine uncertainty in Mineral Exploration processes, which is a mayor subject in quantitative geosciences. This study investigates the ability of Dempster-Shafer Theory and modified rules to treat uncertainties in processing geophysical and remote sensing data and in their combination. Tarom polymetallic zone in north-western Iran has been selected to perform and test DST rules in mineral exploration.

Mineral exploration involves detection and prospection as well as reserve calculation and site selection of ore and mine places. GIS techniques and mathematics are proper tools for geoscientists to work with in this case. Exploration is a multi-stage activity that begins at a small scale and progresses to a large scale, ultimately leading to the selection of sites as targets for drilling and mining. Error, incompleteness and other uncertainties come with the data and arise from changing scale during the analyses. Among the mathematical methods to determine uncertainty, Dempster-Shafer Theory (DST) is a knowledge-driven method. This method is appropriate to determine uncertainties especially for low-accuracy data.

Application of Dempster-Shafer Theory contains two steps. The first part presents a method to evaluate uncertainty on every data layer separately coming from individual sources. The second part relates to evaluation of data layer uncertainties from multiple sources with effect on each other. For the first part, DST's mass and belief functions have been applied and in the second part combination rules needs to be specified. Alternatively to DST's combination rules there are other combination rules which are applicable on weighted evidences by mass functions and can be used instead of DST's combination rules.

The main objective is related to the second part of DST and the adaption of other relevant combination rules to detect prospection areas based on various geophysical and remote sensing data layers. Results of these different rules to propagate uncertainty are compared here to discuss advantages and disadvantages of these rules to combine geospatial information. Several rules are discussed in detail: Dempster-Shafer theory and Yager's modified combination rules, Discount + Combine method and Mixing-or-Average method, Yager's modified Dempster's rule, Inagaki's unified combination rule, Dubois and Prade's disjunctive consensus rule, Convolutive X-Average and Zhang's center combination rule.

All data processing is performed in GIS environment. Precondition and an extensive part of the work were to collect all data in digital form and to create a consistent spatial database. Images and spatial data tables were integrated in addition to information from reports and all data was transferred and transformed respectively. For mathematical calculations, programming in MATLAB and within the GIS environment has been used.

With regard to processing, all DST's combination rules show similar results. "Dubois and Prade's disjunctive consensus rule" apparently shows smoother results in the graphs but with regard to algebraic properties, results have low accuracy. Though results are similar, regarding algebraic theory there are conflicts in setting up mass functions for Dempster's rule and regarding algebraic conditions Yager's rule is more advantageous compared with Inagaki's rules. In addition to that calculation based on Yager's rule show better correspondence with index points that can be used for validation purpose here. Consequently, this research suggests Yager's combination rule to calculate uncertainty for processing geophysical and remote sensing data in GIS environments for mineral exploration.

Zusammenfassung

In dieser Arbeit werden mathematische Methoden und GIS Techniken angewendet, um Genauigkeiten und Unsicherheiten bei der Erkundung von Lagerstätten zu bestimmen, die eine Hauptaufgabe der quantitativen Geowissenschaften ist. Es wird das Potential der Dempster-Schafer Theorie (DST) mit modifiziertem Regelsatz untersucht, um Unsicherheiten bei der Verarbeitung geophysikalischer Messungen und von Fernerkundungdaten sowie bei deren Verknüpfung zu untersuchen. Die polymetallische Vererzungszone Tarom im Nordwesten Irans wurde als Testgebiet für den Einsatz der DST in der Lagerstättensuche gewählt.

Die Erkundung von Lagerstätten beinhaltet sowohl die Bestimmung und das Auffinden von Erzen als auch die Vorratsberechnung und Standortsuche für Abbauorte. Für diese Aufgaben sind GIS Techniken und mathematische Methoden die richtigen Werkzeuge. Erkundung ist ein mehrskaliger Prozess vom Kleinen ins Große, der mit der Festlegung bestimmter Orte für Bohrungen und Bergbauaktivitäten endet. Messfehler, Unvollständigkeiten und andere Fehlereinflüsse kommen mit den Daten und Entstehen bei der Prozessierung und bei Skalenübergängen. Aus der Menge der mathematischen Methoden ist die DST eine wissensbasierte Methode, um Fehlereinflüsse zu behandeln. Diese Methode ist besonders geeignet, um Daten mit großen Unsicherheiten und Fehleranteil zu verarbeiten.

Die Anwendung der DST erfolgt in zwei Schritten. Der erste Teil beinhaltet eine Methode, um die Unsicherheit für jeden einzelnen Datensatz aus jeder einzelnen Quelle zu bestimmen. Im zweiten Teil werden Unsicherheiten bestimmt, die z.B. für Zwischenprodukte in der Datenverarbeitung unterschiedliche Ursachen haben und sich gegenseitig beeinflussen können. Im ersten Schritt werden Gewichts- oder „Vertrauens-" Funktionen bestimmt, die im zweiten Schritt mit zu spezifizierenden Verknüpfungsregeln vereinigt werden. Alternativen zu den DST-Verknüpfungsregeln existieren.

Das Hauptanliegen in dieser Arbeit ist der zweite Teil der DST mit der Adaptierung alternativer Verknüpfungsregeln zur Festlegung der Aufsuchungsgebiete basierend auf unterschiedlichen geophysikalischen Messungen und Fernerkundungsdaten. Die Ergebnisse der Anwendung unterschiedlicher Regelsätze werden diskutiert und verglichen, um die jeweiligen Vor- und Nachteile der Methoden zu beschreiben. Folgende Verknüpfungsregeln wurden untersucht: Dempster-Shafer Theorie und Yagers modifizierte Verknüpfungsregel, Discount + Combine Methode und Mixing-or-Aaverage Methode, Yagers modifizierte Dempster Regel, Inagaki's vereinheitlichte Verknüpfungsregel, Dubois‘ und Prades disjunctive consensus Regel, Convolutive X-Average und Zhangs center combination Regel.

Alle Datenauswertungen sind in einer GIS-Umgebung erfolgt. Voraussetzung dafür und ein besonderer, umfangreicher Teil der Arbeit waren die Sammlung, Transformation und Vorverarbeitung der verschiedenen Datensatze, um eine konsistente Geodatenbank zu erzeugen. Dazu wurden Satellitenbilder und Messwerttabellen integriert sowie Mess- und Ergebnisprotokolle ausgewertet. Für die mathematischen Berechnungen wurden MATLAB Programme geschrieben und Funktionen von ArcGIS genutzt.

Im Ergebnis der unterschiedlichen Auswertungen kann festgestellt werden, dass alle untersuchten Verknüpfungsregeln ähnliche Ergebnisse liefern. Dubois‘ und Prades disjunctive consensus Regel zeigt in den Abbildungen einen gelglättteten Verlauf aber in den Berechnungsergebnissen eine geringe Genauigkeit. Obwohl ähnliche Ergebnisse erzielt werden können, ist die Aufstellung der Gewichtsfunktion mittels der Dempster Regel problematisch. Yagers Regel ist vorteilhaft im Vergleich mit der nach Inagaki. Zusätzlich sind die Ergebnisse basierend auf Yagers Regel in besserer Übereinstimmung mit den Informationen an den als Referenzdaten verwendeten Indexpunkten. Konsequenterweise schlagen wir Yagers

modifizierte Verknüpfungsregel zur Berechnung der Unsicherheiten bei der Auswertung geophysikalischer und fernerkundlicher Datensätze zur Lagerstättensuche vor.

Acknowledgment

This dissertation would not have been possible without the guidance and the help of several individuals who in one way or another contributed and extended their valuable assistance in the preparation and completion of this thesis.

I would like to express my sincere gratitude to my supervisors Prof. Wolfgang Busch and Prof. Hossein Tudeshki for their constant and invaluable guidance, assistance, suggestions and tutelage that they have shown throughout the entire research work.

I am sincerely grateful to my colleagues and staff in Institute of Geotechnical Engineering and Mine Surveying of TU-Clausthal, especially Dr. Knospe for his consultations.

It is a pleasure to thank those who made possible facilities in Geological Survey of Iran; Mohammad Taghi Koreei president of GSI, my colleagues in Geomatics, GIS, Remote Sensing and Airborne Geophysics Departments.

My thanks and gratitude go to Geological Survey of Iran, Technology Transfer Institute in Iran and Carl Duisberg Center in Germany for giving me the opportunity to conduct my PhD research in Germany.

It is my great pleasure to express sincere gratitude to all family members especially my parents, friends, and all those who supported me during my PhD research.

Clausthal-Zellerfeld, January 2012 Seyedeh Roghayeh Mousavi

Contents

Chapter 1: General

1.1 Introduction

In this research the main purpose is using of some mathematical rules to determine uncertainty in geological sciences. Mineral exploration is a subject that always has been fascinated by geologist and mining experts and today GIS and mathematics come to help experts to determine uncertainties in this framework, so this object has been chosen to study of ability of Dempster-Shafer theory rules in solving of uncertainties in geological sciences.

Mineral exploration is the process of finding ore and mine, mineral exploration is a multi-stage activity that begins at a small scale and progresses to a large scale, at the end leading to the selection of sites as targets for drilling for buried deposits. At a small scale, at first must delineate general zones that may be of potential interest for mineral deposits of a selected type, usually based on broad geological considerations. At a medium scale, parts of these general zones are selected for more detailed follow-up exploration, based on evidence from geological mapping, regional geochemical and geophysical surveys and the locations of known mineral occurrences. Having identified those more specific zones of favorability, targets may be selected directly, or a further stage of detailed survey work undertaken. At the end, this process leads to a large-scale map showing the locations and ranking of potential sites.

1.2 Mineral potential mapping and conceptual model

Before analyzing it is necessary to provide mineral deposit models of the study area in large scale. The models can guide an expert in applying of suitable mathematic rules and mathematic models to determine of uncertainties and that also indicate which data should be gathered for analyzing. In this research by study of mineral deposit models and making correlation between study area and models some models can be exist in the area selected to explanation. This chapter tries to introduce the area and ability of the area for appropriate mineral deposit models.

Figure 1-1 shows a flowchart of operations that in this research to be applied. Conceptual models are important for all kinds of GIS applications. Mineral deposits can be classified into different types, depending on their characteristics. Conceptual models of metallogenesis and mineral deposit usually described by words and diagrams; they describe the typical characteristics of deposit groups; are accompanied by an interpretation of the processes of deposit formation, and are useful for providing criteria for mineral exploration (Hodgson, 1990).

In according to the flowchart; exploration database and geological knowledge base help to achieve conceptual models. By the way exploration database to be applied to prepare evidential data. Analyzing need the data in unique condition so after unifying the data and recognizing Uncertainties and criteria by conceptual model, then we can apply favorite mathematical modeling on the unified data. The modeling results are binary favorability map that after validation give mineral potential map.

The deposits occur within thick sequences of subaqueous volcanic rocks and are found mainly in felsic lava flows, but also in other volcanic rock types. Proximity to the contact between felsic flows and volcaniclastic units may be important. The volcanic rocks are associated with large felsic intrusions, believed to act as a subvolcanic heat source driving a hydrothermal circulation. Seawater is thereby pumped through the volcanic rocks, from which metals are dissolved and re-deposited at or near vents to the seafloor. The vent areas are associated with dykes and vertical fractures that cut through the volcanic rocks, localizing the upward flow of hydrothermal fluids. Heat from the intrusive dykes also helps to drive the circulation. The hydrothermal fluids react with the volcanic rocks to produce alteration minerals. Silicification and the presence of amphibole minerals occur in large zones, semiconformable with the volcanic stratigraphy. Ankerite occurs in more restricted zones. Weathering and erosion of deposits produces a dispersion halo of metallic elements in drainage sediments and till. Regional magnetic surveys show variations in magnetic susceptibility of the rocks, mainly due to differences in rock type. Sharp gradients in the magnetic field measurements usually reflect changes in rock type at geological contacts. Geophysical data can be particularly important evidence for VMS deposits, which have distinctive electrical characteristics. Airborne and ground EM data are widely used to explore for these deposits, particularly in association with magnetic data.

Figure 1-1: present a flowchart of GIS processing for mineral exploration.

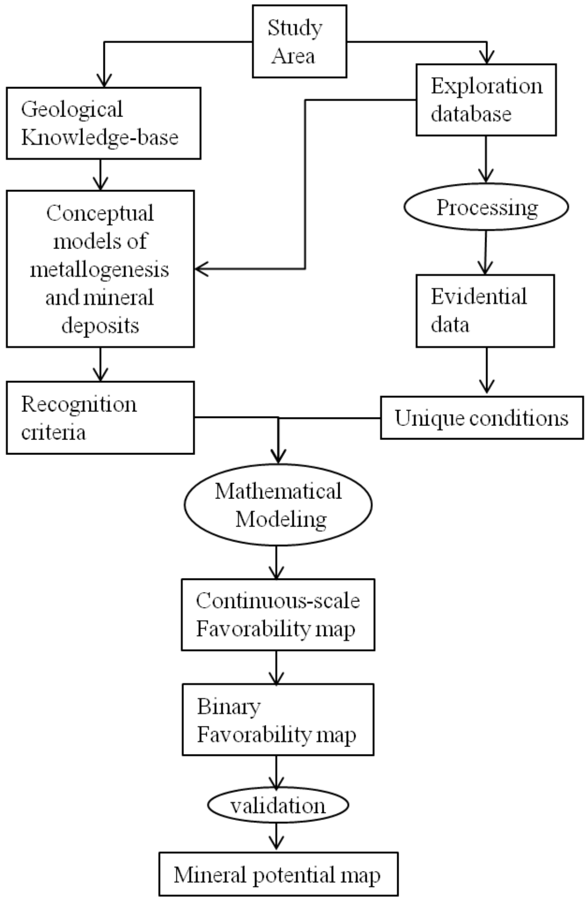

These criteria constitute part of the deposit model used in the GIS study, providing a framework for data selection and analysis.

Volcanogenic massive sulfide ore deposits are formed at volcanic vents on the ocean floor. For a description of the characteristics and genesis of VMS deposits in general, (Lydon 1984, 1988). The Chisel Lake VMS deposit occurring in the lower proterozoic Snow Lake greenstone belt (Bailes and Galley 1989), who summarize the geology and mineral deposits of the Anderson-Chisel-Morgan Lake area. In the study area the principal characteristics of the deposits useful for potential mapping are as follows.

Mostly a GIS project to be performed in three steps including of building spatial database, data processing and applying of data model as illustrated in figure 1-2. In mineral exploration for providing of mineral potential map there are also three steps.

In first step the appropriate data are assembled into a GIS database, the choice of geospatial data type need mineral exploration knowledge. In this research with attention to situation of the study area and existence of many evidences in study area show which type of mineralization has the most possibility.

Step1	Defining conceptual models of metallogenesis and mineral deposits (Building spatial data base)	Spatial data inputs	Bedrock geology		Structures	Ore-Forming Processes (OFP)
			Heat Sources	Host Geology		
			- Major batholiths (Exposed) - Satellite porphyries - Hidden igneous bodies - Tectono-magmatic Features	- Felsic magmatic massive - Subvolcanic porphyries - Eocene volcanic - Neogene Sediments - Pre-Eocene Carbonate	- Deep Major Lineaments - Transverse structures - Regionally Extensional Suites	- Hydrothermal Alteration - Ore Deposits / indications - magnetic anomalies - K - Alteration Anomalies U.K/Th Anomalies
Step 2	Spatial Data Processing and analysis	Operation to extract spatial features relevant to mineral deposit model	-Reclassification -Select contacts and quantify spatial association with known mineral deposits		Quantify spatial association with known mineral deposits	Extractable from RS(ETM) data and geophysics airborne data
		Derived maps to be used as evidence	-Favorable host rocks -Favorable distances to heat sources - Favorable entropy		Favorable distances to Structures	Favorable Alteration
Step 3	Integration Modelling	Combine spatial evidence maps	Data and knowledge driven methodologies			
		Final predictive map	Prognoses map of mineral potential			

Figure 1-2: Conceptual model of GIS processing for mineral exploration in 3 steps.(modified from Bonham Carter ' s model 1994)

Tarom magmatic arc lie in Alp-Himalaya orogeny range. The area are covered by Eocene volcanic arc rocks and in some place with intrusive rocks so it would be expecting minerals that relevant to this type rocks in addition existing of some ancient mining show this place has potential for mineralization in volcanic host rocks and plutonic rocks, plutonic rocks can be heat source as can be host rock for mineralization. Majorly rocks expose batholiths, porphyries, hidden igneous bodies, tectono-magmatic Features, felsic magmatic massive, subvolcanic porphyries, Eocene volcanic, neogene sediments, pre-eocene Carbonate.

Fractures make special conditions on the host rocks for creating of place on the rocks for settlement of the minerals. These fractures are usually associated with geological structures. Alteration zone are other factor can help us to find mineralization complex area.

In second step to be manipulate the data for extracting and deriving those spatial patterns relevant to the aims of the project in this step all necessary data have been extracted from different original source and prepared to use in geographic information system (GIS). In the third step, derived evidence combine to predict mineral potential area, applying of combining method depend on the type of data and trusting to data accuracy. Every step must be done precisely for acquisition of best conclusion.

1.3 Application of Geographic Information System (GSI) in mineral exploration

This part discuss about application of GIS for Geology with mineral exploration intent. A Geographic Information System (GIS) is a computer system capable of analyzing and displaying geographically referenced information, in other word spatial data identified by their location; the word geographic implies that locations of the data items are known, or can be calculated, in terms of geographic coordinates (latitude, longitude). In this research GIS is a tools and a context for mineral exploration.

The use of GIS in mineral exploration is now widespread, allowing the integration of disparate digital datasets into a single and unified database. The methods of combining multiple maps in a GIS encompass a wide variety of models. The purpose of a mineral explorer from using of GIS is assembling spatial data in the form of a mineral potential map to decide priorities for future exploration. Mineral exploration require the concurrent consideration of many kinds of spatial evidence for mineral deposits like the geology, structure, geochemical and geophysical and remote sensing characteristics of region as well as the location type of past discoveries. The interaction of many processes must be considered, and the concurrent analysis of multiple datasets is absolutely necessary.

1.4 GIS and relevant computer software

There are a number of close software in the family of GIS software that to be producted and developed for handling with spatial data. ArcGIS is one of them that have been improved to high utilization. In this software there are analyses and management tools and its capabilities have been increased for preparing and digitalizing of data. That is compatible with different resource data. In some case that will be need some another software for preparing original like Envi for remote sensing data. In this project ArcGIS, Oasis montaj, Envi and some programing and calculator software have been used. Other programs often used in associated with GIS for specialized tasks like Microsoft Excel. Following figure 1-3 shows place of GIS software in a diagram for geoprocessing states.

1.4.1 ArcGIS Desktop

ArcGIS Desktop is a comprehensive set of professional GIS methods used to solve problems, to

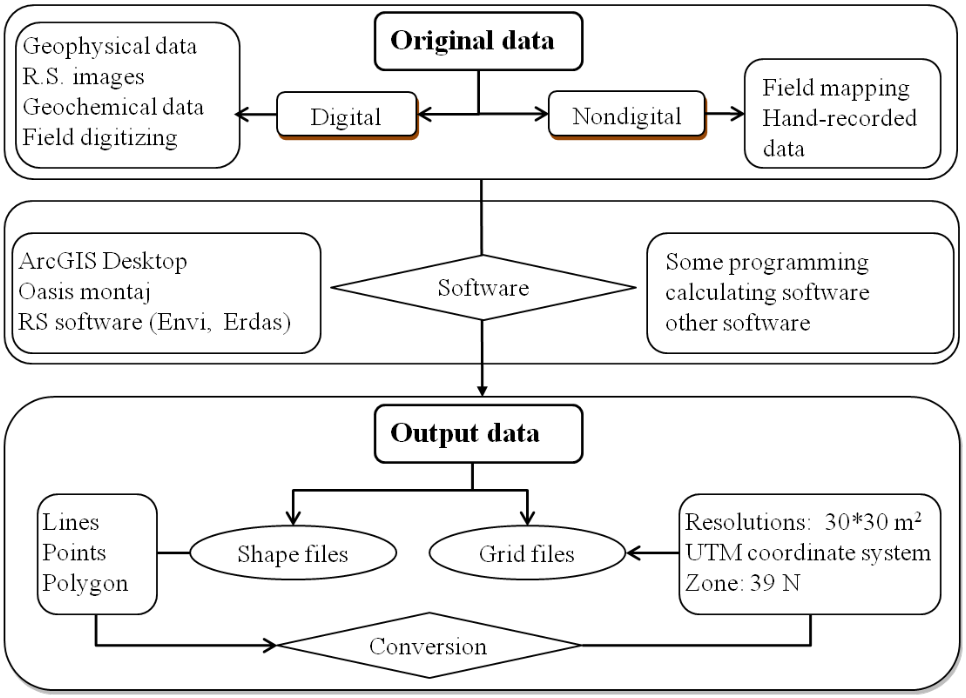

Figure 1-3: diagram of original data and software used for the processing.

meet a mission, to increase efficiency, to make better decisions; and to communicate, to visualize; and understand an idea, a plan, a conflict, a problem, or the status of a situation. It is available at three functional levels : ArcView, ArcEditor, and ArcInfo; ArcView focuses on comprehensive data use, mapping, and analysis, ArcEditor adds advanced geographic editing and data creation, ArcInfo is a complete, professional GIS desktop containing comprehensive GIS functionality, including rich geoprocessing tools. Additional capabilities can be added to all seats through a series of ArcGIS Desktop extension products from ESRI and other organizations.

1.4.2 RS Software

Envi, Erdas Imagine, Er Mapper and Geomatica are software products that usually to be used for digital image analyses. For this research Envi and Erdas Imagine were accessible. Envi and Erdas Imagine are the ideal software for the analysis, visualization and presentation of digital imagery, this software combine remotes sensing and GIS capabilities. Those enable users to create geospatial data, extract the most information and update their existing GIS data. Envi image-processing package includes advanced, yet easy-to-use, spectral tools, geometric correction, terrain analysis, radar analysis, raster and vector GIS capabilities, extensive support for images so this software has been choose for the most part of image processing application.

1.4.3 Geosoft (Oasis montaj)

Oasis montaj is planned by Geosoft Company; the company is headquartered in Toronto, Canada. Oasis montaj help to access of geophysics data and analysis of them. That also has some ability for GIS geoprocessing. The Oasis montaj software package includes a rich set of built-in data import, processing, visualization, mapping, and integration capabilities. It features Geosoft's complete library of basic and advanced gridding utilities, and plotting functionality.
A variety of montaj extensions and montaj plus extensions are available for advanced geophysics and geochemical data processing, analysis, quality control and modeling. These

extensions make Oasis montaj more powerful and comprehensive for geoscience mapping and processing systems. In this case that has been used only for geophysics data analysis.

1.5 Map projection

The location of a spatial data on the earth is defined in mathematical terms using either geographical coordinates, or planar coordinates according to some projection. For a GIS is possible to store and manipulate all spatial data in geographical coordinates (latitudes and longitudes. The Universal Transverse Mercator (UTM) is one of the most widely-used coordinate system which in this project also has been used. UTM system, established in 1936 by the International Union of Geodesy and Geophysics, and adopted by many national and international mapping organizations. The UTM grid utilizes the transverse Mercator projection, which results from wrapping the cylinder round the poles inverse of the ordinary Mercator projection. The globe is subdivided into sixty UTM zones, numbered from west to east, starting with zone 1 at 180°W. Each zone is thus six degrees of longitude wide, and extends from 84°N to 80 °S.

The study area is located in zone 39 UTM system. All data have been transferred to UTM map projection for GIS processing.

1-6 Geology of the study area

Tarom polymetallic Zone is a part of west Alborz mountain range that in Eocene epoch has been formed by mainly volcanic rocks eruption. Rock sequences are equivalent of Karaj formation and associated with volcanic lavas of basalt, andesite, basaltic andesite and trachyte that are all intruded by Oligocene intrusive bodies. Figure 1-4 represent position of the study

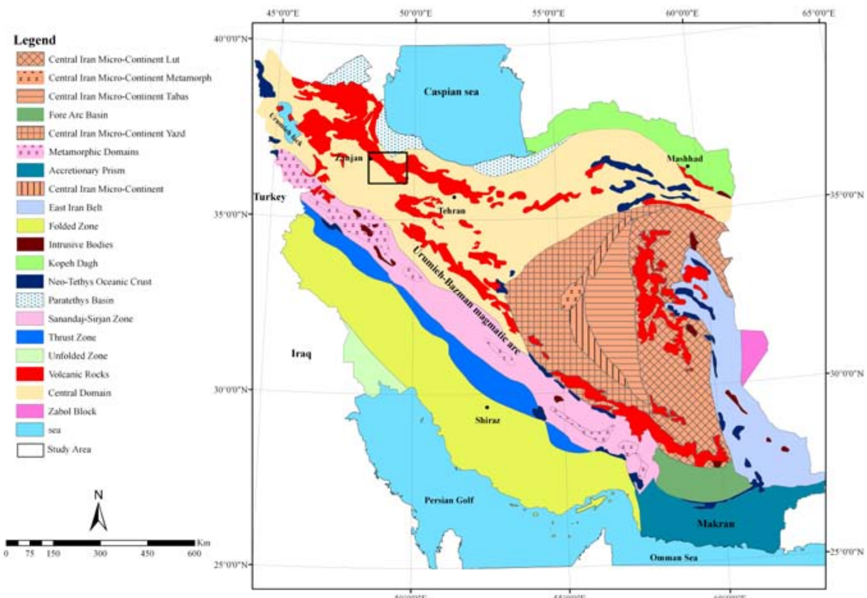

Figure 1-4: shows situation of the study area and Cenozoic igneous rocks in Iran plateau map, the area lie in west Alborz where intersects Zagros mountain range and in central domain of Iranian plateau division. There are two trends of igneous rocks along the Alborz and Zagros Mountains and the igneous rocks of Tarom zone occupy intersection of between them. (Aghanabati, 2004)

area in geological map of Iran, in this map can see the area located in northwest of Iran on the west part of Alborz Mountain range. The red colour on figure 1-4 indicates that volcanic rocks dominate on the study area.

Table 1-1 shows position of the Eocene epoch between other epochs and age of them. The role of calc-alkaline to shoshonitic intrusive rocks in formation of mineral deposits is essential. Lead, zinc copper, iron, manganese, gold, tungsten and minor molybdenum mineralization are reported in this field.

Table 1-1: shows era, period, epoch and age of some lithological units in the study area.

ERA	PRIOD	EPOCH/AGE	AGE
CENOZOIC	QUATERNARY		
	NEOGEN	PLIOCENE	5.3 ma
		MIOCENE	23.8
	PALEOGEN	OLIGOCENE	33.7
		EOCENE	54.8
		PALEOCENE	65
MESOZOIC			248.2
PALEOZOIC			540
PRECAMBRIAN			2500

Karaj formation in west Alborz has been divided in two major parts, upper and lower parts, Kordkand is lower part with 2400m thickness and name of the upper part is Amand with 1400m thickness. Every part has some units; it has reported only some units from Amand part in Tarom zone like Ea.4, Ea.5, Ea.6 units. Ea.4 covers horizontally an extensive region and includes alternate of acidic and intermediate magmatic rocks with dacite, rhyolite and andesite occurrence. Ea.5 consist acidic rocks mainly in lava, Tuff, breccia forms. Ea.6 has 300m thickness with acidic and intermediate components of tuff and lava (appendix).

Next studies for providing of geological map in scale 1/100,000 are more particular about geological units of the Tarom zone. In the attachment can see the table of descriptions for the rocks that occurred in the study area. Tarom zone contains parts of every 7 map sheets so there are 7 individual describes for volcanic rocks that in the next sections of thesis have been tried making a unit map by integrating with RS images. Table in the attachment represent rock type of the area in 7 geological map sheets (scale 1/100,000) and age of them in the table there are a column that show a rank that has been given to lithological unit according to aim in prospecting models, lithological units with number 1 have high capability to mineralization for Cu or Au and units with range 5 have low capability for mineralization of epithermal models minerals or porphyry minerals.

Figure 1-5 has been provided from 7 geological sheets. In this map (Figure 1-5), the lithological unites are separated by different colours for intrusive, extrusive (volcanic) and sedimentary rocks. At first volcanic lava have been erupted in a submarine environment, abundance of tuff and another submarine rocks indicate this matter, and then volcanic activity can be seen on the land because of pyroclastic rocks occurrence. According to the diagram of An+Ab'+Or of Irvine (figure1-6) and Baragar, 1971 the volcanic rocks of the area have been classified by Zarei (1992) generally to alkali-potassic, some alkali-sodic and rarely calc-alkaline in characters with alkali-potassic rhyolite, quartz trachyte, andesite, andesite basalt, basalt and shoshonite in the norm.

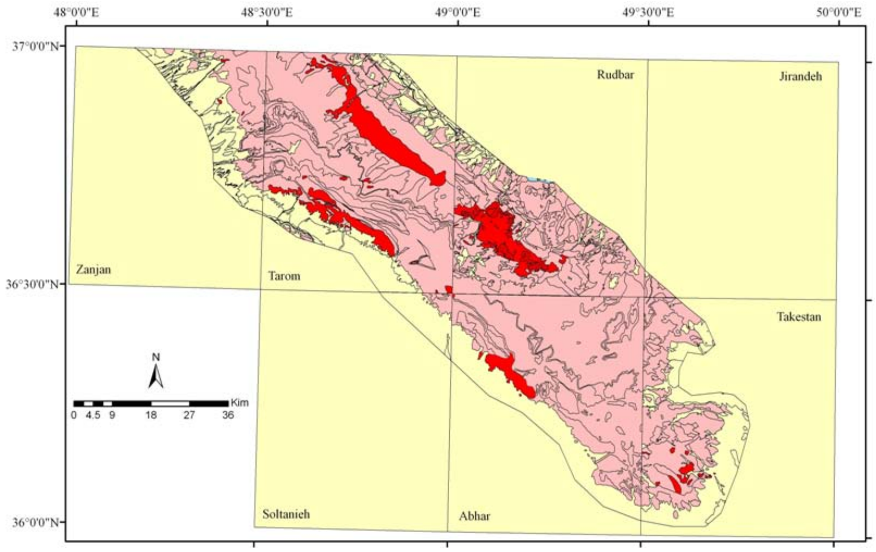

Figure 1-5: represent lithological units in Eocene era with pinkish (extrusive rocks) and red (intrusive rocks) colour yellow colour related to sedimentary rocks.

Figure 1-6: Represent geochemical composition volcanic rocks of the area in diagram of An+Ab'+Or. (Zarei, 1992)

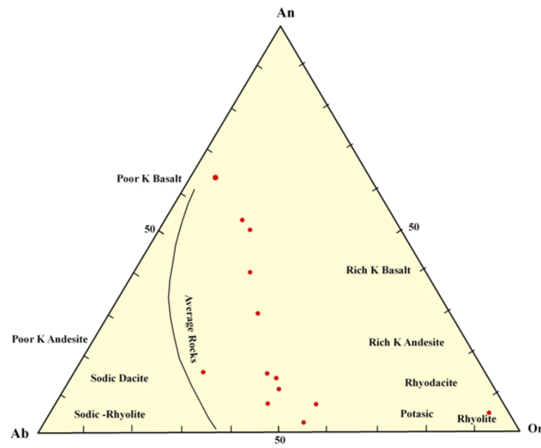

According to Baragar, 1971, there isn’t geochemical connection between acidic and basic terms, probably that due to crustal source of rocks. He believes these magmatic rocks are more related to island arc in continental margin relative to continental rifts. Figure 1-7 illustrate tectonic situation of the area, with regard to submitted tectonic model for area in figure 1-7 can result the area has continental margin arc position.

It is possible basaltic magma come from partial melting of metasomatized mantle due to fractional melting of olivine in intermediate term. In additional there are crustal pollution because of abundance of rare element like Sr, Rb, Ba and irregular distributing of them in different terms. As mentioned, another reason that indicates crustal source of rocks is geochemical connection lacks between basic, acidic and intermediate rocks.

In this area there are some masses of plutonic igneous rocks that after Eocene intrude in the volcanic rocks along the northwest-southeast direction and that can be seen mainly in alkali granite, granite, granodiorite, quartz monzonite, quartz monzodiorite, quartz syenite occurrence. According to Peyrovan researches (1992), intruding of the plutonic masses was the last magmatic activities in the area and occurred after Pyrenean orogeny (early Oligocene). Plutonic rocks mainly are silica-oversaturated and in microscopic study has 1-35 percent quartz. Granite rocks originate from mantle or lower crustal this researcher believe granite type is I and in comparing with another granite in the world in geochemical and mineralogical characters, intrusive rocks in Tarom zone are CCG+CAG+IAG type and in one case is POG. Geochemical characteristic similarity between plutonic and volcanic rocks can be possible because of the same source for them.

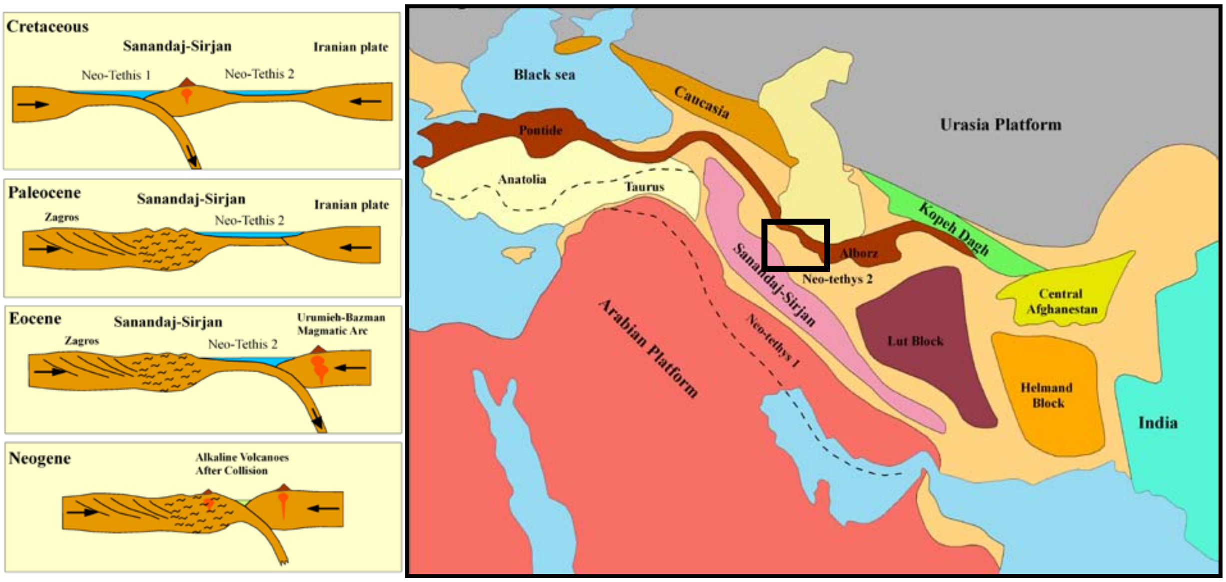

Figure 1-7: tectonic situation of the area (Aghanabati, 2004)

In figure 1-5 can distinguish intrusive masses in 4 major outcrops and in some small masses by red colour. This lithological unites in the maps table (in the appendix) show g, gd, G1 and G2 with northwest-southeast trend in the same trend of the volcanic rocks. In Takestan sheet intrusive rocks outcrops in southwest of the sheet and in the table have been named by g and include micrograntie that has been surrounded by alteration zone in around in addition there are in this area some dike with the same type rocks. A great mass has been set in southwest of the Rudbar sheet and contains granite, monzonite and aplite in light gray till pink colour. In Tarom sheet there are two great masses in the same direction of the volcanic rocks other small outcrops can be seen in some place, in basic, acidic and intermediate type but basic rocks are very less, the masses in this area contain quartz diorite, quartz monzonite, syenogranite, granite and rarely diorite and gabbro, this rocks are older than others in additional there are aplitic veins that related to the youngest magmatic phase, also tourmaline veins in intrusive rocks indicate Br metasomatism. Another large mass outcrops in Abhar sheet with alkali granite, granite, granodiorite, quartz monzonite, quartz monzodiorite, quartz syenite. Magmatic activities in this place have been issued by tectonic activities including orogeny phases.
Certainly Pyrenean orogeny is effective action in occurring of Eo-Oligocene intrusive igneous rocks in the area. Two separate groups for plutonic rocks have been defined the first alkali granite, granite, granodiorite, monzonite, quartz monzodiorite. These rocks make a continuous series and probably quartz monzonite is a mother magma for them, this magma with fractioning by partial crystallization create basic rocks include quartz monzodiorite beside of acidic rocks include granite, granite, granodiorite. These rocks can be originated from upper mantle or lower crust that has been melted by influencing of water that comes from a subducting oceanic crust. Second group include quartz syenite and alkali quartz syenite and probably originate from melting of lower crust in some stage.
According to tectonic classification; Iran plateaus situated between Urasia and Arabian platform. Figure 1-6 shows this matter where geologists believe it was an oceanic environment with continental environment in some place. 650 million years ago Alborz area was a part of gondwana continent as Tethys Ocean separated it from Eurasia continent, about 220-270 million

years ago this ocean has been replaced by neotethys oceans, figure 1-6 shows that, this happened after closing of Tethys ocean, that time Alborz was a part of Eurasia continent how Neotethys create between Eurasia and Arabian plate in gondwana. This events are contemporary with Alpine orogeny, this event formed the mountain ranges of the Alpide belt include the mountains from the Alps range in west to the Himalaya mountain range in east as well as caused closing of the Tethys and neotethys oceans, in additional caused Alborz and Zagros mountains forming in Iran plateaus, this activity have been begun from Mesozoic until now and itself has several phases.

By closing of neotethys Ocean and subduction of oceanic crust under continental crust, igneous activity occurred along the Alborz area and Sanandaj-Sirjan zone, neotethys2 was closed in the Eocene as the figure 1-6 shows while volcanic activity accompanied this event. Pyrenean orogeny is one of several phases in Alpine orogeny which has more effect upon the Alborz area that caused intrusive magma activity in the study area.

1.7 Metallogeny of the study area

Ore deposit can form in different condition by different source but in this case we are connected to igneous rocks. There are many different types of ore deposit that can be formed in igneous rocks just as a host rocks or host and source rocks. As regard to the last comment, here there are approximately intermediate and alkaline rocks that have been arise in a volcanic arc environment in Eocene epoch, these characteristics create some condition for epithermal and porphyry mineralization so has been tried to describe some model of ore forming in these cases.

1.7.1 Epithermal mineralization

Epithermal mineralization in this case is more possible with according to abundance of alteration area. This type mineralization is formed in a geothermal system; today's active geothermal systems occupy the same tectonovolcanic place as those hydrothermal systems, preserved from the past. The near-surface (0-1000 m) formations of epithermal ore deposits in the Tertiary[1] volcanic rocks are formed in the Circum-Pacific region and elsewhere formed at deeper levels (2-5 km or so) beneath calc-alkaline volcanoes in these same volcanic rocks (Ulitoe, 1973; Henley and McNabb, 1978), porphyry- type copper and molybdenum deposits are preserved in both Tertiary and much older hydrothermal systems (Heleney, 1986).

This mineralization has been formed in a hydrothermal circulation; hydrothermal circulation in its most general sense is the circulation of hot water; hydrothermal circulation occurs most often in the vicinity of sources of heat within the Earth's crust. That commonly occurs near volcanic activity, but can occur in the deep crust related to the intrusion of granite, or as the result of orogeny or metamorphism. In additional geothermal systems are abundant in the tectonically active zones of the earth's crust. Chemical differences arise from the sources of recharge water and contribution of gases from magmatic or metamorphic sources. Hot water springs occur in the tectonically stable crust where the deep crustal penetration of groundwater in favorable sedimentary formations, like limestone.

The source of fluids for geothermal system in non-marine environment is atmospheric water versus marine environment, which will be need abundant rainfall in non-marine environment for forming of ore deposits so in contrast; marine environment has more accessibility to fluids and more ability to forming of the ore deposit. In marine environment active geothermal systems are corresponded to convection circulation and provide heat energy from discharging of that in

[1] the first period of the Cenozoic Era

oceanic crust magma. Figure 1-8 generalized structure of a typical geothermal system in silicic-volcanic rocks.

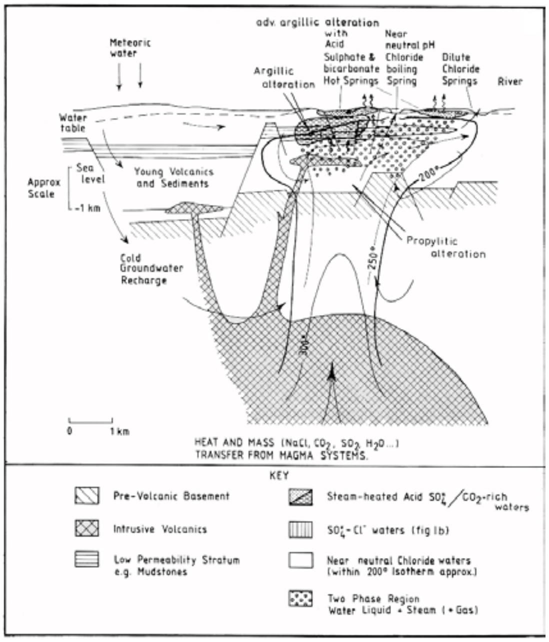

Figure 1-8: Generalized structure of a typical geothermal system in silicic-volcanic rocks (extracted from Cox and Singer 1996).

Usually in non-marine environment water penetrate downward to the depth by fractures, to the hot intrusive rocks, as they go to deeper, the temperature increase also the solubility of fluids; they acquire a part of heat energy from surrounding rock in their route, when they arrive to the intrusive rocks, they provide the greatest portion kinetic energy from heat energy of intrusive rocks where magma are solidifying and becoming colder. Magma implements two actions, not only that charge heat energy for fluids motions in geothermal system but also provide a big part of solution substances for fluids.

In the active geothermal system for non-marine environment hot water can be influenced to 5 Km depth and it is possible to extend for several million years. Near of the surface temperature has a range between 50-100C but in deeper increase to 350-400C. Today’s active geothermal systems are more common in tectonic area and associate magma activity especially in boundaries of the tectonic plates so these are seen in volcanic structures that occur on divergent and convergent plate borders and are more associate with volcanic activity of andesite, dacite and rhyolite than basaltic activity (Ellis, 1979). Some indications for these systems are hot water springs, geysers, and fumaroles mudpots.

Volcanic areas like Yellowstone National Park, U.S.A., Iceland, or in the Taupo Volcanic Zone of New Zealand, but other terrines also host hydrothermal activity even though subsurface temperatures may be relatively low and surface features less impressive. Warm springs in the Rocky Mountains, the European or New Zealand Alps or in the sedimentary massifs of central Europe are examples with active geothermal system. (Henley 1986).

Circulation route and influence area of the fluids depend on geological characteristics, usually the fluids penetrate in a vertical or approximately vertical axle and commonly are conducted by fractures and faults, in some place due to horizontal penetrable area it is possible horizontal expanding. The fluids in their circulation toward the surface lose gradually their energy as their solubility and settle some associated substances and elements from solution, usually settle in fractures as veins because there are adequate spaces in this geological structure, finally on the surface appear as hot springs and remainder settled on the surface. Due to gradual settlement there are a zonation for geothermal mineralization system, in depth that to be accompanied with Te, Zn, Bi, Pb and Cu on surface with W, As, Sb, Au, Ag and Tl. There are several models for Au epithermal deposits from Cox and Singer 1996, on the following to try explaining 5 models which have relationship with falsic volcanic rocks. several case of epithermal mineralization in different part of Iran can see, some of them that are relatively near of the region; Zareshuran and Dandi deposit in a district with about 200 km distance at west and Dashkassan deposit with about 300 km distance in southwest.

1.7.1.1 Model of hot-spring Au-Ag

In this model fine-grained silica and quartz in silicified breccias are associated with gold, pyrite, and Sb and As sulfides, rock types are commonly rhyolite with porphyritic and brecciated textures also age range mainly Tertiary and Quaternary. Depositional environments usually are subaerial rhyolitic volcanic centers, rhyolite domes, and shallow parts of related geothermal systems. Tectonic settings include through-going fracture systems related to volcanism above subduction zones, rifted continental margins and leaky transform faults.

1.7.1.2 Model of creed epithermal veins

Approximate synonym for this model is Epithermal gold (quartz-adularia) alkali-chloride-type and polymetallic veins. In this model galena, sphalerite, chalcopyrite, sulfosalts, tellurides, gold in quartz-carbonate veins; hosted by felsic to intermediate volcanic rocks. Older miogeosynclinal evaporites or rocks with trapped seawater are associated with these deposits. Host rocks are andesite, dacite, quartz latite, rhyodacite, rhyolite, and associated sedimentary rocks. Mineralization related to calc-alkaline or bimodal volcanism with porphyritic texture, age Range Mainly Tertiary, depositional environments are Bimodal and calc-alkaline volcanism. Deposits related to sources of saline fluids in prevolcanic basement like evaporates or rocks with entrapped seawater. Generally in tectonic structure similar through-going fractures systems; major normal faults, fractures related to doming, ring fracture zones, joints associated with calderas has been creating. Underlying or nearby older rocks of continental shelf with evaporite basins, or island arcs that are rapidly uplifted. Associated deposit types are Placer gold, epithermal quartz alunite Au and polymetallic replacement.

1.7.1.3 Model of Comstock epithermal veins

This mode is very similar to last mode though approximate synonym for this model is epithermal gold (quartz-adularia) alkali-chloride type. In this model; Gold, electrum, silver sulfosalts, and argentite seated in vuggy quartz-adularia veins and to be hosted by felsic to intermediate volcanic rocks that overlie predominantly elastic sedimentary rocks, and their metamorphic equivalents.

Rock types of host rocks are andesite, dacite, quartz latite, rhyodacite, rhyolite; and associated sedimentary rocks. Mineralization related to calc-alkaline or bimodal volcanism with porphyritic textures and age Range Mainly Tertiary.

Depositional environment is Calc-alkaline and bimodal volcanism and associated intrusive activity over basement rocks composed of elastic sedimentary rocks and their metamorphic equivalents. Volcanic-related geothermal systems lack access to saline fluids from basement sources. Tectonic settings are through-going fracture systems, major normal faults, fractures related to doming, ring fracture zones, joints. Associated deposit types are placer gold and epithermal quartz-alunite Au.

1.7.1.4 Model of Sado epithermal veins

In this model gold, chalcopyrite, sulfosalts, and argentite in vuggy veins are hosted by felsic to intermediate volcanic rocks that overlie older volcanic sequences or igneous intrusions.

Rock types of host rocks are andesite, dacite, quartz latite, rhyodacite, rhyolite, and associated sedimentary rocks, mineralization related to calc-alkaline or bimodal volcanism with porphyritic texture, age range mainly Tertiary.

Depositional environment is calc-alkaline and bimodal volcanism and associated intrusive activity over basement rocks composed of thick and older volcanic sequences or igneous intrusive (batholiths), volcanic-related geothermal systems lack access to saline fluids from basement sources. Tectonic settings contain through-going fracture systems, major normal faults, fractures related to doming, ring fracture zones, joints. Associated deposit types are placer gold and quartz-alunite Au.

Mineralogy composed of Gold, argentite, electrum, chalcopyrite, Sulfosalts and tellurides are moderate, galena and sphalerite are sparse and gangue minerals consisting of quartz, pyrite, adularia, calcite, chalcedony, adularia, kaolinite, rhodochrosite, chlorite, sericite, and barite are moderate to sparse. That can be seen banded veins, open space filling, lamellar quartz, stockwork, breccia pipes texture and structure.

1.7.1.5 Model of epithermal quartz- alunite Au

Approximate synonym for this model has been used acid-sulfate, or enargite gold by Ashley, 1982. And that was described with gold, pyrite, and enargite[2] in vuggy[3] veins and breccias in zones of high-alumina alteration related to felsic volcanism.

Environment rock types contain volcanic rocks similar dacite, quartz latite, rhyodacite, rhyolite and hypabyssal[4] intrusions or domes, with porphyritic texture, age range generally Tertiary, but can be any age. Depositional Environment Within the volcanic edifice, ring fracture zones of calderas or areas of igneous activity with sedimentary evaporates in basement.

Tectonic settings are through-going fracture systems contain keystone graben structures, ring fracture zones, normal faults, fractures related to doming, joint sets. Associated deposit Types are porphyry copper, polymetallic replacement, volcanic hosted Cu-As-Sb. pyrophyllite, hydrothermal clay, and alunite deposits.

Deposit mineral composed of Native gold, enargite, pyrite, silver-bearing sulfosalts, chalcopyrite, bornite, precious-metal tellurides, galena, sphalerite, huebnerite[5] and May have hypogene oxidation phase with chalcocite, covellite, luzonite with late-stage native sulfur. Veins, breccia pipes, pods, dikes; replacement veins often porous, and vuggy, with comb structure and crustified banding are common texture and structure in ore deposits.

1.7.2 Porphyry mineralization

Another mineralization system in the study area can be Cu-Au porphyry mineralization; Au in this system is a subordinate deposit and commonly appears as associated element of copper

---

[2] An iron-black mineral of metallic luster, occurring in small orthorhombic crystals, also massive. It contains sulphur, arsenic, copper, and often silver

[3] A small cavity in a rock or vein, often with a mineral lining of different composition from that of the surrounding rock.

[4] Solidifying chiefly as a minor intrusion, especially as a dike or sill, before reaching the earth's surface.

[5] hubnerite is a mineral consisting of manganese tungstate (chemical formula: MnWO4).

porphyry deposits also in this system that is mineralized commonly as an autochthonous[6] inverse of epithermal deposit.

The major products from porphyry copper deposits are Cu-Mo or Cu-Au but sometimes another precious metals similar Ag, Pb, Sn, W, Ur, Pt have been exploited from this deposit. The deposits occur close to or in felsic-intermediate intrusive rocks (I-type granitoids ± their volcanic equivalents) that have porphyritic texture. There are usually several occurrence of intrusive activity, so expect swarms of dykes and intrusive breccias. Copper porphyritic deposits commonly were submitted in two types that come in fallowing:

A- Calc-alkaline deposits: which are associated with intermediate porphyritic plutonic rocks. These deposits classify into:

1- Cordilleran Porphyry Cu type: that is associated with quartz monzonites and granodiorite. This type is characterized by grades of 0.45 - 1.2 % Cu, 0.01 - 0.03 % Mo.

2- Island Arc Porphyry Cu: Associated with quartz diorites and granodiorites, and grades of 0.35 - 0.7 % Cu, but < 0.001 % Mo. Generally, these deposits appear to have a higher Au/Cu and lower Mo/Cu ratios in contrast with the cordilleran types.

B- Alkaline Porphyry Cu deposits: which are associated with alkaline rocks (monzonite, syenodiorite), and are characterized by grades of 0.45 - 1% Cu, < 0.001% Mo, and an overall lower concentration of S. Significant amounts of Au may occur in these deposits as well.

It is important to note that the island arc and alkaline type deposits often contain significant amounts of Au and/or Ag.

In follow to be described model of porphyritic deposit with Cu-Au that has been submitted by By Dennis P. Cox (Cox and Singer 1996). These deposits are formed in stockwork veinlets of chalcopyrite, bornite, and magnetite in porphyritic intrusions and coeval volcanic rocks. Ratio of Au (ppm) to Mo (percent) is greater than 30. Environment rock types are tonalite to monzogranite; dacite, andesite flows and tuffs coeval with intrusive rocks, also syenite, monzonite, and coeval high-K, low-Ti volcanic rocks (shoshonites). Textures Intrusive rocks are porphyritic with fine- to medium-grained aplitic groundmass. Age changes between Cretaceus to Quaternary. Tectonic settings contain island-arc volcanic setting, especially waning stage of volcanic cycle, also continental margin rift-related volcanism. Associated deposit consist of porphyry Cu-Mo; gold placers.

Geochemical properties are characterized by Cu, Au, Ag; peripheral Mo. Peripheral Pb, Zn, Mn anomalies may be present if late sericite pyrite alteration is strong.

Example in Iran for this model is Sarcheshme mine in south, near of Kerman city, in this mine Au exploit as a minor production.

1.8 Model in the Tarom zone

According to the explanation about epithermal and porphyry deposit and with regards to economic geology reports (Geochemical analysis table of some instance in the appendix) beside of the lithological information (table 1-2) in the area there are both type of mineralization. About epithermal, except of hot-spring model all model is possible and also there isn't any evidence about active hot-sprig or sediment of them but other four models are possible.

There is similarity between other models in characteristics in addition there isn't adequate information for discriminating of them in the area.

[6] Originating or formed in the place where found

The study area composed of the Tertiary volcanic rocks that some where intrusive rocks intrude in border and in some places around of river can be seen Quaternary sediments. Here some common characteristics according to models have been brought.

Epithermal model for area:

For discrimination of the models have been used some properties which can drive from geological map similar host rocks type, age range, texture of rocks, and some structures (figure 1-9).

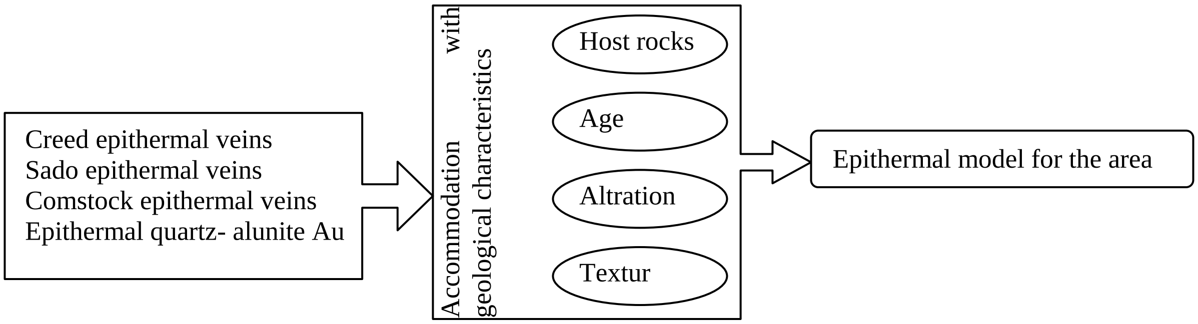

Figure 1-9: for extracting of epithermal models some information have been attended like age, host rocks, alteration and texture.

In the attribute of the geological map in GIS environment have been created several field that show age, host rocks and texture and by this way some lithological units that was suitable for epithermal mineralization have been discriminated.

Figure 1-10 shows porphyritic and epithermal mineralization related to porphyry model, which can be accorded to the study area model (extracted from Cox and Singer 1996). In this model, some brunch of intrusive rocks have been outcropped on the ground but the main mass body hides under surface. Around of the intrusive rocks there is alteration area.

Figure 1-10: porphyritic and epithermal mineralization related to porphyry model, which can be accorded to the study area model (extracted from Cox and Singer 1996).

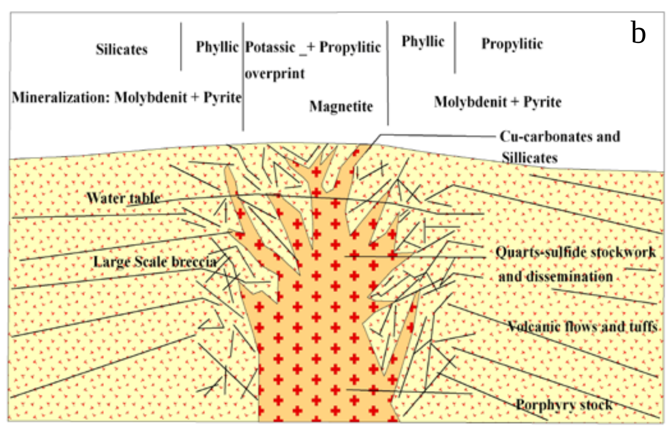

Faults are fractures along the relative sliding movement of the blocks. These fractures create appropriate condition to epithermal mineralization. We recognize them by various criteria:

1) Layers of different types and ages of rock units sit side-by-side

2) Abrupt topographic discontinuities of landforms

3) Depressions along the fault trace (broken rock is more easily eroded)

4) Scarps or cliffs

5) Sudden shifts of drainage courses.
6) Abrupt changes in vegetation patterns

These structures also have been extracted from different data layers for applying in the GIS processing.

For area has been use four geology sheets that every of them has been provided by different geologists with different standards so there are in two lithological unit in adjacent sheets different description and that increase confidence.

Chapter 2: Methodology

2.1 Introduction

Today GIS technology has developed in different scientific cases also in mineral exploration. GIS technology capabilities have been increased step by step. Now we can use mathematic rules easily in this environment. This chapter tries to introduce the purpose of the thesis and discuss mathematical rules that can help to solve uncertainty in GIS context for the study area. Dempster-Shafer theory rules are here the main used mathematical rules which details and analysis is explained in this chapter.

2.2 History of economic geology studies in the area and GIS projects

Bonham-Carter has developed GIS applying technologies in geosciences through geologists and some GIS experts that have tried to use that. In this case and has gathered all research results in his book 1994 systematically. In this book he indicates several methods to integration of spatial data in GIS context by mathematic rules. He classifies integration manners to data-driven and knowledge-driven. Bonham-Carter explains three steps: data gathering, processing and integrating of data.

Bonham-Carter contributed with GIS group in Geological Survey of Iran (GSI). He helped and introduced initial capability of GIS instrument to Iranian experts. The first project was performed by Dr Daneshfar & et al. 1998 in Saqqez sheet west of Iran. Conclusions have been presented in some papers and reports. GIS group have done many projects in different regions and different scales by these methods as Tarom Mountain.

Tarom Mountains due to its situation and ancient mines already have been considered for mining and mineral exploration also by outlander experts. Russian scholars have done the first scientific researches on mines before Second World War in this area. Molly 1963 has mentioned ore deposits and mines in north of Zanjan and in Tarom area. D. Bazin & H. Hubner 1969 in a report have remarked and explained some ores, indices and mines in this area. Ladam 1945 had a research on the mineralization in west part of Alborz Mountains Range; where cover this area too.

Mobasher, 1986 submitted a report about systematic exploration in Aliabad-e-musavi region. There are some reports from Kymiaghalam 1987, Tadaion-Eslami 1989, Moaied 1991, Jamshidi 1991, Mehrparto-babakhani 1995, Sh. Rahmani 1997, Amini& fazaeli 1999, Rahmani 2004 and etcetera. They individually have reported about ore deposits in this area.

Geological Survey of Iran has divided the area of Iran for some investigation to quadrangles in 1/100,000 and 1/250,000 scales. Hence, geological study be done in these quadrangles but sometimes, depend on purposes, some zones determine for studies like Tarom zone. Tarom zone situates in west part of Albourz Mountain Range and has special structure for mineralization.

Usually in geological maps and reports, there is some information about economic geology besides lithologic information. Hence for this thesis, economic and lithologic information have been derived from map reports.

Geological map and report of Zanjan are in 1/250,000 scale and Stöcklin & et al., 1969 provided that. There are report and map from Annells, 1975 for Qazvin-Rasht quadrangle in 1/250,000 scale. Also there are some reports for geological maps of area in 1/100,000 scale quadrangles.

Some projects in GSI have used GIS techniques to mineral exploration in the study area. These projects have been performed in two division systems. First, projects investigate in quadrangles division systems with scale: 1/100,000 (division system in Iran for providing of geological maps). Then, another project investigates in zonation system. The study area contains Tarom zone in the zonation system and some parts of seven quadrangles. Already GIS techniques have been implemented for mineral exploration only in some parts of study area. In the following some advantages and disadvantages of previous methods in the two division systems are discussed:

Quadrangle division system with weight of evidence method:

Weight of evidence method has been performed for three quadrangles with considering to Bonham-Carter work 1994. This method depends on Bayesian theory and uses probability framework. The main concepts in Bayesian theory is the idea of prior and posterior probability. The ArcView Spatial Analyst extensions have been used for this method. These extensions help to create spatial models for geographic areas. In this method, indication points and old mines have been used besides other data layers like faults, geological units, geochemical data and geophysical data after converting of them to polygon layers as evidence.

A weak point is to determine quadrangle area for modeling and processing in the former studies. In the quadrangle sheets, it is possible to see several disparate districts with different economic geological potential. Sometimes, mineralizations have conflict with each other in this division system; all of them are processing in one unit system and unit condition, also unit standards so that make unreliable conclusions. For example, there are Eocene epoch lithology units as volcanic rocks with especial potential in metal ore deposit in northwest of Abhar sheet. But, that can be seen another structure related to Mesozoic era and sedimentary lithology with non-metal ore deposit potentials in south west of Abhar sheet. In addition tectonic mechanisms are different in northwest and southwest of Abhar sheet hence different tectonic structure create different conditions for ore deposit.

Another weak point of this method in quadrangle division system was precision. Weight of evidence model needs precise data to give desirable results. imprecise data are not suitable for weight of evidence model, especially indication points are important and data layer with low accuracy from geology maps and another data layer make unreliable data so that affect on posterior probabilities.

Zonation division system and index overlay method:

In zonation system, GSI exploration researchers have divided Iran into 20 zones with mineralization capability. Tarom zone is one of them and situated northwest of Iran. This zone covers wide area and it has north-west to south-east direction. From south-east, it is limited by Qazvin area in central Alborz. Then to north-west, Tarom mountain continue in west Alborz mountain where named Tarom Zone. In north, the zone is adjacent to Hashtjin zone and in west it is adjacent to Soltanieh Mountain.

Index overlay method has been used for mineral potential modeling in this zone. This method is more appropriate with regard to wide study area and applying primitive data with low accuracy. In the end of the model processing, some favorable area have been proposed for next expert investigations. Due to Tarom zone capability, that needs more investigations with other methods.

Bonham-Carter 1994 implies Dempster-Shafer theory as knowledge-driven type for data processing and combination. Dempster-Shafer theory is the method that this thesis investigates for mineral exploration. This theory also known as belief functions theory, Dempster-Shafer theory takes its name from A. P. Dempster (1968) and Glenn Shafer (1976). In fact, the theory reasoning found as far back as the seventeenth century. The theory came to the attention of AI researchers in the early 1980s, when they were trying to adapt probability theory to expert systems.

The Dempster-Shafer theory is based on two ideas: first, the idea of obtaining degrees of belief for one question from subjective probabilities for a related question; second, Dempster's rule for combining such degrees of belief when they are based on independent items of evidence (Shafer, 1992). Hence, this method found on statistical methods and based on Bayes' theorem also.

P. An 1992 applied Dempster-Safer Theory rules for mineral exploration. Caranza, 2002 applied several methods for mineral exploration beside of Dempster-Shafer rules and compared their conclusions. Other previous researching related to Tangestani & Moore, 2001 who used this theory for copper mineral exploration in south of Iran.

2.3 Type of uncertainty in geological application

The uncertainty term is used in science and technology generally. It is discussed by theoretical mathematicians as a fundamental term and is defined by them as lack of certainty in describing an object, a feature or a process. Helton 1997 describes the dual nature of uncertainty with the following definitions:

Aleatory Uncertainty: the type of uncertainty which results from the fact that a system can behave in random ways also known as stochastic uncertainty, type A uncertainty, irreducible uncertainty, variability, objective uncertainty.

Epistemic Uncertainty: the type of uncertainty which results from the lack of knowledge about a system and that is a property of the analysts performing the analysis and also known as: subjective uncertainty, type B uncertainty, reducible uncertainty, state of knowledge uncertainty, ignorance.

Zimmermann 2000 defines uncertainty phrase as: “Uncertainty implies that in a certain situation a person does not dispose about information which quantitatively is appropriate to describe, prescribe and predict deterministically and numerically a system”. This definition should hold also for geological uncertainty.

Dubois and Prade 2000 distinguished in mathematical respect the following three types of uncertainties:

Imprecision or inaccuracy, expressing the deviation of measurements forms a true value. In this context the term accuracy expresses the closeness of the measurement to the true value. The term error represents the numerical difference of the measurement from a true value. All measurements inevitability results in some even very small error. The term bias is also frequently used in the case of consistent under or over estimation of the true value.

Vagueness or ambiguity expresses the uncertainty of non-statistical or object. In these cases the measurements are replaced by observations and linguistic descriptions (“semantic ambiguity”). Several researchers of information theory concluded that this type of uncertainty cannot be properly handled by stochastic methods, but must be treated by the possibility theory (Smithson, 1989) or other uncertainty theories.

Incompleteness is a type of uncertainty, occurring when the amount of information or knowledge (measurement or descriptions) is insufficient to perform an adequate evaluation of the given population. The phrase population is used here in mathematical sense. Often the phrase approximation is used for the result of the evaluation of such situations.

Zimmermann 2000 distinguishes further two sources of uncertainties: conflicting evidence, when considerable information is available pointing to certain evidence, but there might be some further information contradicting and pointing to the another evidence. It is often very difficult to find out which of the evidence is true. Belief is the last source of uncertainty distinguished by Zimmermann. In his opinion there are situation in which all available information is subjective, as a kind of belief. He emphasize that any human being develops on the basis of available data. This occurs in a way which is largely unknown for experts and produces belief about a system, which can call expert's opinion.

B´ardossy 2004 imply distinguishing of objective information contain measurement, observation, descriptions etc. from subjective information based on the expert's opinion. The different type of uncertainty may need different modes of representation.

The sources of uncertainties are undoubtedly valid the geological problems as well. However the amount and the complexity of the most geological uncertainties require a more detailed classification. The lack of such a classification is one of the main reasons why many geological uncertainties have not been evaluated and solved so far. B´ardossy distinguished uncertainty in geological area to uncertainties due to natural variability, and uncertainty due to human imperfections and incompetency. Variability (heterogeneity) is an inherent natural property of all geological features, objects and processing. Theoretically, complete lack of variability could also exist and called homogeneity but this never takes place in geological systems. Even the minerals, consider in the past as completely homogenous objects are heterogeneous, their real crystal structures being far away from the theoretical, perfect structure (B´ardossy 2004).

The degree of variability of geological feature or object may be quit varied depending on the related geological processes and environment. Generally, the higher the variability of a geological feature or object, the larger will be the uncertainty of its evaluation (measurements or description, as outlined above). It is also obvious that highly variable features require more investigation, collection of more of input data, that only slightly variable ones. A significant particularity of geological objects is that their features can be structured and unstructured. The structured variability, called also trends, show more or less regular spatial and temporal changes that can be described by the well known methods of trend-surface-analysis. Examples of spatial trends are gradual compositional transitions of one rock into the other or cyclic repetition of sedimentary features in a sequence of layers. On the other hand, unstructured variability may occur unexpectedly in a geological object and their spatial position and /or magnitude cannot be exactly predicted. They appear in the trend-surface-analysis as residuals and outliers. There are no perfectly structured or unstructured geological objects, rather a mixture of the two types. The higher the proportion of the unstructured locations, the higher is the overall uncertainty of the given object.

The uncertainties due to human shortcomings, incompetency or inadequate conditions may occur in all stages of geological investigations and they are extremely different. Their main sources are incomplete knowledge of the given geological object or process, shortcomings in modeling, the inaccurate application of mathematical methods and finally financial, economic, temporal or other natural limitations of the investigation.

Uncertainties in the phase of preparing the input data contain:

1- Lack of representative sampling, 2- Insufficient laboratory measurements, 3- Errors of laboratory measurements, 4- Another possibility is the ranking of all collected qualitative data 5- Uncertainties due to time estimation and in the phase of geological evaluation and reasoning contain, 6- Conceptual and model uncertainties, 7- Uncertainties due to subjective information, 8- Uncertainties of mathematical modeling, 9- Uncertainties due to the incorrect application of mathematical methods and 10- Uncertainties of the final conclusions of a geological investigation or project (György 2003).

In source of geological uncertainties and errors, it should be attended that the natural variability is a property of nature and it is not dependent on human shortcomings. Natural variability can be studied, quantified and described, but it cannot be diminished. On the other hand, there are the uncertainties and errors due to human shortcomings and that can be diminished to a certain extent, but they cannot be completely eliminated. There is a possibility to estimate their approximate amount, applying both mathematical calculations and subjective judgment. This gives a more realistic base for scientific and practical decisions. Finally, it is not enough to identify and to determine uncertainties for each variable separately, but for geological purposes; generally the calculation of the total uncertainty is required.

2.3.1 Uncertainty in geospatial environment

In geology the spatial position of the geologic objects and processes is important. For the spatial evaluation spatial coordinates (X, Y, Z) must be added to each variable and they must be part of all calculations. Spatial predictions can be performed by point and block kriging and the standard error of the prediction can be calculated (Bardossy 2001). Matheron's theory 1971 has some limitations, like the requirement of first and second order stationarity in the studied area. A further limitation is that semiquantitative and qualitative data cannot be evaluated by this method. However, indicator kriging can model certain types of semiquantitative data. Geostatistics have been applied broadly during the last two decades in mineral exploration, mining and in the petroleum industry (Schuenemeyer & Power, 2000). Much has been published on the method and on practical experiences. The development of fuzzy geostatistics and particularly of fuzzy-kriging was an essential step for the handling of spatial uncertainty in geology. But Bardossy 2001 believes spatial equivalents can be developed for all the nonspatial uncertainty analysis methods. They would complete the evaluation of uncertainty and error in the spatial domain.

2.3.2 The risk in geological applications

B´ardossy 2001 has cited the main application of uncertainty in geology by risk term. He discusses about risk term and put mineral exploration as a risk in geology environment. Risk is a common term in science, economy and industry that is a complex and difficult concept. There is not still agreement how risk should be defined. According to the definition of the society of risk analysis:

Risk is the potential for the realization of unwanted consequences of a decision or an action. Risk analysis is the process of quantification of the probabilities and expected consequences of risks. Note that decision analysis, a joint application of procedures for choosing optimal decisions in the face of uncertainty, is a subject very close to the risk analysis, only more general than the latter one. B´ardossy 2001 believes the rich experiences of decision analysis should be applied to the analysis of risks in geology as well.

The main goal of risk analysis is to predict-as accurately as possible - the likelihood of the unwanted or accidental events and to clarify the uncertainties that impede the producing of reliable predictions. B´ardossy 2001 has cited risks in two groups. The first group is related to natural geological processes, such as earthquakes, volcanic activities, landslides, asteroid impacts etc. They are often called natural hazards. These risks exist in many regions on the earth without recognition of them and without trying to define their amount and possible consequences. In this context, risk identification is a deliberate procedure with the aim to review and if possible to anticipate the consequence of these natural hazards.

According to B´ardossy 2001investigations, other risks are related to human geological activities, e.g. mineral exploration, mining projects, landslides induced by construction activities, ground water contamination etc.

In the recent years a growing demand appeared for the perfection of the risk analysis methods, as it became clear that risk quantification cannot be achieved by the traditional statistical approaches only (T.Nilsen 2003, T.Aven 1998). Today, it is unrealistic to be able to determine the exact risk of a given decision or action. The different sources of uncertainties cannot be clarified entirely and forever those remain as certain proportion of risk that cannot predict (B´ardossy 2001).

2.3.3 Uncertainty in mineral exploration and objects

Mathematical methods are increasing applied in geology and there are mathematical treatments that help for decreasing uncertainties. As mentioned before, the main purpose is applying and verifying of Dempster-Shafer theory (DST) and some supplemental relevant theory for evaluation of uncertainty in geospatial environments, in this case geospatial data has been used for define of Au and Cu mineral prospect area.

Uncertainties appear first on the level of the input data and propagate along the evaluation process then in the final data can contain less or more uncertainties. Conventional, there are two steps in every geospatial case studies first evaluation of uncertainty in input data layers from multiple sources and second applying of that data layers for next processing for different purposes which this second has capability to do that. There are some relevant theories to DST; these theories have been presented as Dempster-Shafer Theory supplements. Till now, these theories have not been used for geospatial data. The thesis focuses on the verifying of the theories and their capabilities in GIS context and finally compares the results.

DST presents traditional probabilistic theory as a mathematical solution of uncertainty. The significant ability of this theory is that it allows the allocation of a probability mass to sets or intervals. DST doesn't need an assumption regarding the probability of the individual constituents of the set or intervals. This is a potentially valuable tool for evaluation of geospatial applications; when it is not possible to obtain a precise measurement by experiments, or when knowledge is obtained from low precise data. In this theory, combination of evidences and modeling of conflicts between them are possible while evidences come from different sources. There are supplemental combination rules for DST structures that has been applied in this research. That contains Yager's modified, Inagaki's unified combination rule, Zhang's center combination rule, Dubois and prade's disjunctive consensus rule and Mixing or Averaging rule.

The reason for applying Dempster-Shafer theory and their relevant theories for this thesis and mineral exploration can be characterized by the following concepts:

1. The first reason relates to the nature of the existing geospatial evidences. There are varieties of accurate and low accurate evidences from different sources and in the consequent there are different reliabilities to the evidences. The Belief function of the Dempster-Shafer theory can effectively solve the problem of the evidences with different reliability.The capability of combining rules of the Dempster-Shafer theory combine different types of evidences that obtained from multiple sources.
2. The relation of Dempster-Shafer theory to traditional probability theory and set theory.
3. The relatively high degree of theoretical development among the nontraditional theories for characterizing uncertainty that can be used to improve DST.
4. There are a few numbers of case studies that apply this theory for evaluation of geospatial uncertainties.

2.4 Type of evidence in GIS context

Evidences in GIS context contain spatial data like polygons, lines and points with certain location in certain geographic coordinate system. With respect to purposes, these data are extracted from raw geospatial information like RS images, geological maps, geochemical maps and etc. as digital data. For mineral exploration also all the geospatial information is applied those after weighting by different methods to be compiled also by various methods depend on type and precision of data.

In DST, there are two critical and related issues, concerning the combination of evidence that obtained from multiple sources. One is the type of evidence involved and the other is how to handle conflicting evidence. Kari 2002 considers four types of evidence from multiple sensors that impact the choice of how information is to be combined: consonant evidence, consistent evidence, arbitrary evidence, and disjoint evidence in geospatial environment can consider the multiple sensors like geospatial multiple data layers that come from different sources.

Consonant evidence can be represented as a nested structure of subsets where the elements of the smallest set are included in the next larger set those all of elements are included in the next larger set and so on. This can correspond to the situation where information is obtained over time that increasingly narrows or refines the size of the evidentiary set. Take a simple example from target identification. Suppose there are five sensors with varying degrees of resolution: sensor 1; sensor 2; sensor 3; sensor 4; sensor 5.

Each of these possible configurations of evidence from multiple sources has different implications on the level of conflict associated with the situation. Clearly in the case of disjoint evidence, all of the sources supply conflicting evidence. With arbitrary evidence, there is some agreement between some sources but there is no consensus among sources on any one element. Consistent evidence implies an agreement on at least one evidential set or element (figure 2-1) Consonant evidence represents the situation where each set is supported by the next larger set and implies an agreement on the smallest evidential set. However, there is a conflict between the additional evidence that the larger set represents in relation to the smaller set. Traditional probability theory cannot handle consonant, consistent, or arbitrary evidence without resorting to further assumptions of the probability distributions within a set. Also, probability theory can not express the level of conflict between these evidential sets. Dempster-Shafer theory is a framework that can handle these various evidentiary types by combining a notion of probability with the traditional conception of sets. In addition, in Dempster Shafer theory, there are many ways which conflict can be incorporated when combining multiple sources of information.

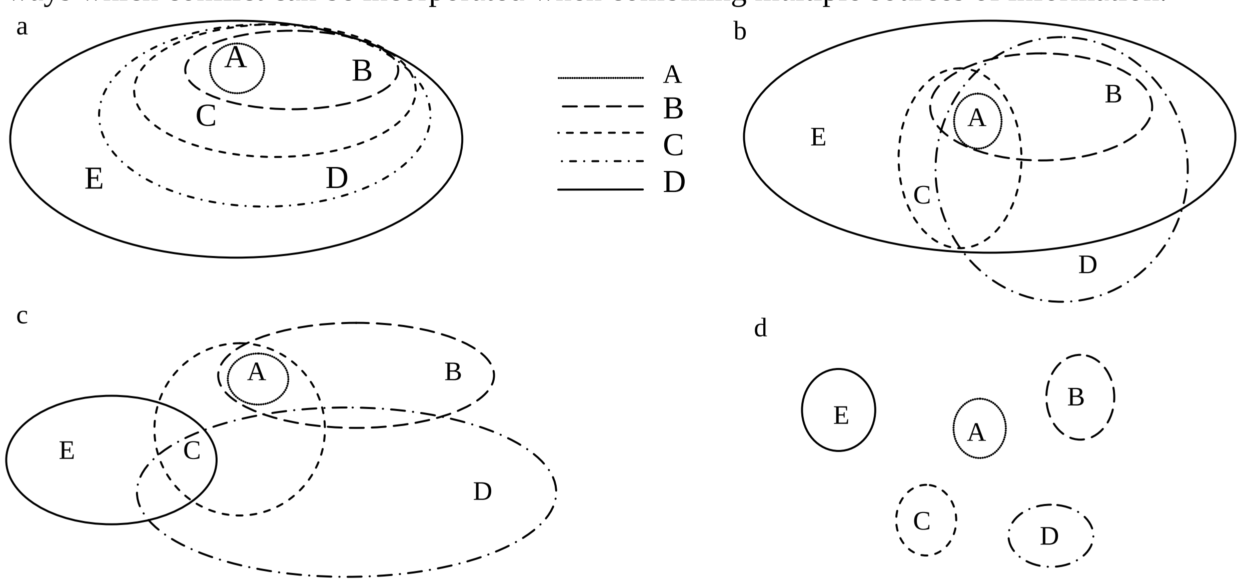

Figure 2-1: Represent in a- consonant evidence, b- consistent evidence, c- arbitrary evidence, d- disjoint evidence (Sentz, K. 2002).

Figure 2-1-a shows consonant evidence obtained from multiple sources, Sensor 1 detects a target in vicinity A. Sensor 2 detects two targets; one in vicinity A and one in vicinity B. Sensor 3 detects three targets; one in vicinity A, one in vicinity B, one in vicinity C. Sensor 4 detects four targets: one in vicinity A, one in vicinity B, one in vicinity C, one in vicinity D. Sensor 5 detects five targets: one in vicinity A, one in vicinity B, one in vicinity C, one in vicinity, one in vicinity E.

Consistent evidence (Figure 2-1-b) obtained from multiple sensors; consistent evidence means that there is at least one element that is common to all subsets. From our target identification, this could look like; Sensor 1 detects a target in vicinity A. Sensor 2 detects two targets; one in vicinity A and one in vicinity B. Sensor 3 detects two targets; one in vicinity A, one in vicinity C. Sensor 4 detects three targets; one in vicinity A, one in vicinity B, one in vicinity D. Sensor 5 detects four targets; one in vicinity A, one in vicinity B, one in vicinity C, one in vicinity E.

Arbitrary evidence (Figure 2-1-c) obtained from multiple sensors; arbitrary evidence corresponds to the situation where there is no element common to, all subsets, though some subsets may have elements in common. One possible configuration in our target identification example; Sensor 1 detects a target in vicinity A, sensor 2 detects two targets; one in vicinity A and one in vicinity B, sensor 3 detects two targets: one in vicinity A, one in vicinity C, sensor 4 detects two targets; one in vicinity C, one in vicinity D and sensor 5 detects two targets: one in vicinity C, one in vicinity E.

Disjoint evidence (Figure 2-1-d) obtained from multiple sensors disjoint evidence implies that any two subsets have no elements in common with any other subset. Sensor 1 detects a target in vicinity A, sensor 2 detects a target in vicinity B, sensor 3 detects a target in vicinity C, sensor 4 detects a target in vicinity D and sensor 5 detects a target in vicinity E.

In the geospatial evidence, every four states are possible but the arbitrary evidences are more common.

2.5 Dempster-Shafer theory

Dempster-Shafer Theory is a mathematical theory of evidence and usually has been abbreviated by DST or DS theory. The major work on the subject is related to Shafer investigations 1976 and is an expansion of Dempster investigations 1967. Dempster-Shafer theory can be interpreted as a generalization of probability theory where probabilities are assigned to sets as opposed to mutually exclusive singletons. There are three important functions in Dempster-Shafer theory: the basic probability assignment or mass function (bpa or m), the Belief function (Bel), and the Plausibility function (Pl).

In traditional probability theory, evidence is associated with only one possible event. In DST, evidence can be associated with multiple possible events, e.g., sets of events. As a result, evidence in DST can be meaningful at a higher level of abstraction without having to resort to assumptions about the events within the evidential set. Where the evidence is sufficient enough to permit the assignment of probabilities to single events, the Dempster-Shafer model collapses to the traditional probabilistic formulation. One of the most important features of Dempster-Shafer theory is that the model is designed to cope with varying levels of precision regarding the information and no further assumptions are needed to represent the information. It also allows for the direct representation of uncertainty of system responses where low accurate input data can be characterized by a set or an interval and the resulting output is a set or an interval. The following expressions show traditional probability theory expressions. p (A) shows the probability P of some event A.

$0 \le p(A) \le 1 \qquad \forall A \in F$ Where F is event space and A is any event in F.

$p(\varnothing)=0$ (2-1)

$p(A) = 1- p(\overline{A})$ (2-2)

Figure 2-2 illustrates probability position in comparison with DST, according to Kolmogorov axioms. In figure 2-2, the probability P of some event A to be denoted by p (A). Figure 2-2a shows traditional probability. Figure 2-2-b and c illustrate DST: the Belief function the Plausibility function and uncertainty between of them.

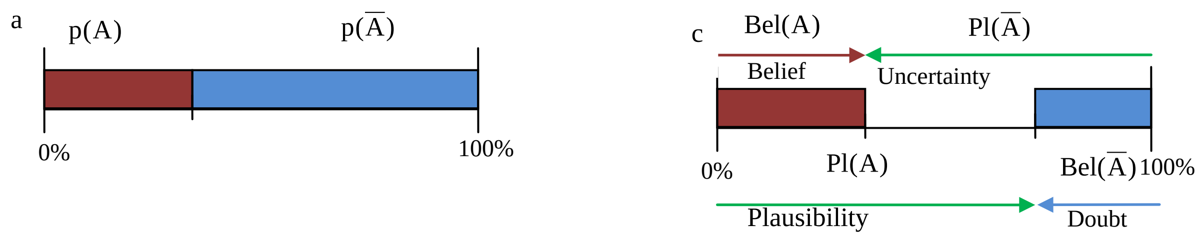

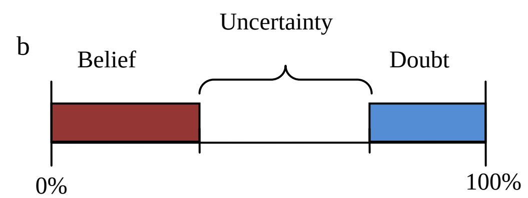

Figure 2-2: represent in a classical probability theory and in b and c position of belief, plausibility, uncertainty and doubt (Extracted from http://www2.cs.uni-paderborn.de/ cs/ ag-klbue /de/courses/ss04/confdiag04/diagnosis-stat2-ss04-slides.ps.nup.pdf).

2.5.1 The basic probability assignment (bpa) or Mass function

The basic probability assignment (bpa) is a primitive of evidence theory and some literatures use mass function term. In general speaking, the term “basic probability assignment” does not refer to probability in the classical sense. In expressions, the bpa to be represented by m and defines a mapping of the power set to the interval between 0 and 1(expression 2-3). With consider to expression 2-4 and 2-5, where the bpa of the null set is 0 and summation of the bpa for all the subsets of the power set is 1. The value of the bpa for a given set A (represented as m (A)), expresses the proportion of all relevant and available evidence that supports the claim that a particular element of X (the universal set) belongs to the set A but to no particular subset of A (Klir, 1998). The value of m (A) pertains only to the set A and makes no additional claims about any subsets of A. Any further evidence on the subsets of A would be represented by another bpa, in other words B $\subset$ A, m (B) would the bpa for the subset B.
Formally, descriptions for m can be represented by the following three expressions:

$$m : \mathrm{P(X)} \rightarrow [0,1] \qquad (2\text{-}3)$$

$$\mathrm{m}\ (\varnothing) = 0 \qquad (2\text{-}4)$$

$$\sum_{\mathrm{A} \in \mathrm{P(X)}} \mathrm{m(A)} = 1 \qquad (2\text{-}5)$$

Where P (X) represents the power set of X, $\varnothing$ is the null set, and A is a set in the power set (A$\in$ P(X)) (Klir, 1998).
Some investigators have found that suitable to interpret the basic probability assignment as a classical probability, such as Chokr & Kreinovich, 1994. The framework of Dempster-Shafer theory can support this interpretation. The theoretical implications of this interpretation are well developed in (Kramosil, 2001). This is a very important and appropriate interpretation of Dempster-Shafer theory but it does not demonstrate the full scope of the representational power of the basic probability assignment. With respect to the bpa’s inherent nature, the bpa cannot be equated with a classical probability in general.

2.5.2 Belief and Plausibility functions

From the basic probability assignment, the upper and lower bounds of an interval can be defined. This interval contains the accurate probability of a set of interest (in the classical sense) and is bounded by two non-additive continuous measures called Belief and Plausibility.

The lower bound Belief for a set A is defined as the sum of all the basic probability assignments of the proper subsets (B) of the set of interest (A) ($B \subseteq A$). The upper bound, Plausibility, is the sum of all the basic probability assignments of the sets (B) that intersect the set of interest (A) ($B \cap A \neq \emptyset$). Formally, for all sets A that are elements of the power set ($A \in P(X)$), (Klir, 1998)

$$Bel(A) = \sum_{B|B \subseteq A} m(B) \tag{2-6}$$

$$Pl(A) = \sum_{B|B \cap A \neq \emptyset} m(B) \tag{2-7}$$

The two measures, Belief and Plausibility are non-additive. This can be interpreted as is not required for the sum of all the Belief measures to be 1 and similarly for the sum of the Plausibility measures.

It is possible to obtain the basic probability assignment from the Belief measure with the following inverse function:

$$\mathrm{m(A)} = \sum_{\mathrm{B}|\mathrm{B} \subseteq \mathrm{A}} (-1)^{|\mathrm{A-B}|} \mathrm{Bel(B)} \tag{2-8}$$

Where, |A-B| is the difference of the cardinality of the two sets.

In addition to deriving these measures from the basic probability assignment (m), these two measures can be derived from each other. For example, Plausibility can be derived from Belief in the following way:

$$\mathrm{Pl(A)} = 1 - \mathrm{Bel}(\overline{\mathrm{A}}) \tag{2-9}$$

$$\mathrm{Bel}(\overline{\mathrm{A}}) = \sum_{\mathrm{B}|\mathrm{B} \subseteq \mathrm{A}} \mathrm{m(B)} = \sum_{\mathrm{B}|\mathrm{B} \cap \mathrm{A} = \emptyset} \mathrm{m(B)} \tag{2-10}$$

Where $\overline{\mathrm{A}}$ is the classical complement of A.

This definition of Plausibility in terms of Belief comes from the fact that all basic assignments must sum to 1.

$$\mathrm{Bel(A)} = \mathrm{P(A)} = \mathrm{Pl(A)} \tag{2-11}$$

The probability is uniquely determined if Bel (A) = Pl (A). In this case, which corresponds to classical probability, all the probabilities, P (A) are uniquely determined for all subsets A of the universal set X (Yager, 1987). Otherwise, Bel (A) and Pl (A) may be viewed as lower and upper bounds on probabilities, respectively, where the actual probability is contained in the interval described by the bounds. Upper and lower probabilities derived by the other frameworks in generalized information theory cannot be directly interpreted as Belief and Plausibility functions. (Dubois & Prade, 1992)

Höhl ,1998 has clarified mass function with this instance:

$\Theta = \{A, B, C\}$,

$P(X) = \{\emptyset, \{A\}, \{B\}, \{C\}, \{A, B\}, \{A, C\}, \{B, C\}, \Theta\}$

Two examples of possible state for a mass function:

$m_1(\{C\}) = 0.6$, $m_1(\{A, B\}) = 0.3$, $m_1(\Theta) = 0.1$

$m_2(\{A\}) = 0.8$, $m_2(\Theta) = 0.2$

Table 2-1 shows Calculation of Bel, Pl and Pl-Bel interval range based on the follow mass functions m, m ({C}) = 0.23, m_1 ({A}) = 0.62, m_1 ({A, B}) = 0.11, m_1 (Θ) = 0.04
Figure 2-3 illustrates their theoretic connections.

Table 2-1 shows Calculation of Bel, Pl and Pl-Bel interval range

	Bel	Pl	Pl-Bel
Ø	0	0	0
{A}	0.62	0.62+ 0.11+ 0.04 = 0.77	0.15
{B}	0	0.11+ 0.04=0.15	0.15
{C}	0.23	0.23+ 0.04=0.27	0.04
{A,B}	0.62 + 0.11 = 0.73	0.62+ 0.11+0.04 = 0.77	0.04
{A,C}	0.62 + 0.23 = 0.85	0.62+ 0.11+0.23 + 0.04 = 1	0.15
{B,C}	0.23	0.11+ 0.23+0.04 = 0.38	0.15
Θ	0.62 + 0.23 + 0.11+ 0.04 = 1	0.62 + 0.11+ 0.23 + 0.04 = 1	0

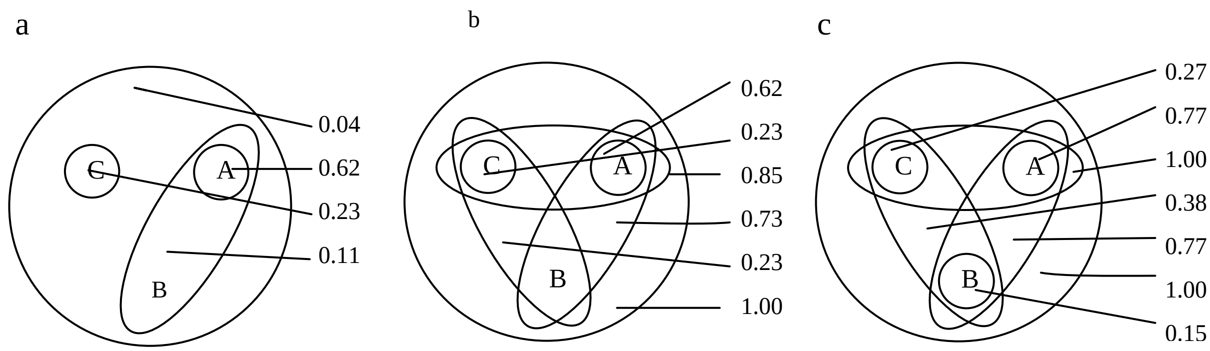

Figure 2-3: Illustrates theoretic connection between mass function (a), belief function (b) and plausibility function (c) (Höhl 1998).

In mineral exploration after evaluation of uncertainty with bpa, bel, pl functions that would be needed combining of outcome evidence for detection of anomalies area or prospect area. DST has an operation, Dempster's rule of combination, for the pooling of evidence from a variety of sources. This rule aggregates two independent bodies of evidence defined within the same frame of discernment into one body of evidence. In addition of DST rule for combination there are some other rules for combining of weighted evidences by DST rules.
Familiar examples of aggregation techniques include arithmetic averages, geometric averages, harmonic averages, maximum values, and minimum values (Ayyub, 2001). Combination rules are special types of aggregation methods for data obtained from multiple sources. These multiple sources provide different assessments for the same frame of discernment and Dempster-Shafer theory is based on the assumption that these sources are independent. The requirement for establishing the independence of sources is an important philosophical question. From a set theoretic standpoint, these rules can potentially occupy a continuum between conjunction (AND-based on set intersection) and disjunction (OR-based on set union) (Dubois and Prade, 1992). In the situation where all sources are considered reliable, a conjunctive operation is appropriate (A and B and C…). In the case where there is one reliable source among many, that can justify the use of a disjunctive combination operation (A or B or C…). However, many combination operations lie between these two extremes (A and B or C, A and C or B, etc.).
Dubois and Prade (Dubois, Prade, 1992) describe these three types of combinations as conjunctive pooling ($A \cap B$, if $A \cap B \neq \emptyset$), disjunctive pooling ($A \cup B$), and tradeoff (There are many ways a tradeoff between $A \cap B$ and $A \cup B$ can be achieved).

There are multiple operators available in each category of pooling by which a corpus of data can be combined. One means of comparison of combination rules is by comparing the algebraic properties they satisfy. With the tradeoff type of combination operations, less information is assumed than in a Bayesian approach and the precision of the result may suffer as a consequence. On the other hand, a precise answer obtained via the Bayesian approach does not express any uncertainty associated with it and may have hidden assumptions of additively or Principle of Insufficient Reason. (Dubois and Prade, 1992)

In keeping with this general notion of a continuum of combination operations, there are multiple possible ways in which evidence can be combined in Dempster-Shafer theory. The original combination rule of multiple basic probability assignments known as the Dempster rule is a generalization of Bayes' rule. (Dempster, 1967) This rule strongly emphasizes the agreement between multiple sources and ignores all the conflicting evidence through a normalization factor. This can be considered a strict AND-operation. The use of the Dempster rule has come under serious criticism when significant conflict in the information is encountered. (Zadeh, 1986; Yager, 1987)

Consequently, other researchers have developed modified Dempster rules that attempt to represent the degree of conflict in the final result. This issue of conflict and the allocation of the bpa mass associated with it is the critical distinction between all of the Dempster-type rules. To employ any of these combination rules in an application, it is essential to understand how conflict should be treated in that particular application context.

In addition to the Dempster rule of combination, that will discuss four modified Dempster rules: Yager's rule; Inagaki's unified combination rule; Zhang's center combination rule; and Dubois and Prade's disjunctive pooling rule. Three types of averages will be considered: discount and combine convolutive averaging and mixing. All of the combination rules will be considered relative to four algebraic properties: commutativity, $A * B = B * A$; idempotence, $A * A = A$; continuity, $A * B \approx A' * B$, where $A' \approx A$ (A' is very close to A); and associativity, $A * (B * C) = (A * B) * C$; where * denotes the combination operation. The motivation for these properties is discussed at length in (Ferson and Kreinovich, 2002).

Figure 2-4 illustrates the concept of using a DST approach to fuse multi-sensor identity data and has been derived from Hall 2004 concepts for mathematical combination of evidence from multi-sensor identity data. Hall, 2004 believe combination rules in DST are analogous to Bayesian approach. Individual sensors collect parametric data and assign evidence for the identity of an observed entity. This identity declaration is quantified via probability mass function. DST's rules of combination provide a prescription for combination these declarations, resulting in a joint evidential interval for each possible hypothesis. Here the support for a hypothesis is a measure of evidence that lends credence to a hypothesis being true, while the plausibility is a measure of the evidence that fails to refute plausibility.

The identity fusion process proceeds much like the Bayesian approach, instead of sensor inputs of probabilities of alternate hypotheses the DST sensors assign probability masses to multiple propositions. These probability masses are combined via combination rules, and a set of evidential intervals computed. Just as the Bayesian fusion did not prescribe the decision logic to choose a prevailing hypothesis, neither does the DST approach prescription the decision logic to

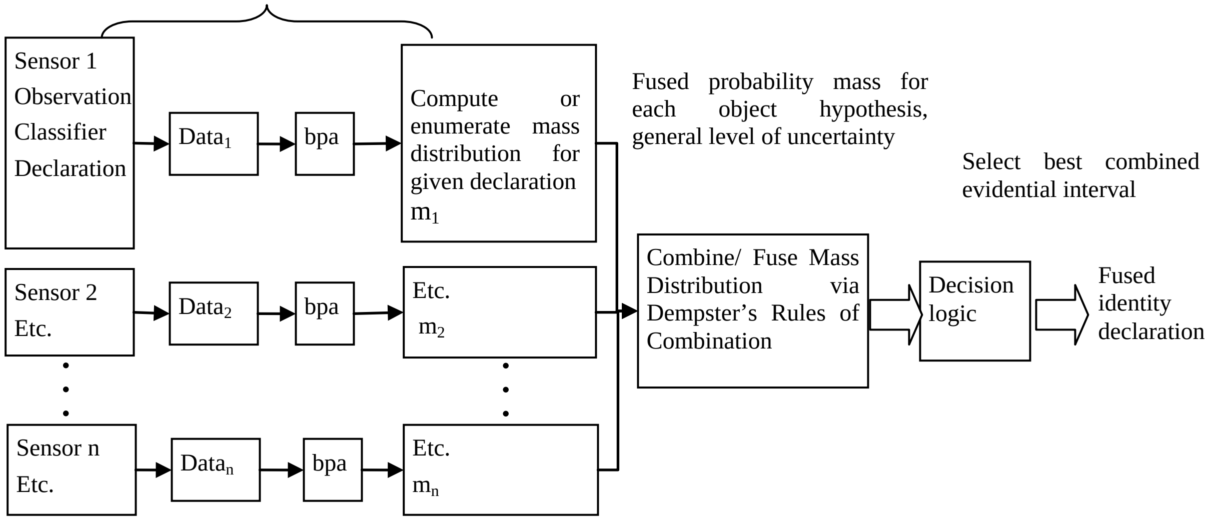

Figure 2-4: Transformation from observation space to mass distribution. (Modified from Hall, 2004)

choose a proposition as being true. The possibility still exists for so –called weak decisions, in which there is insufficient evidence to declare a hypothetical winner from among competing hypotheses.

A useful feature of the DST approach is the ability to establish a general level of uncertainty. Hence, unlike the Bayesian approach, the DST method provides a means to explicitly account for unknown possible causes of observational data.

Sentz, 2002 clarified the differences between the various combination rules for discrete and interval type data. The following provisions show the data given by discrete and the data given by intervals. For more apprehension about DST combination rules in every combination rules, that have been explained combination of the data given by discrete and interval types.

In data given by discrete values suppose two experts are consulted regarding a system failure. The failure could be caused by Component A, Component B or Component C. The first expert believes that the failure is due to Component A with a probability of 0.99 or Component B with a probability of 0.01 (denoted by m_1 (A) and m_1(B), respectively). The second expert believes that the failure is due to Component C with a probability of 0.99 or Component B with a probability of 0.01 (denoted by m_2(C) and m_2(B), respectively). The distributions can be represented by the following:

Expert 1:

m_1 (A) = 0.99 (failure due to Component A)

m_1 (B) = 0.01 (failure due to Component B)

Expert 2:

m_2 (B) = 0.01 (failure due to Component B)

m_2(C) = 0.99 (failure due to Component C)

In Data given by intervals Using the operations discussed above, now that will be consider the aggregation of three sources of information where the information is given as intervals. Interval-based data is common to problems involving parametric uncertainty for physical parameters like conductivity, diffusivity, or viscosity. Suppose there is an experiment that provides multiple intervals for an uncertain parameter from three sources A, B, and C that must be combined. The intervals are associated with sources A, B, and C that summarized in the Tables 2-2, 2-3 and 2-4, respectively. Figures 2-5, 2-6 and 2-7 present the intervals and the basic probability assignments graphically with a “generalized cumulative distribution function” (gcdf). This is the probabilistic concept of cumulative distribution function generalized to Dempster-Shafer structures where the focal elements (intervals) are represented on the x-axis and the cumulative basic probability assignments on the y-axis (Yager, 1986).

Table 2-2: The interval-based data for A and the basic probability assignments.

Interval	m1
[1,4]	0.5
[3,5]	0.5

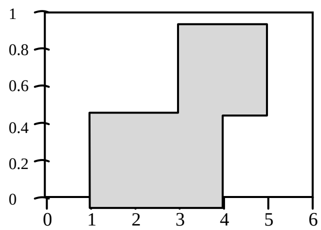

Figure 2-5: The gcdf of A.

Table 2-3: The interval-based data for B and the basic probability assignments.

Interval	*m*2
[1,4]	0.3333
[2,5]	0.3333
[3,6]	0.3333

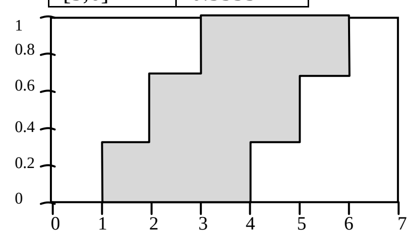

Figure 2-6: The gcdf of B.

Table 2-4: The interval-based data for C and the basic probability assignments.

Interval	*m*3
[6,10]	0.3333
[9,11]	0.3333
[12,14]	0.3333

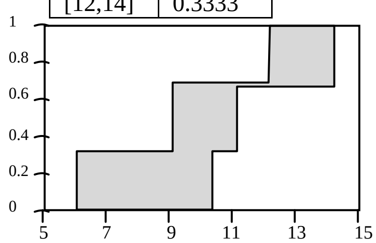

Figure 2-7 the gcdf of C.

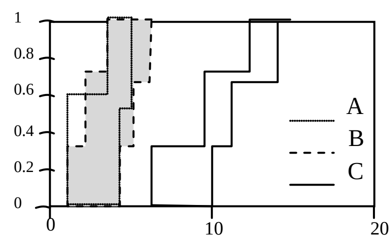

Figure 2-8: The gcdf’s of A, B, and C without any combination operation.

Without any combination operation, the gcdf’s of A, B, and C are represented in figure 2-8.
As is evident in figure 2-8 and Tables 2-2, 2-3 and 2-4, the data for A and B is consistent with each other. However the data for A and C are disjoint. First, that will be consider the combination of consistent data (A and B) and then the combination of the disjoint data (A and C) with the combination rules that discussed in next sections with every rules too.

2.5.3.1 The Dempster rule of combination

The Dempster rule of combination is critical to the original conception of Dempster-Shafer theory. The measures of Belief and Plausibility are derived from the combined basic assignments. Dempster’s rule combines multiple belief functions through their basic probability assignments (m). These belief functions are defined on the same frame of discernment, but are based on independent arguments or bodies of evidence. The issue of independence is a critical factor when combining evidence and is an important research subject in Dempster-Shafer theory. The Dempster rule of combination is purely a conjunctive operation (AND). The combination rule results in a belief function based on conjunctive pooled evidence (Shafer, 1986, p.132). Specifically, the combination (called the joint $m_{1,2}$) is calculated from the aggregation of two bpa’s m_1 and m_2 in the following manner:

$$m_1 \otimes m_2(A) = \frac{\sum_{B \cap C = A} m_1(B) m_2(C)}{1-K} \qquad \text{When } A \neq \emptyset \qquad (2\text{-}12)$$

$$m_1 \otimes m_2(\emptyset) = 0 \qquad (2\text{-}13)$$

$$\text{Where } K = \sum_{B \cap C = \emptyset} m_1(B) m_2(C) \qquad (2\text{-}14)$$

K represents basic probability mass associated with conflict. This is determined by summing the products of the bpa's of all sets where the intersection is null. This rule is commutative, associative, but not idempotent or continuous. The denominator in Dempster's rule, 1-K, is a normalization factor. This has the effect of completely ignoring conflict and attributing any probability mass associated with conflict to the null set (Yager, 1987). Consequently, this operation will yield counterintuitive results in the face of significant conflict in certain contexts. The problem with conflicting evidence and Dempster's rule was originally pointed out by Lotfi Zadeh 1984.

Zadeh 1984 provides a compelling example of erroneous results. Suppose that a patient is seen by two physicians regarding the patient's neurological symptoms. The first, Zadeh 1984 believes that the patient has either meningitis with a probability of 0.99 or a brain tumor, with a probability of 0.01. The second physician believes the patient actually suffers from a concussion with a probability of 0.99 but admits the possibility of a brain tumor with a probability of 0.01. Using the values to calculate the m (brain tumor) with Dempster's rule, that find that m(brain tumor) = Bel (brain tumor) = 1. Clearly, this rule of combination yields a result that implies complete support for a diagnosis that both physicians considered to be very unlikely. (Zadeh, 1984)

In light of this simple but dramatic example of the counterintuitive results of normalization factor in Dempster's rule, a number of methods and combination operations that have been developed to address this problem posed by strongly conflicting evidence. That will be discussing many of these alternatives in the following sections as well as the importance of conflict and context in the rule selection. That will be find that in addition to the level or degree of conflict is important in determining the propriety of using Dempster's rule, the relevance of conflict also plays a critical role.

Sentz, 2002 give calculation example for data given by discrete values calculation results for data given by interval values in the following provisions.

In discrete data the combination of the masses associated with the experts is summarized in Table 2-5. For them, expressions 2-12 to 2-14 have been used.

With regard to table 2-5, to calculate the combined basic probability assignment for a particular cell, simply multiply the masses from the associated column and row. Where the intersection is

Table 2-5: Dempster Combination of Expert 1 and Expert 2.

			Expert 1		
			A	B	C
			0.99	0.01	0
Exper 2	Failure Cause	*m*2			
	A	0	$m1(A)\ m2(A) = 0$	$m1(B)\ m2(A) = 0$	$m1(C)\ m2(A) = 0$
	B	0.01	$m1(A)\ m2(B) = 0.0099$	$m1(B)\ m2(B) = 0.0001$	$m1(C)\ m2(B) = 0$
	C	0.99	$m1(A)\ m2(C) = 0.9801$	$m1(B)\ m2(C) = 0.0099$	$m1(C)\ m2(C) = 0$

nonempty, the masses for a particular set from each source are multiplied, e.g., m_{12} (B) = (0.01) (0.01) = 0.0001. Where the intersection is empty, this represents conflicting evidence and should be calculated as well. For the empty intersection of the two sets A and C associate with Expert 1 and 2, respectively, there is a mass associated with it. m_1 (A) m_2(C) = (0.99) (0.99) =

(0.9801). Then sum the masses for all sets and the conflict. The only nonzero value is for the combination of B, m_{12} (B) = 0.0001. In this example there is only one intersection that yields B, but in a more complicated example it is possible to find more intersections to yield B. For K, there are three cells that contribute to conflict represented by empty intersections. Using expression 2-13, K = (0.99)(0.01) + (0.99)(0.01) + (0.99)(0.99) = 0.9999 Using expression 2-11, calculate the joint, m_1(B) m_2(B) = (.01)(.01) / (1-0.9999) = 1

Though there is highly conflicting evidence, the basic probability assignment for the failure of Component B is 1, which corresponds to a Bel (B) = 1. This is the result of normalizing the masses to exclude those associated with conflict. These consider the inconsistency when Dempster's rule is used in the circumstances of significant relevant conflict, which was pointed out by Zadeh, 1984.

For intervals-type data the calculation of Dempster's rule has been used expression 2-12, 2-13 and 2-14 and is summarized in Table 2-6.

Table 2-6: Combination of A and B with Dempster's Rule

			A			
			Interval	m	Interval	m
			[1, 4]	0.5	[3, 5]	0.5
B	Interval	m				
	[1, 4]	0.33333	[1, 4]	0.16667	[3, 4]	0.16667
	[2, 5]	0.333333	[2, 4]	0.16667	[3, 5]	0.16667
	[3, 6]	0.333333	[3, 4]	0.16667	[3, 5]	0.16667

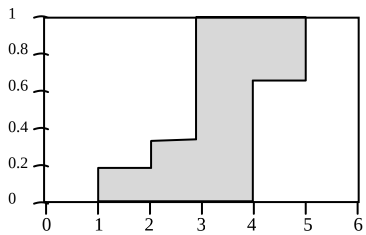

Figure 2-9: The gcdf of the combination of A and B using Dempster's rule.

Note that the intersection of two intervals is defined by the maximum of the two lower bounds and the minimum of the two upper bounds corresponding to an intersection. With regard to table 2-6, the bpa's for like intervals are summed, i.e. [1,4] has a value for m of 0.166667; [2,4] has an m value of 0.166667; [3,4] has a value of 0.33334; and [3,5] has an m value of 0.33334. The resulting structure of the combination of A and B using Dempster's rule is illustrated in figure 2-9.

The combination of A and C using Dempster's rule is not possible due to the normalization factor.

2.5.3.2 Discount + combine method

This method was initially discussed in (Shafer, 1976) and deals with conflict just in the manner that the name implies. Specifically, when an analyst is faced with conflicting evidence, he can discount the sources first, and then combine the resulting functions with Dempster's rule (or an alternative rule) using a discounting function. This discounting function must account for the absolute reliability of the sources. Absolute reliability implies that the analyst is qualified to make distinctions between the reliability of experts, sensors, or other sources of information and can express this distinction between sources mathematically. (Dubois and Prade, 1992) Shafer applies the discounting function to each specified Belief. Let $1-\alpha_i$ be the degree of reliability attributable to a particular belief function, A (Shafer calls this a degree of trust), where $0 \le \alpha_i$

≤1 and i is an index used to specify the particular discounting function associated with a particular belief measure. Bel $_{\alpha i}$ (A) then represents the discounted belief function defined by:

$$Bel^{\alpha\, i}(A) = (1-\alpha_i)Bel(A) \quad (2\text{-}15)$$

Shafer then averages all the belief functions associated with set A ($Bel^{\alpha I}{}_1(A)$, $Bel^{\alpha I}{}_2(A)$…. $Bel^{\alpha I}{}_n(A)$) to obtain an average of n Bel, denoted by Bel .

$$\overline{Bel}(A) = \frac{1}{n}(Bel^{\alpha}1(A) + ... + Bel^{\alpha}n(A)) \qquad (2\text{-}16)$$

For all subsets A of the universal set X.

Consequently, the discount and combine method uses an averaging function as the method of combination. This is to be used when all the belief functions to be combined are highly conflicting and the discounting rate is not too small. This can also be used to eliminate the influence of any strongly conflicting single belief function provided that the remaining belief functions do not conflict too much with each other and the discount rate is not too small or too large. Alternatively, for this case one could also eliminate the strongly conflicting belief altogether if that is reasonable. (Shafer, 1976)

2.5.3.3 Yager's modified Dempster's rule

The most prominent of the alternative combination rules is a class of unbiased operators developed by Ron Yager (Yager, 1987a). Yager points out that an important feature of combination rules is the ability to update an already combined structure when new information becomes available. This is frequently referred to as updating and the algebraic property that facilitates this is associativity. Dempster's rule is an example of an associative combination operation and the order of the information does not impact the resulting fused structure. (Yager, 1987b)

Yager points out that in many cases a non-associative operator is necessary for combination. A familiar example of this is the arithmetic average. The arithmetic average is not itself associative, i.e., one cannot update the information by averaging an average of a given body of data and a new data point to yield a meaningful result.

However, the arithmetic average can be updated by adding the new data point to the sum of the pre-existing data points and dividing by the total number of data points. This is the concept of a quasi-associative operator that Yager introduced in (Yager, 1987b). Quasi-associativity means that the operator can be broken down into associative suboperations.

Through the notion of quasi-associative operator, Yager develops a general framework to look at combination rules where associative operators are a proper subset.

To address the issue of conflict, Yager starts with an important distinction between the basic probability mass assignment (m) and what he refers to as the ground probability mass assignment (designated by q). The major differences between the basic probability assignment and the ground probability assignment are in the normalization factor and the mass attributed to the universal set. The combined ground probability assignment is defined in expression 2-16.

$$q(A) = \sum_{B \cap C = A} m_1(B)m_2(C) \qquad (2\text{-}17)$$

where A is the intersection of subsets B and C (both in the power set P (X)), and q(A) denotes the ground probability assignment associated with A. Note that there is no normalization factor. This rule is known as Yager's combination rule or sometimes the Modified Dempster's Rule.

Though the Yager rule of combination is not associative, the combined structure q(A) can be used to include any number of pieces of evidence. Assume m_1, m_2,…m_n are the basic probability assignments for n belief structures. Let F_i represent the set of focal elements associated with the i_{th} belief structure (m_i) which are subsets of the universal set X. A_i represents an element of the focal set. Then the combination of n basic probability assignment structures is defined by (Yager, 1987a):

$$q(A) = \sum_{\cap_{i=1}^{n} A_i = A} m_1(A_1) m_2(A_2) \ldots m_n(A_n) \qquad (2\text{-}18)$$

Through the quasi-associativity that Yager describes, the combined structure q(A) can be updated based on new evidence. This is performed by combining the ground probability assignment associated with the new evidence and the ground probability assignment of the already existing combination through the above formulas (expression 2-16) and then converting the ground probability assignments to basic probability assignments described below. (Expressions 2-19 to 2- 21)

As previously mentioned, one obvious distinction between combination with the basic and the ground probability assignment functions is the absence of the normalization factor (1-K). In Yager's formulation, he circumvents normalization by allowing the ground probability mass assignment of the null set to be greater than 0, i.e.

$$q(\emptyset) \geq 0 \qquad (2\text{-}19)$$

$q(\emptyset)$ is calculated in exactly in the same manner as Dempster's K (conflict) in Expression 2-13. Then Yager adds the value of the conflict represented by $q(\emptyset)$ to the ground probability assignment of the universal set, q(X), to yield the conversion of the ground probabilities to the basic probability assignment of the universal set $m^Y(X)$:

$$m^Y(X) = q(X) + q(\emptyset) \qquad (2\text{-}20)$$

Consequently, instead of normalizing out the conflict, as that find in the case of the Dempster rule, Yager at the end attributes conflict to the universal set X through the conversion of the ground probability assignment to the basic probability assignments. The interpretation of the mass of the universal set (X) is the degree of ignorance.

Dempster's rule has the effect of changing the evidence through the normalization and the allocation of conflicting mass to the null set. Yager's rule can be considered as an epistemologically honest interpretation of the evidence as it does not change the evidence by normalizing out the conflict. In Yager's rule, the mass associated with conflict is attributed to the universal set and thus enlarges this degree of ignorance. (Yager, 1987a)

Upon inspection of the two combination formulas it is clear that Yager's rule of combination yields the same result as Dempster's rule when conflict is equal to zero, (K = 0 or $q(\emptyset) = 0$). (Yager, 1987a) The basic algebraic properties that this rule satisfies are commutativity and quasi-associativity, but not idempotence or continuity.

The ground probability assignment functions (q) for the null set, $\emptyset$, and an arbitrary set A, are converted to the basic probability assignment function associated with this Yager's rule (m^Y) by (Yager 1987a):

$$m^Y(\emptyset) = 0 \qquad (2\text{-}21)$$

$$m^Y(A) = q(A) \qquad (2\text{-}22)$$

The basic probability assignments associated with Yager's rule (m^Y) are not the same as with Dempster's rule (m). Yager provides the relation between the ground assignments and Dempster's rule (Yager 1987a):

$$m(\text{Ø}) = 0 \qquad (2\text{-}23)$$

$$m(X) = \frac{q(x)}{1 - q(\text{Ø})} \qquad (2\text{-}24)$$

$$m(A) = \frac{q(A)}{1 - q(\text{Ø})} \qquad \text{For } A \neq \text{Ø}, X \qquad (2\text{-}25)$$

To summarize, these are the important attributes of Yager's rule of combination:
1. The introduction of the general notion of quasi-associative operators and the expansion of the theoretical basis for the combination and updating of evidence where the associative operators are a proper subset of the quasi-associative operators.
2. The introduction of the ground probability assignment functions (q) and their relation to the basic probability assignments (m_Y) associated with Yager's rule and the basic probability assignments (m) associated with Dempster's rule.
3. The rule does not filter or change the evidence through normalization.
4. The allocation of conflict to the universal set (X) instead of to the null set ($\emptyset$).
Thus mass associated with conflict is interpreted as the degree of ignorance.
Sentz, 2002 give calculation example for data given by discrete values calculation results for data given by interval values in the following provisions.
In data given by district value Yager's rule will yield the almost the same matrix as with Dempster's rule. However, there are some important exceptions in the nomenclature and eventually the allocation of conflict: 1. Instead of basic probability assignments (m), Yager calls these ground probability assignments (q) and 2. Instead of using K to represent the conflict, Yager uses the q(Ø) which is calculated in the exact same way as K. (expression 2-14)
Using expression 2-17, the combination is calculated: $q_{12}(B) = m_{12}(B) = (0.01)(0.01) = 0.0001$
Here the combination is not normalized by the factor (1-K). When Yager converts the ground probability assignments (q) to the basic probability assignments (m), the mass for a particular joint remains the same and the mass associated with conflict is attributed to the universal set X that represents the degree of ignorance (or lack of agreement). So in this case the m(X) is 0.9999. To convert the basic probability assignment to the lower bound Bel, the Bel(B) is equal to the m(B) (Bel (B) = .0001), as this is the only set that satisfies the criteria for Belief ($B \subseteq B$). This approach results in a significant reduction of the value for Belief and a large expansion of Plausibility. Note that the value of Belief is substantially smaller than either the experts' estimates would yield individually in such a case, this may be counterintuitive.
As the evidence from A and B is consistent, the calculations for Yager's rule are same as in Table 2-6. The resulting structure of the combination of A and B using Yager's rule (figure 2-11) is also the same as with Dempster's rule.
In interval-type data, for evidence from A and B the yager's rule calculations are same as table 2-6. The resulting structure of the combination of A and B is also the same as figure 2-9.
For evidence from A and C, it is different of the Dempster's case; Yager's rule can be calculated for the combination of A and C. However, since the evidence is entirely conflicting, all of the basic probability mass is attributed to the universal set. In the continuous domain this corresponds to the real line, figure 2-10 shows the structure for that. As mentioned earlier, the

mass allocated to the universal set is interpreted as the degree of ignorance or the degree of lack of agreement among sources.

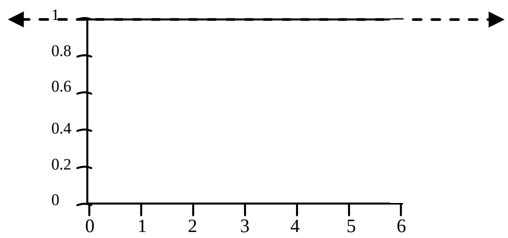

Figure 2-10: The gcdf of the combination of A and B using Yager's rule.

2.5.3.4 Inagaki's unified combination rule

This combination rule was introduced by Toshiyuki Inagaki. (Inagaki, 1991) Inagaki takes advantage of the ground probability assignment function (q) that Yager defined in (Yager, 1987a) to define a continuous parameterized class of combination operations which subsumes both Dempster's rule and Yager's rule. Specifically, Inagaki argues that every combination rule can be expressed as:

$$m(C) = q(C)+f(C)\, q(\text{Ø}) \qquad \text{Where } C \neq (\text{Ø}) \qquad (2\text{-}26)$$

$$\sum_{C\subset X, C\neq \text{Ø}} f(C) = 1 \qquad (2\text{-}27)$$

$$f(C) \geq 0 \qquad (2\text{-}28)$$

From expression 2-26 the function, f, can be interpreted as a scaling function for q(∅), where the conflict (represented by the parameter k) is defined by:

$$k = \frac{f(C)}{q(C)} \quad \text{For any } C\neq X, \text{Ø} \qquad (2\text{-}29)$$

Inagaki restricts consideration to the class of combination rules that satisfy the following property:

$$\frac{m(C)}{m(D)} = \frac{q(C)}{q(D)} \qquad (2\text{-}30)$$

For any nonempty sets C and D which are distinct from X or ∅. By maintaining the ratio between m and q consistently, this expression implies that there is no "meta-knowledge" of the credibility or reliability of sources/experts. If an analyst applied a weighting factor to the evidence based on some extra knowledge about the credibility of the sources, in general, this would change the ratio and the equality would not hold. As a result of this restriction and its implication, Inagaki's rule applies only to the situations where there is no information regarding the credibility or reliability of the sources. (Inagaki, 1991)

From the general expression (expression 2-26) and the restriction (expression 2-26) and the definition of k (expression 2-29), Inagaki derives his unified combination rule denoted by m^U.

$$m_k^U(C) = [1 + kq(\text{Ø})]q(C), \quad \text{Where } C\neq X, \text{Ø} \qquad (2\text{-}31)$$

$$m_k^U(X) = [1 + kq(\text{Ø})]q(X) + [1 + kq(\text{Ø}) - k]q(\text{Ø}) \qquad (2\text{-}32)$$

$$0 \le k \le \frac{1}{1 - q(\varnothing) - q(X)} \qquad (2\text{-}33)$$

The parameter k is used for normalization. The determination of k is an important step in the implementation of this rule, however, a developed well-justified procedure for determining k is lacking in the literature reviewed here. Tanaka and Klir 1999 refer to the determination of k either through experimental data, simulation, or the expectations of an expert in the context of a specific application. In addition, they provide an example for the determination of k and the resulting affect on m for monitoring systems (Tanaka and Klir, 1999). In Inagaki 1991, Inagaki poses the optimization problem for the selection of k to be an open and critical research question. Despite this, Inagaki discusses the rules in the context of an application where he demonstrates the values of Belief and Plausibility as a function of k and the implications on the choice of a safety control policy.

The value of k directly affects the value of the combined basic probability assignments and will collapse to either Dempster's rule or Yager's rule under certain circumstances. When k = 0, the unified combination rule coincides with Yager's rule.

When $$k = \frac{1}{1 - q(\varnothing)}$$

The rule corresponds to Dempster's rule. The parameter k gives rise to an entire parametrized class of possible combination rules that interpolate or extrapolate Dempster's rule. (Inagaki, 1991) This is schematically represented in the figure 2-11 from (Inagaki 1991):

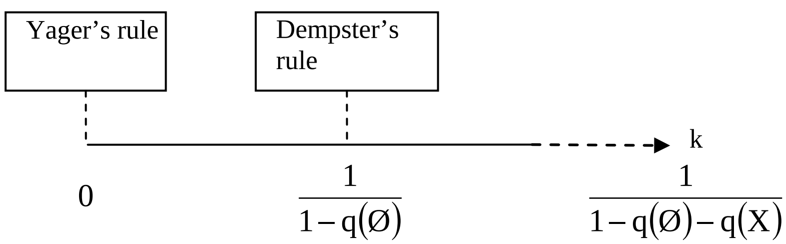

Figure 2-11: The Possible Values of *k* in Inagaki's Unified Combination Rule.

The only combination rule of this parametrized class that is associative is the one that corresponds to Dempster's rule. Every combination rule represented by the unified combination rule is commutative though not idempotent or continuous. Inagaki considers the effect of non-associativity in applications to be an open research question. (Inagaki, 1991)

As is pointed out by Tanaka and Klir (Tanaka and Klir 1999), the most extreme rule (referred to as "the extra rule" and denoted by the parameter k_{ext}) availed by this formulation is when k is equal to the upper bound:

$$m^{U}_{k_{ext}}(C) = \frac{1 - q(X)}{1 - q(X) - q(\varnothing)} q(C) \qquad \text{For } C \neq X, \qquad (2\text{-}34)$$

$$m^{U}_{k_{ext}}(X) = q(X) \qquad (2\text{-}35)$$

As can be seen in expression 2-34, the value of q(C) is scaled by the factor, $\frac{1-q(X)}{1-q(X)-q(\varnothing)}$ to yield the corresponding basic probability function $m^{U}_{k_{ext}}$. The interpretation of the extreme rule of Inagaki's class is that both conflict (represented by $q(\varnothing)$) and the degree of ignorance (represented by the probability mass associated with the universal set, q(X)) are used to scale the resulting combination. This acts as a filter for the evidence.

Inagaki studied the ordering relations of the three rules: Dempster's rule, Yager's rule, and this "extra rule" and the propriety of their application in fault-warning safety control policy. (Inagaki, 1991) Tanaka and Klir point out that the selection of the parameter k essentially determines how to cope with conflicting information. Yager's rule (k=0) assigns conflict to the universal set and does not change the evidence. Dempster's rule ($k=1/(1-q(\varnothing))$) tremendously filters the evidence by ignoring all conflict. Inagaki's extreme rule ($k=1/(1-q(\varnothing)-q(X))$) also filters the evidence by scaling both conflict and ignorance, but the degree of influence of the scaling is determined by the relative values of q(X) and $q(\varnothing)$. k has the effect of scaling the importance of conflict as it is represented in the resulting combination. The greater the value of k, the greater it will be the change to the evidence. As noted earlier, a well-justified procedure for the selection of k is as essential step toward implementing this rule in an application.

The important contributions of Inagaki's Unified rule of combination can be summarized as follows:

1. The use of Yager's ground functions to develop a parameterized class of combination rules that subsumes both Dempster's rule and Yager's rule.
2. Inagaki compares and orders three combination rules: Dempster's rule, Yager's rule, and the Inagaki extra rule, in terms of the value of m in the context of an application.

Sentz, 2002 give calculation example for data given by discrete values calculation results for data given by interval values in the following provisions.

In the data given by discrete value, again the matrix is calculated in the same manner as in case of the Dempster rule. Inagaki uses the ground probability functions similar to Yager. At the end, the value of $m_{1,2}(B)$ obtained by Inagaki's rule depends on the value of k which is now a parameter. Figure 2-12 demonstrates the behavior of the Inagaki combination as a function of the value of k for this problem.

When k = 0, Inagaki's combination will obtain the same result as Yager's ($m_{12}(B) = 0.0001$). When $k=\frac{1}{1-q(\varnothing)}=\frac{1}{1-0.9999}=10000$, Inagaki's rule corresponds to Dempster's rule ($m_{12}(B) = 1$). Because there is no mass associated with the universal set q(X), in this case, Inagaki's extra rule is the like Dempster's rule. Although, the calculation can be extended beyond Dempster's rule, any value for the combination greater than 1 does not make sense because sums of all masses must be equal to 1. Corresponding to the increasing value of k, is the increase in the filtering of the evidence.

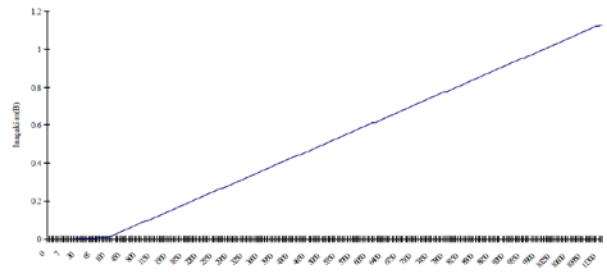

Figure 2-12: The value of m12 (B) as a function of k in Inagaki's rule.

In data given by interval value type, with k=0, that obtain the same calculations as Yager's rule and Dempster's rule figure 2-13 indicate the intervals of A and B when k=0. In figure 2-14 as expected, that find the same calculations for the combination of A and B where k=1.

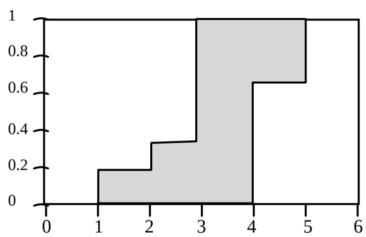

Figure 2-13: The Inagaki combination of A and B for k=0.

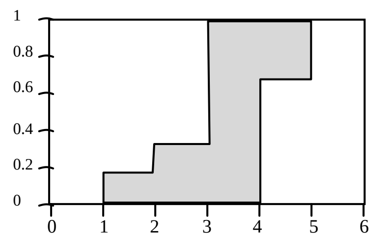

Figure 2-14: The Inagaki combination of A and B where k = 1.

2.5.3.5 Dubois and Prade's disjunctive consensus rule

Dubois and Prade take a set-theoretic view of a body of evidence to form their disjunctive consensus rule in (Dubois, Prade, 1986; Dubois, Prade, 1992). They define the union of the basic probability assignments $m_1 \cup m_2$ (denoted by $m_\cup(C)$) by extending the set-theoretic union:

$$m \cup (C) = \sum_{A \cup B = C} m_1(A) m_2(B) \qquad (2\text{-}36)$$

For all A of the power set X. The union does not generate any conflict and does not reject any of the information asserted by the sources. As such, no normalization procedure is required. The drawback of this method is that it may yield a more imprecise result than desirable.

The union can be more easily performed via the belief measure: Let $Bel_1 \cup Bel_2$ be the belief measure associated with $m_1 \cup m_2$. Then for every subset A of the universal set X,

$$Bel_1(A) \cup Bel_2(A) = Bel_1(A)\, Bel_2(A) \qquad (2\text{-}37)$$

The disjunctive pooling operation is commutative, associative, but not idempotent.

Sentz, 2002 give calculation example for data given by discrete values calculation results for data given by interval values in the following provisions.

In data given by discrete value example, after unions of multiple sets based on the calculations from table 2-5, the results come in table 2-9.

In data given by interval value type, the upper and lower bounds for the disjunctive consensus are defined by the minimum of the lower bounds and the maximum of the upper bounds. The calculations for the joint of the basic probability assignments are the product of the marginal. The intervals and their respective probability assignments are listed in table 2-10. The only like interval is (1,5) where the summed m is equal to 0.33334.

Table 2-9: Unions obtained by disjunctive consensus pooling.

Union	$m \cup$	Linguistic Interpretation
$A \cup A$	0	Failure of Component A
$A \cup B$	0.0099	Failure of Component A or B
$A \cup C$	0.9801	Failure of Component A or C
$B \cup B$	0.0001	Failure of Component B
$B \cup C$	0.0099	Failure of Component B or C
$C \cup C$	0	Failure of Component C
$A \cup B \cup C$	1	Failure of Component A or B or C

Table 2-10: the Disjunctive Consensus Pooling of A and B.

			A			
			Interval	m	Interval	m
			[1, 4]	0.5	[3, 5]	0.5
B	Interval	m				
	[1, 4]	0.333333	[1, 4]	0.16666667	[1, 5]	0.16666667
	[2, 5]	0.333333	[1, 5]	0.16666667	[2, 5]	0.16666667
	[3, 6]	0.333333	[1, 6]	0.16666667	[3, 6]	0.16666667

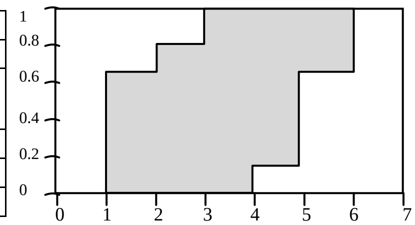

Figure 2-15: the Disjunctive Consensus Pooling of A and B.

It is also possible to calculate the combination of evidence from A and C using disjunctive consensus pooling. Table 2-11 shows calculation results for evidence from A and C and figure 1-16 illustrate structural results for these calculations.

Table 2-11: Calculations for the Disjunctive Consensus Pooling of A and C

			A			
			Interval	m	Interval	m
			[1, 4]	0.5	[3, 5]	0.5
C	Interval	m				
	[6, 10]	0.333333	[1, 10]	0.16666667	[3, 10]	0.16666667
	[9, 11]	0.333333	[1, 11]	0.16666667	[3, 11]	0.16666667
	[12, 14]	0.333333	[1, 14]	0.16666667	[3, 14]	0.16666667

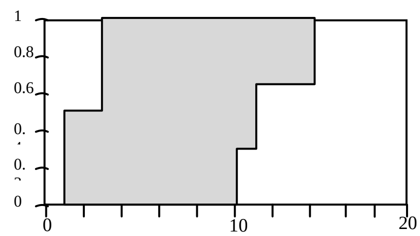

Figure 2-16: the gcdf for the Disjunctive Consensus Pooling of A and C

For more information can see Ferson and Kreinovich, 2002, they compare the disjunctive consensus and the envelope operation.

2.5.3.6 Mixing or average

Mixing (or p-averaging or averaging) is a generalization of averaging for probability distributions. (Ferson and Kreinovich, 2002) This describes the frequency of different values within an interval of possible values in the continuous case or in the discrete case, the possible simple events. The formula for the "mixing" combination rule is just

$$m_{1\ldots n}(A) = \frac{1}{n}\sum_{i=1}^{n} w_i m_i(A) \qquad (2\text{-}38)$$

Where m_i's are the bpa's for the belief structures being aggregated and the w_i's are weights assigned according to the reliability of the sources. This is very similar to the discount and combine rule proposed by Shafer in that they are both averaging operations, but they differ in which structures are being pooled. In the case of mixing, it is the basic probability assignment, m; in the case of discount and combine, it is Bel.

Mixing generalizes the averaging operation that is usually used for probability distributions. In particular, suppose that the input Dempster-Shafer structures are probability distributions, that is, suppose that both structures consist of an element in which each basic probability mass is associated with a single point. If one applies the mixing operation to these inputs, the result will be a Dempster-Shafer structure all of whose masses are also at single points. These masses and points are such that the Dempster-Shafer structure is equivalent to the probability distribution that would have been obtained by mixing the probability distributions, that is, by simply averaging the probabilities for every point. None of the other Dempster-Shafer aggregation rules would give this same answer. Insofar as averaging of probability distributions via mixing is regarded as a natural method of aggregating probability distributions, it might also be considered as a reasonable approach to employ with Dempster-Shafer structures, and that is why it is considered here. Like mixing of probability distributions, mixing in Dempster-Shafer theory is idempotent and commutative. It's not associative but it is quasi-associative.

Sentz, 2002 give calculation example for data given by discrete values calculation results for data given by interval values in the following provisions.

In data given by discrete value, for mixing in this case corresponds to the sum of $m_1(B)(1/2)$ and $m_2(B)(1/2)$. Results can be seen in following calculations after using expression 2-38:

$m_{12}(A) = (1/2)\ (0.99) = 0.445$

$m_{12}(B) = (1/2)\ (0.01) + (1/2)\ (0.01) = 0.01$

$m_{12}(C) = (1/2)\ (0.99) = 0.445$

In data given by interval value, the values for mixing (without weights) are listed in table 2-7, that use expression 2-38. The masses for the like final intervals are summed: (1, 4) has an m value of 0.41667; the remaining distributions remain the same. The resulting structure of the combination of A and B using mixing can be observed in the figure 2-17.

Table 2-7: the mixture of A and B.

Sources	Initial Interval	m	Final Interval	m
Source 1	[1, 4]	0.5	[1, 4]	0.25
	[3, 5]	0.5	[3, 5]	0.25
Source 2	[1, 4]	0.333333	[1, 4]	0.166667
	[2, 5]	0.333333	[2, 5]	0.166667
	[3, 6]	0.333333	[3, 6]	0.166667

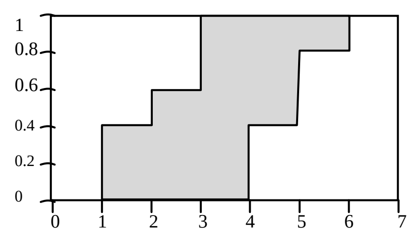

Figure 2-17: the mixture of A and B.

The combination of A and C is possible using mixing. These calculations are summarized in Table 2-8. The resulting structure of the combination of A and C using mixing have been illustrated in figure 2-18.

Table 2-8: the mixture of A and C.

Sources	Initial Interval	m	Final Interval	m
Source 1	[1, 4]	0.5	[1, 4]	0.25
	[3, 5]	0.5	[3, 5]	0.25
Source 2	[6, 10]	0.333333	[6, 10]	0.166667
	[9, 11]	0.333333	[9, 11]	0.166667
	[12, 14]	0.333333	[12, 14]	0.166667

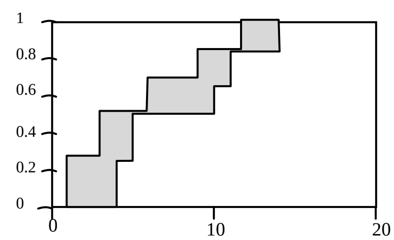

Figure 2-18: the mixture of A and C.

2.5.3.7 Convolutive X-Average

Convolutive x-averaging (or c-averaging) is a generalization of the average for scalar numbers. Ferson and Kreinovich, 2002 give the following expressions Convolutive X-Average calculation:

$$m_{12}(A) = \sum_{\frac{B+C}{2}=A} m_1(B)m_2(C) \qquad (2\text{- }39)$$

Like the mixing average, this can be formulated to include any number of bpa's, n, in the following expression:

$$m_{1....n}(A) \sum_{\frac{A1+....An}{n}=A} \prod_{i=1}^{n} m_i(A) \qquad (2\text{-}40)$$

Suppose that the input Dempster-Shafer structures are scalar numbers, that is, suppose that both structures consist of a single element where all mass is at a single point. If one applies the convolutive average operation to these inputs, the result will be a Dempster-Shafer structure all of whose mass is at a single point, the same point one gets by simply averaging the two scalar numbers. None of the other Dempster-Shafer aggregation rules would give this answer. Insofar as "averaging" is regarded as a natural method of aggregating disparate pieces of information, it might also be considered as a reasonable approach to employ with Dempster-Shafer structures, and that is why it is considered here.

Like averaging of scalar numbers, the convolutive average is commutative. Also like scalar averaging, the convolutive average is not associative, although it is quasi-associative. Unlike scalar averaging, however, it is not idempotent.

Sentz, 2002 gives calculation results for data given by interval values in the following provisions.

Using expression 2-40, that calculate the convolutive x-average for A and B found in Table 2-12. The resulting structure of the combination of A and B using convolutive x-averaging is depicted in figure 2-19.

Figure 2-20 presents the difference between the Dempster rule (solid line) and convolutive x-averaging (dashed line) for the combination of evidence from A and B.

Table 2-12: the Combination of A and B using Convolutive x-Averaging.

			A			
			Interval	m	Interval	m
			[1, 4]	0.5	[3, 5]	0.5
B	Interval	m				
	[1, 4]	0.333333	[1, 4]	0.16666667	[2, 4.5]	0.16666667
	[2, 5]	0.333333	[1.5, 4.5]	0.16666667	[2.5, 5]	0.16666667
	[3, 6]	0.333333	[3, 4]	0.16666667	[3, 5.5]	0.16666667

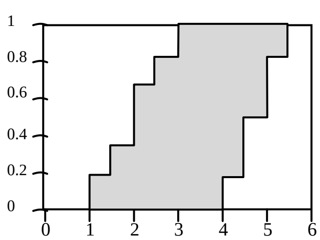

Figure 2-19 the gcdf of the combination of A and B using convolutive x-averaging.

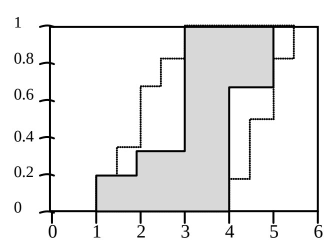

Figure 2-20: The Comparison of Combinations of A and B with Dempster's rule and Convolutive X-Averaging.

As is readily apparent, the bound for the convolutive x-average either is equal to or is significantly larger than the bounds of the Dempster combination.
The combination for evidence from A and C can be performed though the convolutive x-average and the calculation results are presented in table 2-13. Figure 2-21 illustrate structural results for evidence combination from A and C.

Table 2-13: The Combination of A and C using Convolutive x-Averaging.

			A			
			Interval	m	Interval	m
			[1, 4]	0.5	[3, 5]	0.5
C	Interval	m				
	[6, 10]	0.333333	[3.5, 7]	0.16666667	[4.5, 7.5]	0.16666667
	[9, 11]	0.333333	[5, 7.5]	0.16666667	[6, 8]	0.16666667
	[12, 14]	0.333333	[6.5, 9]	0.16666667	[7.5, 9.5]	0.16666667

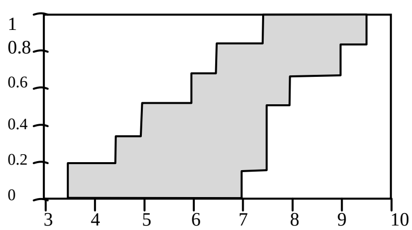

Figure 2-21: The gcdf of the Combination of A and C using Convolutive x-Averaging

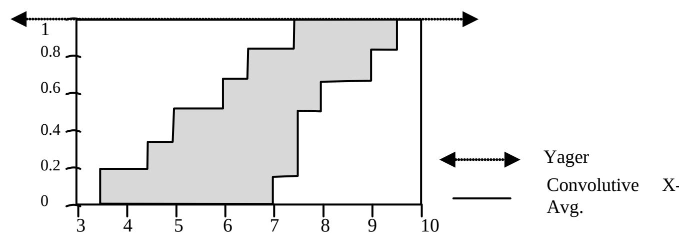

Figure 2-22: Comparison of Yager's rule and Convolutive x-averaging for A and C

The difference between the Yager's rule and convolutive x-averaging rule for the combination of A and C has been illustrated in figure 2-22. This demonstrates the difference between the Yager's combination under complete conflict (which corresponds to the whole real line) and the convolutive x-average. Yager's distribution implies that there is complete ignorance regarding the inputs, whereas the convolutive x-average simply averages them and provides a significantly narrower answer.

2.5.4 Discussion and comparison

Dempster-Shafer Theory essentially combines the Bayesian notion of probabilities with the classical idea of sets where a numerical value signifying confidence can be assigned to sets of simple events rather than to just mutually exclusive simple events. (Bogler, 1992) The theoretical basis for Dempster-Shafer Theory is an attractive one for dealing with a corpus of data that requires different degrees of resolution. From the operational perspective of Dempster-Shafer theory, that finds that the aggregation of evidence from multiple sources is not straightforward, as there are a variety of possible combination rules.
As there are multiple ways of combining data, it would be desirable to develop a formal procedure by which one could select an appropriate combination operation.
Although the algebraic properties may not prove to be useful in designing a comprehensive typology of combination operators, they do provide insight into some of the behavior of the operators. . Kari 2002 has compared and discussed properties of the combination rules in Table 2-14.
For Dubois and Prade, combination operations cannot be discussed solely in terms of algebraic properties because the imposition of too many properties can be too restrictive to solve practical

Table 2-14: Combination Rules and Their Algebraic Properties

	Algebraic Properties			
Combination Rules	Idempotent	Commutative	Associative	Quasi- Associative
Dempster's Rule	No	Yes	Yes	
Yager's Rule	No	Yes	No	Yes
Inagaki's Rule	No	Yes	Depends on value of *k*	Depends on value of *k*
Zhang's Rule	No	Yes		Yes
Mixing	Yes	Yes		Yes
Convolutive x-Average	Yes	Yes		Yes
Disjunctive Consensus Pooling	No	Yes	Yes	

problems. As that can see with the numerous Dempster-type combination rules, they satisfy many of the same algebraic properties. Moreover, as the work of Dubois and Prade points out, (Dubois & Prade 1992), even the definitions of the algebraic properties can be problematic and debatable. Nevertheless, understanding what the desirable properties of a prospective combination rule can be one part of the criteria for rule selection.

Another helpful heuristic for choosing a combination rule is to identify the requirements of the situation as disjunctive pooling, conjunctive pooling or tradeoff.

These correspond to the Dubois and Prade disjunctive pooling method, the Dempster rule, and the remaining operations of Yager's rule, Zhang's rule, discount and combine, mixing, and convolutive x-averaging, respectively. If that requirement alone cannot be determined, it may prove practical to apply Inagaki's rule for many values of k. As Kari has shown here, a number of these rules can be tested and their results compared. Many of the Dempster and the "Dempster-type" combination rules share a common first step, the multiplication of the marginal masses to find the joint. These rules fundamentally differ on how these joint masses are to be combined and where to allocate the mass associated with conflict in the second step.

There are a number of considerations that need to be addressed when combining evidence in itself, the sources of information, the context of the application, and the operation used to combine the evidence that have been depicted in figure 2-23.

As the literature survey on aggregation in generalized information theory reflects, much of the research in the combination rules in Dempster-Shafer theory is devoted to advancing a more accurate mathematical representation of conflict.

With regard to algebraic discussions can conclude: In Dempster's rule the intervals are defined by the minimum of the upper bounds and maximum of the lower bounds. The individual bpa's are calculated by multiplying the bpa's of the marginal. Where the same interval is obtained from multiple combinations, the associated bpa's are summed. There is no mass associated with conflict. Yager's Rule: As there is no conflict, this problem provides the same answer as Dempster's rule. In Inagaki's Rule, we have k=0 and there is no conflict, this problem provides the same answer as Dempster's rule. In Mixing rules, this averaging operation provides different intervals and different bpa's than Dempster's rule. The intervals are either equal to the Dempster intervals or in most cases wider. Convolutive x-Average: The convolutive x-average is quite different from Dempster's rule, Zhang's rule, and mixing in terms of the bounds of the interval and their respective bpa's. The bounds of this average are either equal to those of Dempster's rule or larger. Disjunctive Consensus Pooling is the most imprecise of the combination methods. The intervals are defined by the maximum of the upper bounds and the minimum of the lower bounds and the bpa's are calculated in the same manner as Dempster's rule. Zhang's Rule: Provides a slightly different answer than the other Dempster-type rules. The

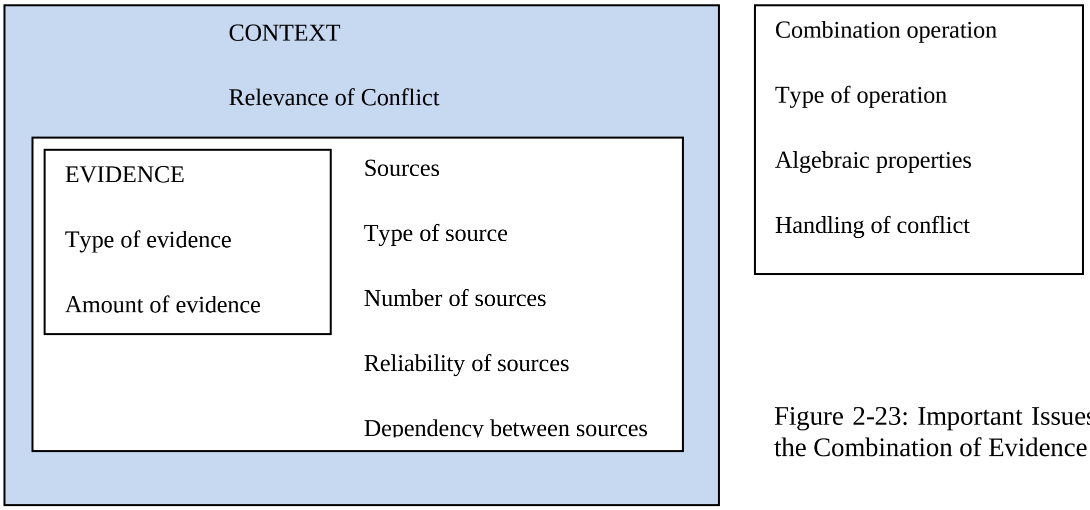

Figure 2-23: Important Issues in the Combination of Evidence

intervals are defined in the same manner but the bpas are scaled differently because of the measure of intersection. Consequently some bpa's are larger than those obtained by Dempster's rule, while others are slightly smaller. The final masses are renormalized so all masses will add to one.

Chapter 3: Gathering and preparing Geospatial Database

3.1 Introduction

The important part of this project is data gathering in digital form and creating a spatial database as in the first chapter to be discussed on the conceptual model. There are various aspects for collecting spatial data and to unite format. Therefore it is necessary to have some information about data acquisition methods and different sensors.

In every project will be needed maps, images and spatial data tables in addition of reported information that can be transferred to spatial data. With regard to previous discussions on mineral exploration, there are four group primary data mainly. These data consist of geology, geophysics, remote sensing and geochemistry. For next processing, these data should be used in GIS context. The following sections explain preparation of data in the GIS context for the integration processing.

Many data can be derived from these primary data with attention to research object. From primary data can drive many different sub-data, e.g. from ASTER image we can extract lithological data and also land use information or vegetation type area. Firstly that will be needed to know which sub-data can extract from primary data. Hence we should have enough information about research subject and object.

In this case study, investigation matter is uncertainty in mineral exploration. So there are questions and uncertainty in place and kind of minerals where and what can be explored in the area. The chapter one discussed about kinds of minerals that can be explored in the area. With regard to chapter one, I determine and prepare the relevant data that can be applied for exploring these specific minerals. This chapter discusses about accessible and relevant data then shows preparing them to apply in GIS context. Next chapter will discuss about defining high potential area for these specific minerals by using the prepared data.

There are some digital and manual data that have been prepared in different standards and formats. Here I use GIS context to compiling of data so it is necessary to bring all data in unique standards and formats in GIS context then eliminate some incorrect data from this data.

3.2 Topographic Data

Available topographic data for the area contain 13 topographic maps on the paper and have been provided from photogrammetry of the airborne photographs by national geographic organization of Iran (NGO 1973 -2003) in scale 1/50,000 with 20m contour lines distance. All maps were digitized in 100 m contour line distance in addition of stream lines but in some place there are gapes for that was tried to apply some software for Dem drawing from ASTER images.

Main applications of this data are georeferencing of RS images and obtaining of DEM maps. Dem map give a good landscape for mapping of some geological terrain like faults. Figure 3-1 shows a part of DEM map and 3D image that to be provided from topographic contour line ASTER image. As in figure 3-1c can see, this *3D Remote Sensing images* give landscape to verify geological structures as mentioned. After extracting lineaments from Remote Sensing images, I use these 3D ASTER images for verifying and adjusting them.

3.3 Remote Sensing data

Remote Sensing can be defined as the collection of data about an object from a distance. Earth scientists use the technique of remote sensing to monitor or measure phenomena found in the Earth's lithosphere, biosphere, hydrosphere, and atmosphere. Remote sensing of the environment is usually done with the help of mechanical devices known as remote sensors.

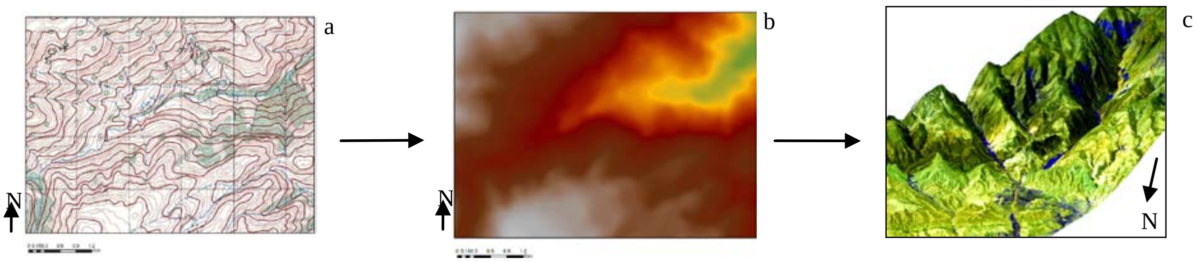

Figure 3-1: present a part of the topographic maps and consequent images from that. a - Topographic map, b- Dem image, c- 3D ASTER image.

These gadgets have a greatly improved the ability to receive and record information about an object without any physical contact. Often, these sensors are positioned away from the object of interest by using helicopters, planes, and satellites. Most sensing devices record information about an object by measuring an object's transmission of electromagnetic energy from reflecting and radiating surfaces. Remote sensing imagery has many different applications in mapping land-use and land cover, agriculture, soils mapping and geomorphologic surveying among other uses. Usually, prospectors use Remote Sensing imagery for mapping lithology, alteration area, geological structures and et cetera. Sometimes the term “Remote Sensing” is abbreviated as RS.

For this project, the images from ETM, ASTER and SPOT satellite sensors are accessible as RS data. Accessible ETM and ASTER images cover all the study area approximately but accessible SPOT image covers a limited place in south east of the study area. Due to wide swath of ETM sensor (185 km); the images come from this sensor cover whole the area but resolutions are lower than ASTER image as spectrum bands are less. Alteration and some lineament data have been derived by RS group of GSI from this image already. In this case I use the result of this data layers for comparing with ASTER images processing results and also as data layers for integration. The Landsat Program is a series of Earth-observing satellite missions managed by NASA and the U.S. Geological Survey. Since 1972, Landsat satellites have collected information about Earth from space. Landsat 7's sensor - the Enhanced Thematic Mapper Plus (ETM+) was built by SBRS, the ETM+ design provides for a nadir-viewing, eight-band multispectral scanning radiometer capable of providing high-resolution image information of the Earth's surface. Figure 3-2 shows situation of the images and covering state of the study area. Figure 3-2a illustrates the study area position on ETM+ images. In figure 3-2, figure 3-2a indicates, two ETM+ images cover all the area. Table 3-1 presents spectrum bands details for ASTER, ETM and SPOT sensors images.

The main studies on Remote Sensing images have been done on the ASTER images. Existing of spectrums in VNIR (visible near infra red), SWIR (short wave infra red) and TIR (thermal infra red) creates relatively high capability to be applied widely in geological subjects. Especially that has good resolution for mapping some lithological terrain and sometimes structural terrains. In table 3-2 can see spectrum bands details for VNIR, SWIR and TIR. ASTER (Advanced Space-borne Thermal Emission and Reflection Radiometer) is an imaging instrument flying on Terra, a satellite launched in December 1999 as part of NASA's Earth Observing System (EOS). ASTER is being used to obtain detailed maps of land surface temperature, reflectance and elevation. ASTER imaging instrument captures high spatial resolution data within a 60*60 km2 scene area in 14 bands with a pixel resolution between 15*15 to 90*90 m2 from the visible to the thermal infrared wavelengths and provides stereo viewing capability for digital elevation model creation.

The study area is covered by 7 scenes, though there is small lack in east part, as can be seen in figure 3-2 b. The images are accessible in 1B level so they don’t need atmospheric corrections and have been georeferenced but those need to be orthorectified. This layer has been used as a reference layer to bring data layers in unique structure like geological data layers. These images obtain ability for determining alteration districts directly which is important in mineral exploration.

SPOT system is the satellite Earth Observation System that was designed by the CNES (the French Space Agency) and developed with the participation of Sweden and Belgium. Its operation has begun science 1986. In this project, high resolution imaging of the SPOT system is useful in some part of the area. The images contain resolution between 2.5- 20 meter in both black-and-white and colour images. The accessible image for the area has 5*5 m^2 resolution and it is acquired in a single panchromatic band (black-and-white) and in the visible spectrums. In this mode, the ground pixel size is 5*5 m^2 with wavelength between 0.48 and 0.71.

Only one scene of SPOT images is available which covers south east part of the area and is accessible in level 1B. I used that for Abhar sheet processing and pan sharpening of ASTER images in the south east of the area. In pan sharpening a high resolution panchromatic image is fused with lower resolution multispectral data to create a colorized high resolution data set. Among the geologic maps, Abhar geologic map has low accuracy, because there is no geological map in scale 1/100,000 for Abhar area. Thus SPOT image is useful to reduce some geologic inaccuracy in this area. Figure 3-2 c indicates the situation of the SPOT image, as mentioned already that covers south east of the area and contains some parts of Abhar, Takestan, Rudbar and Jirandeh geologic sheets. Table 3-1 shows some details of single band of SPOT images.

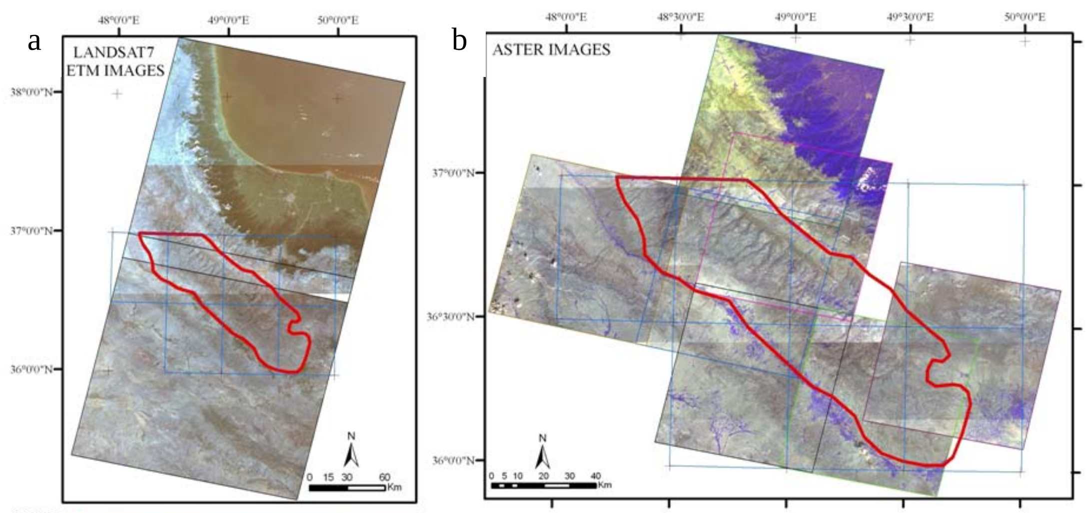

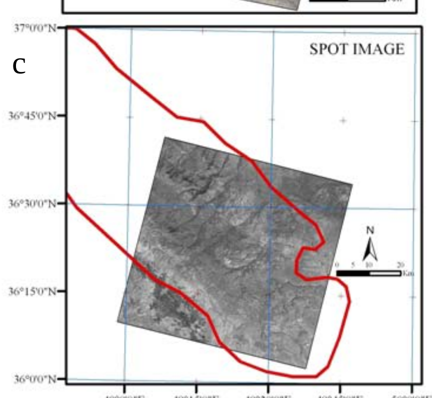

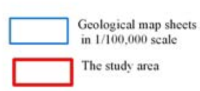

Figure 3-2: That shows position of RS images on the area,
a: represent Landsat7 ETM+ images that consist two images,
b: show 7 Aster image that cover the study area,
c: there are only one SPOT image that cover some part of Abhar, Takestan, Rudbar and Jirandeh sheets.

Table 3-1: That represents spectral properties of ASTER, Landsat7 ETM+ and SPOT images.

	Subsystem	Band No.	Spectral Range (μm)	Spatial Resolution(m^2)	Quantization Levels	Focal Length(mm)	Pixel size on detector(mm)
ASTER	VNIR	1	0.52-0.60	15*15	8 bits	329.0	0.007 * 0.007
		2	0.63-0.69				
		3N	0.78-0.86				
		3B	0.78-0.86			376.3	
	SWIR	4	1.60-1.70	30*30	8 bits		
		5	2.145-2.185				
		6	2.185-2.225				
		7	2.235-2.285				
		8	2.295-2.365				
		9	2.360-2.430				
	TIR	10	8.125-8.475	90 *90	12 bits		
		11	8.475-8.825				
		12	8.925-9.275				
		13	10.25-10.95				
		14	10.95-11.65				
Landsat7 ETM+	NVIR	1	0.45-0.515	30*30	8bits	2438.0	0.1036 * 0.1036
		2	0.525-0.605				
		3	0.63-0.690				
		4	0.75-0.90				
	SWIR	5	1.55-1.75				
	TIR	6L	10.40- 12.5	60*60			
		6H					
	SWIR	7	2.09-2.35	30*30			
	Pan	8	0.52-0.9	13 * 15			
SPOT	Panchromatic		0.48-0.71	5*5	8 bit	580.0	0.0065 * 0.0065

That is necessary preparing Remote Sensing images before applying them in GIS environment, especially geometry correction will be need. With regard to integration method, various data layers should be compiled in unique condition, thus if features in one data layer lie in wrong situation, consequently data will be compiled in wrong situations. Hence, all processes will be conducted us to inaccurate states. Figure 3-3 clarifies this inaccuracy in ETM images by an

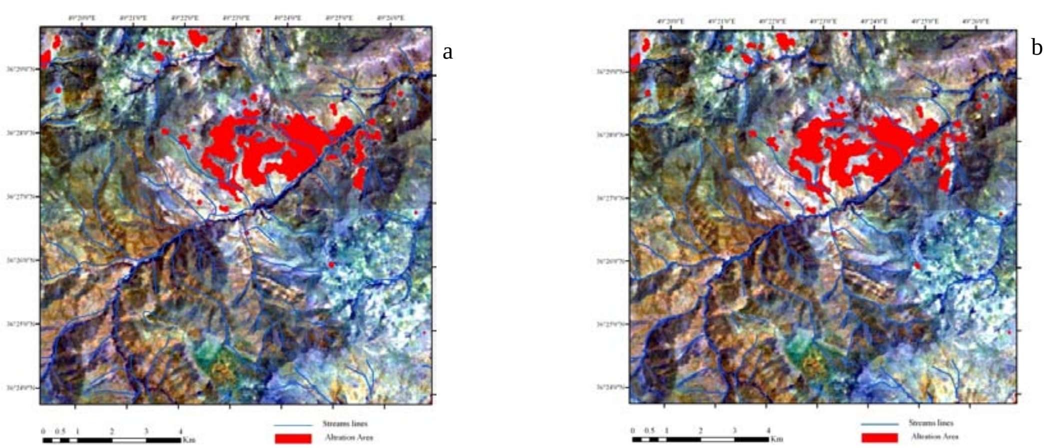

Figure 3-3: figure a presents unconformity between stream lines from topographic map and stream trace on ETM image without geometric correction and alteration area, b shows ETM image after geometric correction.

example. Figure 3-3-a indicate ETM image before geometry correction and figure 3-3b indicate ETM image after geometric correction (involve orthorectifying and georeferencing). In both images, some other data layers like streams and alteration area, that extracted from topographic maps and ASTER image overlay on ETM images. In figure 3-3a, unconformities are clear between stream lines from topographic map and stream trace on ETM image. There is about 280 $\pm$ 20 meters difference between them, in addition alteration area from ASTER images also show this difference. In figure 3-3b, unconformities are adjusted approximately, here streams from topographic map cover stream traces of ETM image well.

For all the images from three different sensors, georeference processing and atmospheric corrections already have been done by production companies but they need still orthorectifying and calibration correction. Remote Sensing image processing has been done mainly by ENVI software. In some processes, GEOMATHICA, ERDAS imagine and ArcMap programs also help me. I use ArcMap to make 3D remote sensing image, this software provide some tools to overlay two layers easily and has a tool for 3D image making. So I have applied that for doing some corrections in lineament data. ERDAS help me to verify SPOT image and GEOMATHICA help me to orthorectify some ASTER images, but ENVI is more user friendly doing that.

Photogrammetric rectification consists of modeling the exterior and interior orientation parameters of the sensor image acquisition geometry in relation to ground coordinates. McGlone (1984) submitted rational polynomial coefficients (RPCs) model, the ground-to-image relationship, as a third-order rational ground-to-image polynomial. ENVI compute RPCs prior to single image orthorectification by building interior and exterior orientation models. Data from each of sensors typically include an accessory RPC file or have the necessary ephemeris data, which ENVI uses to compute RPCs. Another option is to build RPCs for any photograph by using ENVI's Build RPCs function. This function builds RPCs from ground control points (GCPs) or known exterior orientation parameters (XS, YS, ZS, Omega, Phi, and Kappa), then this RPC is used to orthorectify the images.

Both options have been used for orthorectifying of ASTER image but for SPOT and ETM+ have been used second option, both them need ground control point (GCPs). There are some ways for collecting of GCPs: Image-to-Map, Image-to-Image and points derived from a GPS.

For Image-to-map manner that should be used a georeferenced map. In this case topographic maps are available and relatively are more accurate relative to geological map. In addition topographic maps have relatively accurate elevation number which would be need in orthorectifying. Hence I use topographic maps as reference maps to collect points particularly from intersection of stream lines. Intersections of features provide positions that are more accurate points that can be accorded with images easily. For every image at least 3 points will be needed but for more accurate orthorectifying that is better to extract at least 15 point. In some images I use more than 15 points. Also for decreasing of errors, I change situation of points many times.

ETM images as mentioned have been used for situation correction of some data already had been obtained and also have been used in process for recognizing of some lithological terrains as well for comparing of results come from ASTER images. RPC was calculated for rectifying of them from “RPC with GCP” tools of the map menu in ENVI.

ASTER images level 1B was accessible for the study area. In accessible data there were 14 bands in one file, for every bunch of VNIR, SWIR, TIR exist a header file with RPC information and everyone can rectify alone but after rectifying for every bunch would be created individual files. Hence when some processes compile bands that create some shifting and errors. To be suggested before rectify, to create a file with one header file and then calculating of RPC, in this way some errors are possible in RPC calculation but that cause decline of the previous errors. Panchromatic SPOT band also has been rectified by this method. Calculating of RPC need some technical parameters; including focal length, image pixel size on detector, along track incidence angles and across track incidence angles, all these are available on the sensor reports.

In the following provision, processes on the RS images will be explained. That explain how can extract alteration data and how can use these images for correcting lithological units from inaccurate geologic maps.

Main processes are performed on ASTER and ETM images to access alteration area which is very important in mineral exploration. Alteration types of every different mineralization model is particular separate as mentioned in chapter one. e. g. phyllosilicate alteration mainly accompanies epithermal mineralization models and iron oxide alteration accompanies porphyry mineralization models. Other terrains that have been derived from Remote Sensing images are lineaments including of fault and ring structures. Structural data are accessible for GIS experts from process on ETM and RADAR images. Figure 3-4 illustrates spectral properties of the some hydrothermal minerals and that indicate some wavelengths what ASTER and ETM images contain them. Figure 3-4 illustrates spectral reflectance of hydrothermal minerals extracted from USGS library for ASTER and ETM images. As figure 3-4 indicate the first band of ETM image has wavelength 0.4-0.5 μm as table 3-1 show that. Mainly, in ETM image bands, alteration areas have in band 5 more reflectance. Phyllosilicate minerals (montmorillonite, Kaolinite, Alunite, Illite), in ASTER image bands, show more reflectance in band 4, 5 and low reflectance in band 6.

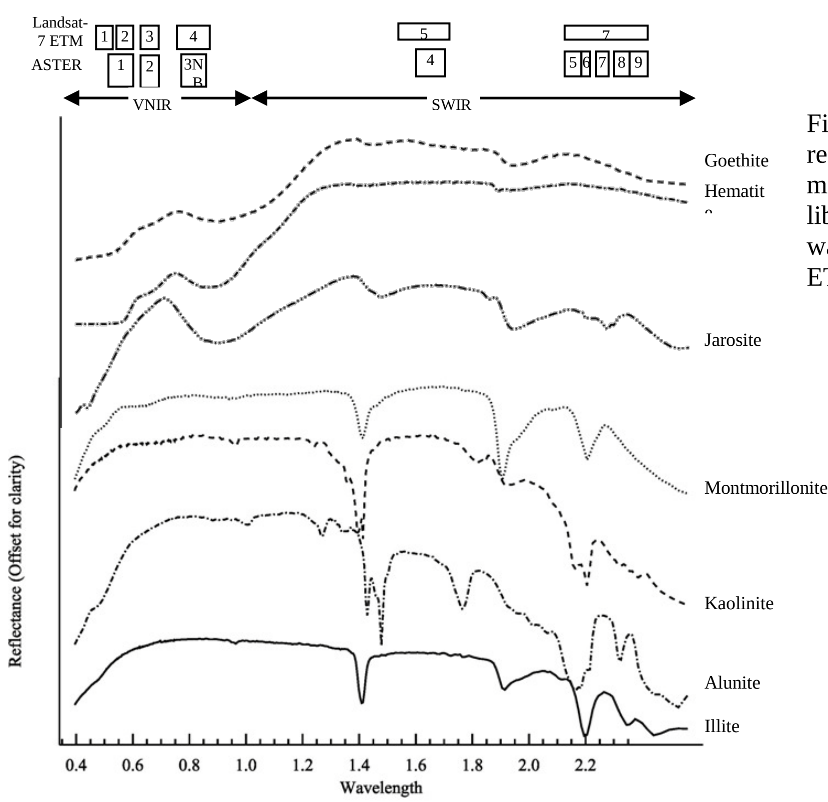

Figure 3-4: illustrates spectral reflectance of hydrothermal minerals. (Extracted from USGS library) also show the band wavelengths that ASTER and ETM images contain.

3.3.1 ETM images processes

As mentioned, ETM images can help to collect some geological data like alteration area. For extracting alteration areas from ETM images, that will be need to consider of the spectrum properties of the bands in table 3-1 and figure 3-4.

3.3.1.1 Alteration minerals area

Two methods have been used to extract alteration area on the ETM images. The first is mathematical operations and other is Principal Component Analysis (PCA). Mathematical operations are a method that can help to enhance place with high reflectance area. The high reflectance areas are related to alteration area or other geological features. Addition, multiplication, division, subtraction are four mathematic operations that to be process on bands. Addition and multiplication operations have similar conclusions on the bands and enhance the same information. In the opposite, subtraction and division operation on bands have similar results and converse results related to addition and multiplication operations. Mainly subtraction and division operations are applied in image processes more than other operations. Sometimes the following normalized ratio has been used:

$$DN = \frac{bi - bj}{bi + bj} \quad , \qquad \text{DN: digital number or pixel value}$$

For all i > j,

In figure 3-4 phyllosilicate alteration minerals show low reflectance in 1.4 - 1.5 and 2.2 wavelength that has accordance with band 6 and 5 of ASTER image and band 7 of ETM images. Ferrous alteration minerals show high reflectance on band 6 and 5 of ASTER image and band 7 of ETM image.

This ratio modifies topographic effects and also that puts the results between 1 and 0. For enhancement of iron oxide alteration including of goethite, hematite and jarosite have been used ratio of band 3 to 1. In this ratio, band 1 has high absorption and band 3 has high reflection hence alterations enhance very well. The ratio of bands 5 to 7 has been processed for distinguishing phyllosilicate alteration areas.

That is possible; some geologic features would be existed with the same spectral reaction in alterations so those appear in processed images also. Hence that has been defined an experiential threshold with high confidence for alteration. To tack away vegetation area in processes, the ratio ETM 5/7 have been applied against of ratio ETM 4/3.

Another applied method for defining of alteration in ETM images is Principal Component Analysis (PCA). I apply this method on ASTER image too so the details will be explained in ASTER processing section. Here has been used feature-oriented PCA and pairwise PCA:

For iron oxide alteration PC4 (1, 3, 4, 5), PC2 (1, 3)

And for phyllosilicate alteration PC4 (1, 2, 5, 7), PC2 (5, 7)

Figure 3-5 represent classification of PC4 results after some corrections for removing vegetation and soils areas. In the figure 3-5 can see alteration areas by red colour on the ETM image.

3.3.1.2 Geological structures

Lineaments are one of important features in geological structures. Lineaments consist of ring structures and faults. Already chapter 1 has discussed about effects of faults (lithological breaking) on mineral deposits. Faults appear on the earth mainly like straight line trace. Ring structure is another structural feature in geology, there are some researches about ring structures and its’ relation with mineral deposits. O'driscoll's, 2007 indicate relationship between rings on rifting tectonic area in southeastern of Australia and mineral deposits. Volkov, 2005 represents

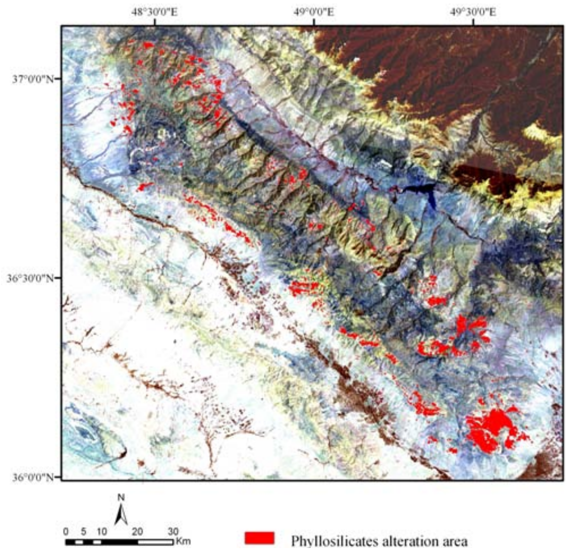

Figure 3-5: represent classification result of PC4 images for phyllosilicates alterations.

connection of epithermal mineralization in southern Macedonia with ring structures. Pavlovic, 2003 in south of Serbia and Kalacheva 2005 in Kuril island of Russia also argue about affects of the ring structures on evolution of hydrothermal alterations. In some case intrusive bodies make ring structures that have connection with Cu porphyry mineralization such as ring structure in Kadica–Bukovik ore district in eastern Macedonia (Volkov 2008).
Figure 3-6 represent faults and ring structures in the area; the diameter of the recognized ring structures and length of the faults range from a few hundred meters to several kilometers.

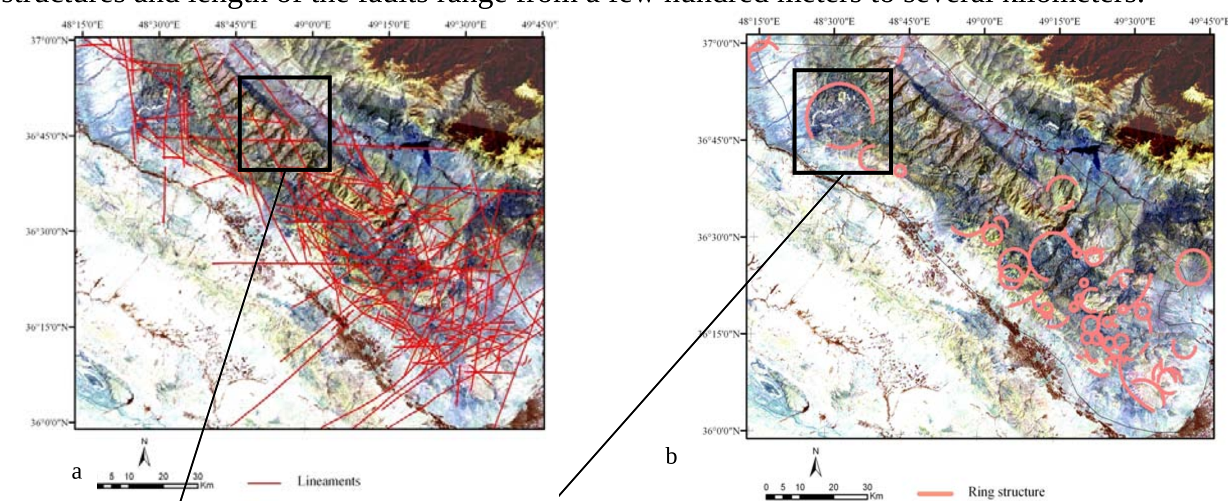

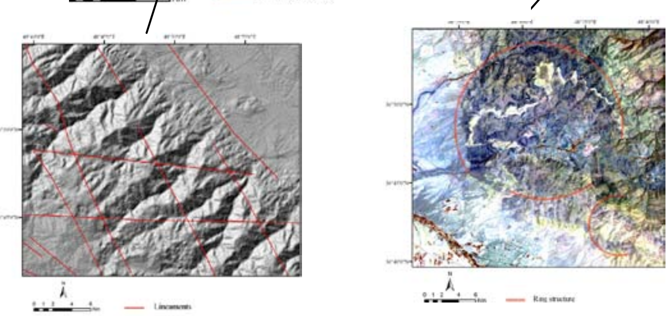

Figure 3-6 a and b indicate lineament structures on ETM image. In a, you can see lineaments including straight lines and in b, you can see ring structures. In a, the part of image has been enlarged indicate straight lines on the 3D hillshade map. In b, the part of the image that has been enlarged is indicating structural traces on the ETM image.

ETM and RADAR image have been applied to extract these structures by geological survey of Iran. Usually high pass filters are used to illuminate of geological structures. In this case, laplacin filter has been applied to enhancement of geological structures. Hill shad images and DEM images have been extracted from ASTER and topographic maps which is useful for verifying of lineaments.

3.3.2 ASTER images processes and extracting of alteration area

The study area contains an oblique structure in direction northwest –southeast, that has been mentioned already. The study area consist parts of 7 geological map sheets in scale 1/100,000 and there are some conflicts between geological map sheets in lithological units especial in map sheets borders. To eliminate these conflicts, it is necessary to make seamless geological map. I used geological map in scale 1/250,000 and Remote Sensing images for acquisition unit geological map with accuracy in scale 1/100,000. Geological maps with scale 1/100,000 are more accurate and also lithological units have more variety relative to geological maps by scale 1/250,000. In the other hand on the borders of the map sheets there are unconformity between lithological units. If the discordances don't adjust, that will create problems in the next processes. Every geological map sheet in scale 1/250,000 contains 6 map sheets in scale 1/100,000. So this would be useful to make seamless lithological units by map sheet in scale 1/250,000, but there is a problem; some units have not been characterized in this scale map. Therefore remote sensing images can help to extract additional data related to map sheet scale 1/250,000 and help to verify the units with conflicts in the sheet borders. I have used ASTER images for this aim too.

ASTER images have 14 channels of spectrum bands NVIR, SWIR and TIR, as considered already. These spectrum bands can use in lithological mapping; detecting igneous, volcanic and sedimentary rock features and hydrothermal alteration area.

Hydrothermal alteration areas create appropriate conditions to deposit of Au and Cu minerals, so they are important indication to mineral exploration. In both types of mineralization models (porphyry and hydrothermal), alteration areas play main role. These areas in porphyry types are not deposit host but more is an evidence for porphyry mineralization in near place. But in hydrothermal type, these areas are directly positions those minerals can deposit in other words they are host rocks. Applying ASTER images are one manner that can help to locate alteration area with Spectrums in 14 bands. Among different method, I used colour composition method, band ratio and Principal Component Analysis (PCA); these methods are common to detect alteration areas in ASTER images.

3.3.2.1 Colour composition

In colour composition method, the image bands are displayed in the blue, green, and red channels. Apparently the processes are simple, but that should be considered choosing bands and colour channels. That should be care which band in which channel can enhance interested features. Colour channel and band selection create colour composition images that features are not in real colours this composition commonly named false colour composition images. Various statistical procedures based on band variance have been indicated here for identification of hydrothermal alteration. Figure 3-7 indicate two false colour composite images of ASTER bands 6-3-1 and 7-4-2 in red, green and blue, respectively. Sericitic and argillic alunitic alteration zones in prospect areas can be recognized by white, bright brown and bright blue colours. Propylitic zones were discriminated by red colour.

3.3.2.2 Band ratio

Band ratio is other technique to discriminate alteration area on the RS images, in this method numerical values in one band divide by another for each pixel and band ratio image can emphasize and quantify spectral difference between these bands.

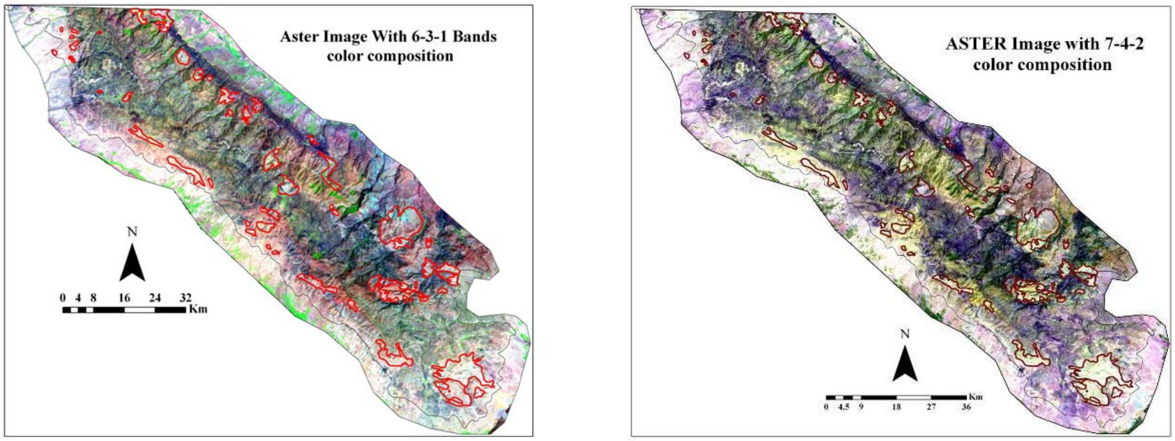

Figure 3-7: indicate two false colour composite images of ASTER bands 6-3-1 and 7-4-2 in red, green and blue, respectively and digitized alteration area.

The produced images have which radiance variation that is proportionally constant from band to band is suppressed and the more interesting radiance variation attributable to spectral reflectance of geological materials is enhanced (Sabine 1999).

With nine VNIR and SWIR bands, there are 36 possible unique ratio combinations that could be produced. For interpretation of the images commonly have been used three colour ratio composition by combining them in the following order R2/1(R), R4/x(G), Rx/2(B) (USGS EROS data center 2004). Table 3-2 represents some ratios for discriminating of alteration and silica minerals and lithological discrimination by Kalinowski 2004. I applied them for recognition of alteration area and making unit geological map; next sections explain that.

Table 3-2: represents some useful band ratio that has been used on the ASTER images in the study area for discriminating of alteration area and lithological units (Kalinowski 2004).

Feature	Band or Ratio	Comments	Feature	Band or Ratio	Comments
Iron			phyllosilicate		
Ferric iron, Fe^{3+}	2/1		Kaolinite	7/5	Approximate
Ferrous iron, Fe^{2+}	5/3 + 1/2		Clay	$(5x7)/6^2$	
Laterite	4/5		Phengitic	5/6	
Gossan	4/2		Muscovite	7/6	
Ferrous silicates (bio, chl, amph)	5/4	Fe oxide Cu-Au alteration	Sericite / muscovite / illite / smectite	(5+7)/6	Phyllic alteration
Ferric oxides	4/3	Can be ambiguous	Alunite / kaolinite / pyrophyllite	(4+6)/5	
Vegetation			Alteration	4/5	
Vegetation	3/2		Host rock	5/6	

Table 3-3 in next page from Kalinowski 2004 suggests some colour compositions, these colour composition also I have applied for recognition of alteration area and unifying of lithological units in different maps.

For recognition of alteration area, bands with high reflectance in alteration minerals are divided by bands with high absorption in alteration minerals. Hence those enhance the alteration area reflectance, where mainly have been formed by hydroxyl-bearing minerals, phyllosilicates and iron oxide alteration area. I used and combined for this research more than 20 colour composition images with simple bands and band ratios, I compare all with each other and by this manner, I drew alteration prospect area in 3 classes for next processing.

Tabl 3-3: shows some colour composition of band ratios can help in recognition of lithological units (Kalinowski 2004).

Features	Red	Green	Blue
AlOH mineral/ advanced argillic altr.	5/6 (phen.)	7/6(musc.)	7/5(kaol.)
Clay, amphibole, laterite	$(5*7)/6^2$ (Clay)	6/8 (amph.)	4/5(lat.)
Gossan, alteration, host rock	4/2(goss.)	4/5 (alt)	5/6 (host)
Gossan, alteration, host rock	6 (goss.)	2 (alt)	1 (host)
Silica	11/10	11/12	13/10
Lithological discrimination for mapping	4/1	3/1	12/14
Lithological discrimination for mapping	4/7	4/1	(2/3) x (4/3)
Lithological discrimination for mapping	4/7	4/3	2/1
Silica, Fe	14/12	(1/2) + (5/3)	1

Figure 3-8 submit only 3 colour compositions that I used for drawing hydrothermal alterations on the digital maps manually. Figure 3-8-a with band ratio 2/1-(5+7)/6-7/5 show red, green and blue colour channels respectively in colour composition image, 2/1 can detect iron oxide minerals, (5+7)/6 and 7/5 ratio enhance sericite and clay minerals respectively. Sericitic and argillic area can be detected by white to bright violate. Bright blue colours show silicic alteration area, green colours show propylitic alteration area; yellow colours detected vegetation areas. In figure 3-8-b 4/2 band ratio indicate gossan (iron oxide alteration mineral) and 4/5 and 5/6 detect other alteration minerals. In this figure, bright green colours signify silicic alteration and light blue colours show prophylactic alteration area. Figure 3-8-c with order 5/6-7/6-7/5 colour composition indicates alteration area with bright blue and bright brown. In this band ratio colour composition image, propylitic alteration area can be recognized by bright cream.

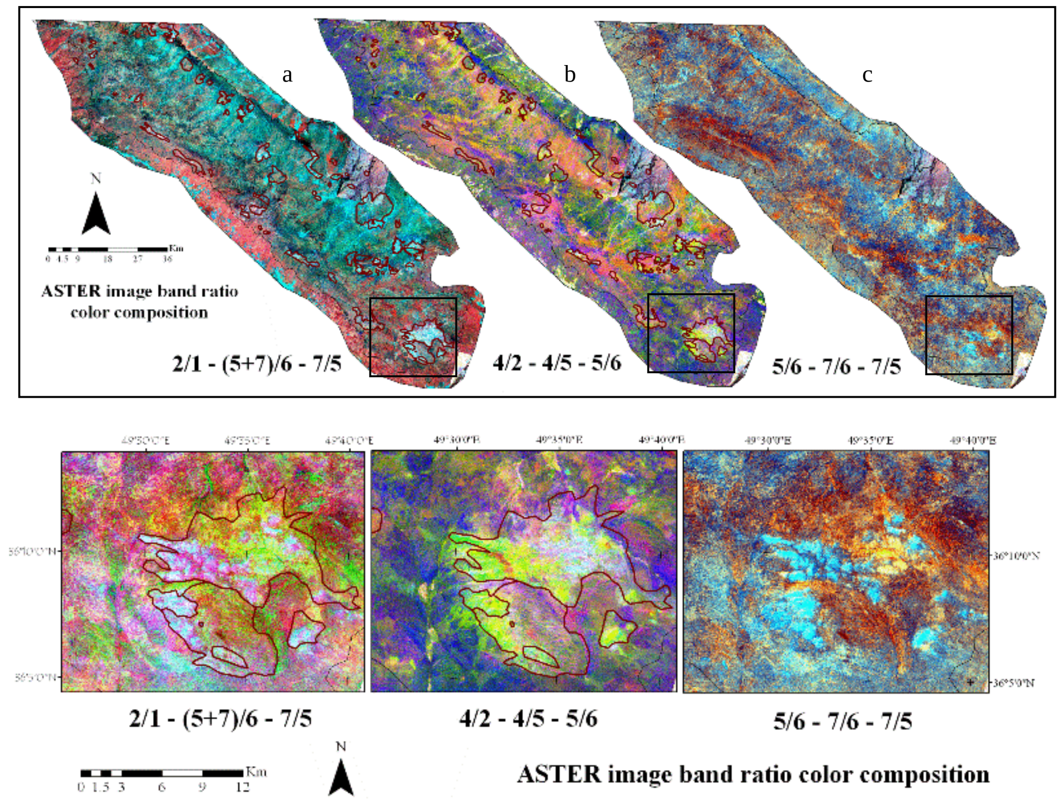

Figure 3-8 represent some band ratio colour composition images and alteration area on them.

In figure 3-8, alteration area in south part has been enlarged to show some colour details. Figure 3-8-a with 2/1-(5+7)/6-7/5 band ratios show red, green and blue respectively. Sericitic and argillic area can be detected by white to bright violate, bright blue colours show silicic alteration area, green colours show propylitic alteration area and yellow colours detected vegetation areas. In figure 3-8-b 4/2 band ratio indicate gossan (iron oxide alteration mineral) and 4/5 and 5/6 detect other alteration minerals. In this figure, bright green colours signify silicic alteration and light blue colours show prophylactic alteration area. Figure 3-8-c with order 5/6-7/6-7/5 in red, green and blue colour composition indicates alteration area with bright blue and bright brown. In this band ratio colour composition image, propylitic alteration area can be recognized by bright cream.

3.3.2.3 Principal Component Analysis (PCA)

Principal component analysis (PCA) is a general method of analysis for correlated multi-variable datasets. Remotely sensed multi-spectral imagery is typical of such datasets for which PCA is an effective technique for spectral enhancement and information manipulation. PCA is based on linear algebraic matrix operations and multi-variable statistics.

This technique is a multivariate statistical technique that selects uncorrelated linear combinations (eigenvector loadings) of variables in such a way that each successively extracted linear combination, or Principal Component (PC), has a smaller variance (Singh and Harrison, 1985).

Higher rank PCs contain significantly less information but it is more relevant to the spectral signatures of specific ground objects. Colour composites of PCs are often very effective for highlighting such ground objects and minerals which may not distinguishable in colour composites of the original bands. In PC colour composites, noise may be exaggerated because the high rank PCs contain significantly less information relative to lower rank PCs and they have very low SNRs. When PC images are stretched and displayed in the same value range, the noise in higher rank PCs is improperly enhanced.

There are Standard PCA and selective PCA, standard PCA to be performed on VNIR + SWIR bands but in selective PCA that can be selected different bands in three, four or six bands for performance. In this case study, I have calculated the general statistics and principal component eigenvectors and eigenvalues for VNIR + SWIR bands, SWIR bands and three bands in different ways. Different alteration maps of this area have been produced by these PCA techniques and their colour compositions. I have chosen image by the better results for mineral and lithological discrimination and the next sections describe them.

Table 3-4 indicates principal component analysis results on 9 bands of VNIR+SWIR. Table 3-4-a shows basic statistic and in 3-4-c can see this components contain 91.39% of the variance of the nine bands.

Basic Stats	Min	Max	Mean	Stdev
Band 1	25.183	227.874	76.834	13.887
Band 2	7.5230	222.399	74.209	16.188
Band 3	12.978	218.948	72.152	12.761
Band 4	0.4895	55.2196	16.310	3.0449
Band 5	-0.1354	17.8789	5.0039	0.9087
Band 6	-0.1036	18.2516	4.7371	0.8771
Band 7	-0.0166	17.2793	4.1816	0.7826
Band 8	-0.0715	13.8232	2.9840	0.6006
Band 9	-0.2419	10.2075	2.2644	0.4265

Table 3-4: represent in a general statistic b (next page) correlation matrix and c eigenvector for 9 bands (VNIR + SWIR).

a

Correlation	Band 1	Band 2	Band 3	Band 4	Band 5	Band 6	Band 7	Band 8	Band 9
Band 1	1	0.979	0.795	0.804	0.845	0.845	0.860	0.856	0.810
Band 2	0.979	1	0.798	0.828	0.874	0.875	0.890	0.889	0.852
Band 3	0.795	0.798	1	0.820	0.776	0.777	0.778	0.765	0.742
Band 4	0.804	0.828	0.820	1	0.951	0.958	0.951	0.932	0.897
Band 5	0.846	0.874	0.776	0.951	1	0.992	0.989	0.985	0.962
Band 6	0.845	0.875	0.777	0.958	0.992	1	0.989	0.986	0.960
Band 7	0.860	0.887	0.778	0.951	0.989	0.989	1	0.992	0.957
Band 8	0.856	0.889	0.768	0.933	0.985	0.986	0.992	1	0.974
Band 9	0.810	0.852	0.742	0.898	0.962	0.960	0.957	0.974	1

b

Eigenvector	PC1	PC 2	PC 3	PC 4	PC 5	PC 6	PC 7	PC 8	PC 9
Band 1	0.568	0.664	0.470	0.109	0.033	0.032	0.029	0.022	0.015
Band 2	-0.313	-0.362	0.875	0.066	0.001	0.001	-0.001	-0.003	-0.001
Band 3	-0.733	0.592	-0.04	0.288	0.088	0.088	0.071	0.060	0.050
Band 4	-0.203	0.274	0.105	-0.858	-0.208	-0.205	-0.174	-0.120	-0.078
Band 5	0.012	-0.041	0.018	-0.400	0.505	0.427	0.392	0.372	0.330
Band 6	-0.008	0.007	0.002	-0.058	0.466	0.241	0.057	-0.346	-0.773
Band 7	-0.005	0.001	0.002	-0.012	-0.372	-0.233	0.725	0.350	-0.399
Band 8	-0.001	0.001	-0.001	0.026	0.568	-0.806	0.112	-0.033	0.113
Band 9	0.001	-0.002	0.000	0.014	0.118	-0.067	-0.519	0.774	-0.335
Covariance									
Eigenvalue	575.55	46.562	5.049	2.446	0.136	0.011	0.009	0.006	0.00177
Variance	91.390	7.3935	0.802	0.388	0.0215	0.002	0.001	0.001	0.0002811

c

Table 3-4 indicates principal component analysis results on 9 bands of VNIR+SWIR. Table 3-4-a shows basic statistic and in 3-4-c can see this components contain 91.39% of the variance of the nine bands.

Eigenvectors band 1 show PC1 and gives information mainly on albedo and topography. PC4 has higher loading of band 4(-0.858), this PC should detect Alteration minerals in dark pixel because of negative contribution of band 4, figure 3-9 indicate alteration areas in PC4 are dark. PC2 has a higher negative loading of band 2 (-0.362) and high positive loading of band 2 is in PC3, this PC can detect iron oxide alteration area, figure 3-9 show PC3 that can applied for iron oxide alteration in bright places. High positive contribution of band 1 (0.664) in PC2 can detect vegetation covered area.

The selective PCA also has been applied for the area and results have been indicated in table 3-5

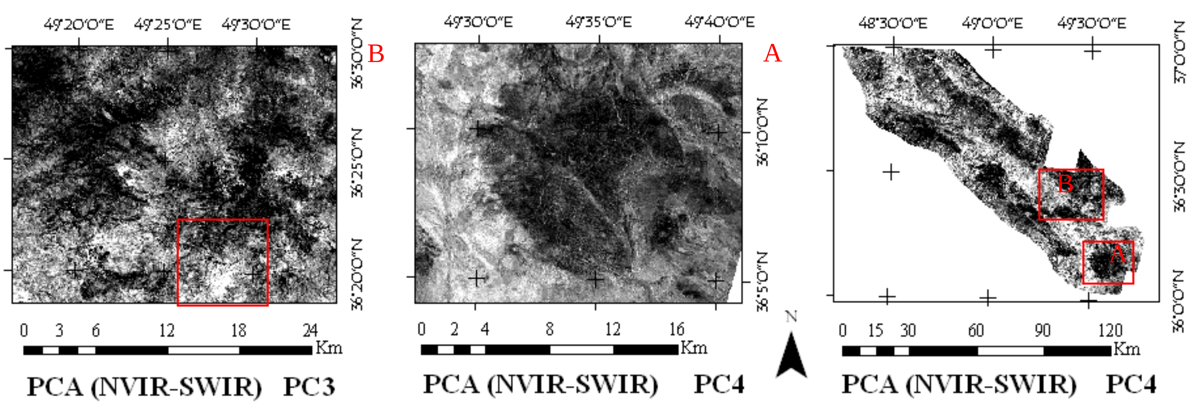

Figure 3-9: represent standard PCA images for recognition of hydrothermal alteration minerals.

and 3-6. Table 3-5 represent PCA results for six bands of SWIR in this table c can see PC1 has higher positive loading of band 4 (0.885) and this PC can discriminate alteration minerals in bright pixels because of positive contribution of band 4. PC6 has the lowest loading of band 4 (0.114) and can show hydrothermal alteration minerals in dark pixels. Table 3-6 represent result of selective PCA on bands 4, 5 and 7. In PC2 because of higher loading of band 4 (0.5799) can detect alunitic alteration area, this PC show this mineral with bright pixels due to positive contributions of band 4 and negative contributions of bands 5 and 7 (figure 3-10c).

In addition of mentioned selective PCA, principle component analysis has been done on 2, 5 and 8 bands and also on 4, 6 and 7 bands separately figure 3-10a and 3-10b show image result of them in PC1 and PC2 respectively. With regard to statics of PCA (4-6-7) in table 3-6, PC1 has higher loading of band 4 (0.94), so that can discriminate clay mineral with bright pixel due to positive contributions of band 4 and negative contribution of bands 6 and 7(figure 3-10a). Statics table of PCA (2-5-8) indicates that PC2 has higher loading of band 2 (0.58), so that can discriminate prophylitic zone with bright pixel due to positive contributions of band 2 and negative contribution of bands 5 and 8 (figure 3-10b).

Colour composition image can help in recognition of the terrains. Result images with 2% enhancement show variation in the images through the different coloring, with overlaying of extracted alteration area from geological maps can find out which colours accord to which alteration type (Kalinowski 2004).

That can look at individual PC images or display three PCs as a colour composite. Colour composition images of PC images are also useful for discriminating lithological units (Guo Liu 2009).

Figure 3-11 show colour composition for PC4-PC5-PC7 in red, green and blue respectively, that come from PCA results for SWIR (figure 3-11a) and also show PCA results for selective bands 4-5-7 in red, green and blue colours composition image (figure 3-11b). In figure 2-11, the rectangles A, B, C and D indicate alteration zones.

Basic Stats	Min	Max	Mean	St dev	Num	Eigenvalue
Band 4	0.489	55.220	16.310	3.045	1	1.793
Band 5	-0.135	17.879	5.0039	0.909	2	0.200
Band 6	-0.104	18.252	4.7371	0.877	3	0.011
Band 7	-0.017	17.279	4.1816	0.783	4	0.095
Band 8	-0.071	13.823	2.9840	0.601	5	0.064
Band 9	-0.242	10.207	2.2644	0.426	6	0.018

Table 3-5: represent in a general statistic b correlation matrix and c eigenvector for 6 bands (SWIR).

Correlation	Band4	Band5	Band 6	Band 7	Band 8	Band 9
Band 4	1	0.951	0.958	0.951	0.933	0.898
Band 5	0.951	1	0.992	0.989	0.985	0.962
Band 6	0.958	0.992	1	0.989	0.986	0.960-
Band 7	0.951	0.989	0.989	1	0.992	0.957
Band 8	0.933	0.985	0.986	0.992	1	0.974
Band 9	0.898	0.962	0.960	0.957	0.974	1

Eigenvector	PC1	PC2	PC3	PC 4	PC 5	PC 6
Band 4	0.885	0.256	0.249	0.221	0.167	0.114
Band 5	0.462	-0.469	-0.410	-0.399	-0.381	-0.305
Band 6	0.053	-0.376	-0.196	-0.199	0.274	0.838
Band 7	-0.007	0.493	0.269	-0.674	-0.406	0.257
Band 8	0.021	0.561	-0.808	0.141	-0.024	0.102
Band 9	-0.015	-0.124	0.071	0.528	-0.766	0.338
Covariance Eigenvalue	11.793	0.200	0.011	0.009	0.006	0.002
Variance(%)	98.098	1.661	0.094	0.080	0.053	0.015

In these images silicic alteration areas are recognized by bright yellow in colour composition image from PCA (4-5-7) for SWIR. Silicic alteration areas have red colour in PCA for selective bands 4-5-7. Alunitic alterations are discriminated by purple colour in PCA for selective bands 4-5-7. Orange colour in zone B of PCA for SWIR shows iron oxide alteration. A. M. Shafaroudi 2009 proposed using of colour composition of PC2 (4-6-7), PC2 (4-5-7) and PC3 (2-5-8) in red, green and blue colours respectively.

Basic Stats	Min	Max	Mean	Stdev
Band 4	0.489562	55.219601	16.310515	3.044901
Band 5	-0.135403	17.878914	5.003913	0.908728
Band 7	-0.016628	17.279345	4.181620	0.782619

Correlation	Band 4	Band 5	Band 7
Band 4	1.000000	0.951422	0.951388
Band 5	0.951422	1.000000	0.989329
Band 7	0.951388	0.989329	1.000000

Eigenvector	PC 1	PC 2	PC 3
Band 4	0.572248	0.579888	0.579881
Band 5	0.820081	-0.404362	-0.404919
Band 7	0.000326	-0.707263	0.706950
Covariance Eigenvalue	10.545438	0.10055	0.007277
Variance(%)	98.98785	0.943842	0.068308

Table 3-6: represent in a general statistic b correlation matrix and c eigenvector for 3 bands (4-5-7).

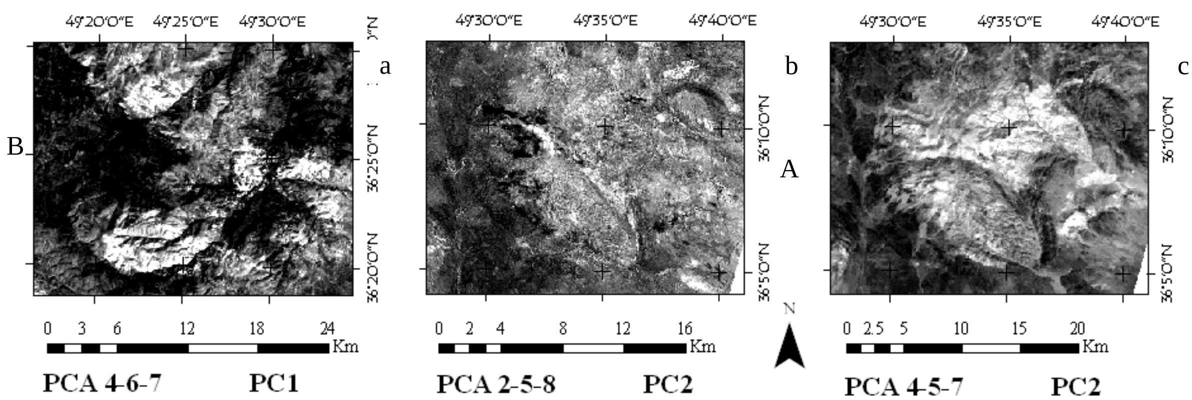

Figure 3-10: show selective PCA for recognition of the hydrothermal alteration minerals. b and c show rectangular area A and B in figure 3-9.

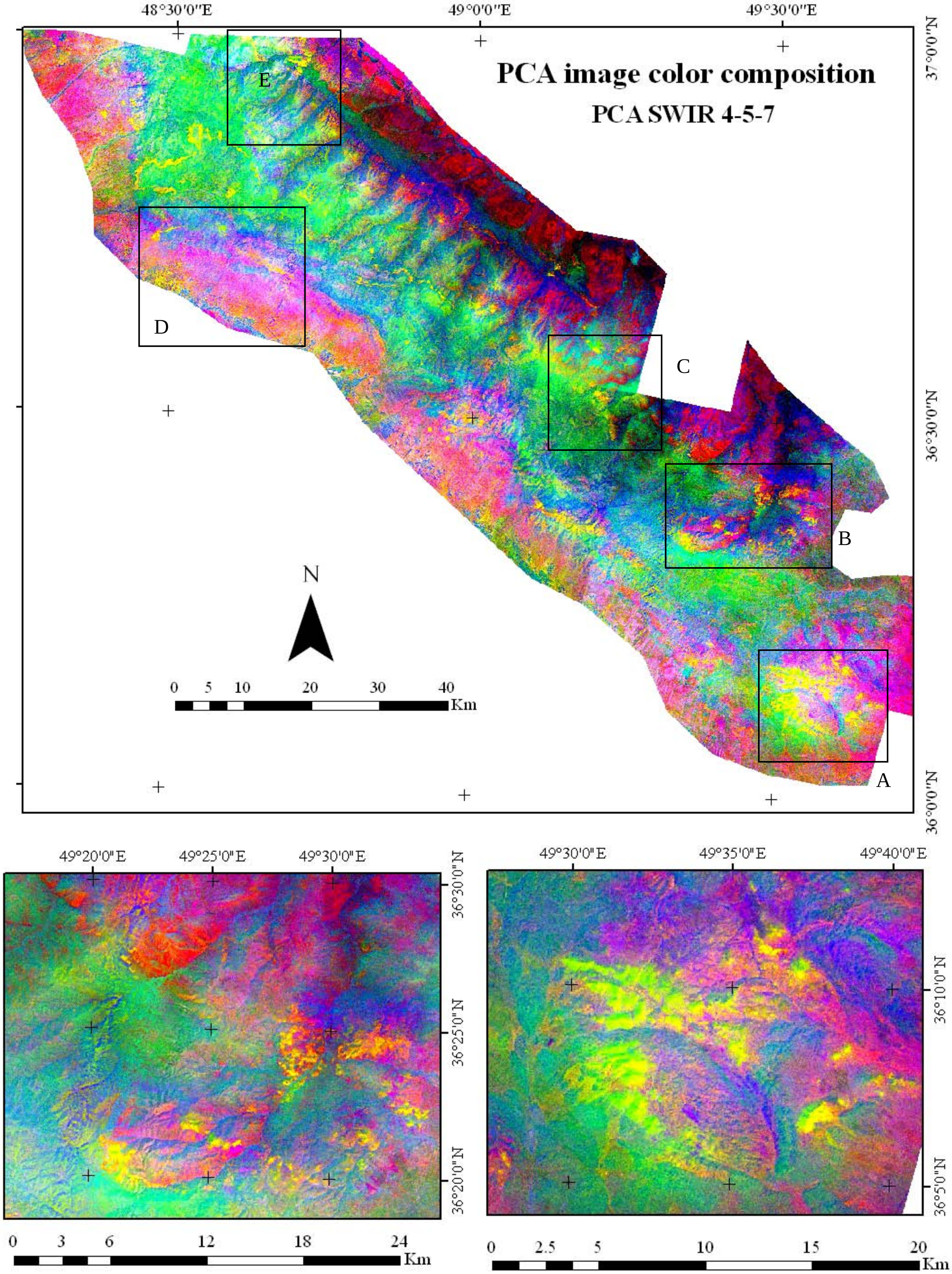

Figure 3-11a: represents colour composition images from PCA for 6 bands (SWIR), 2 alteration zones have been enlarged in the zones A and B, the yellow colour show silicic alteration area.

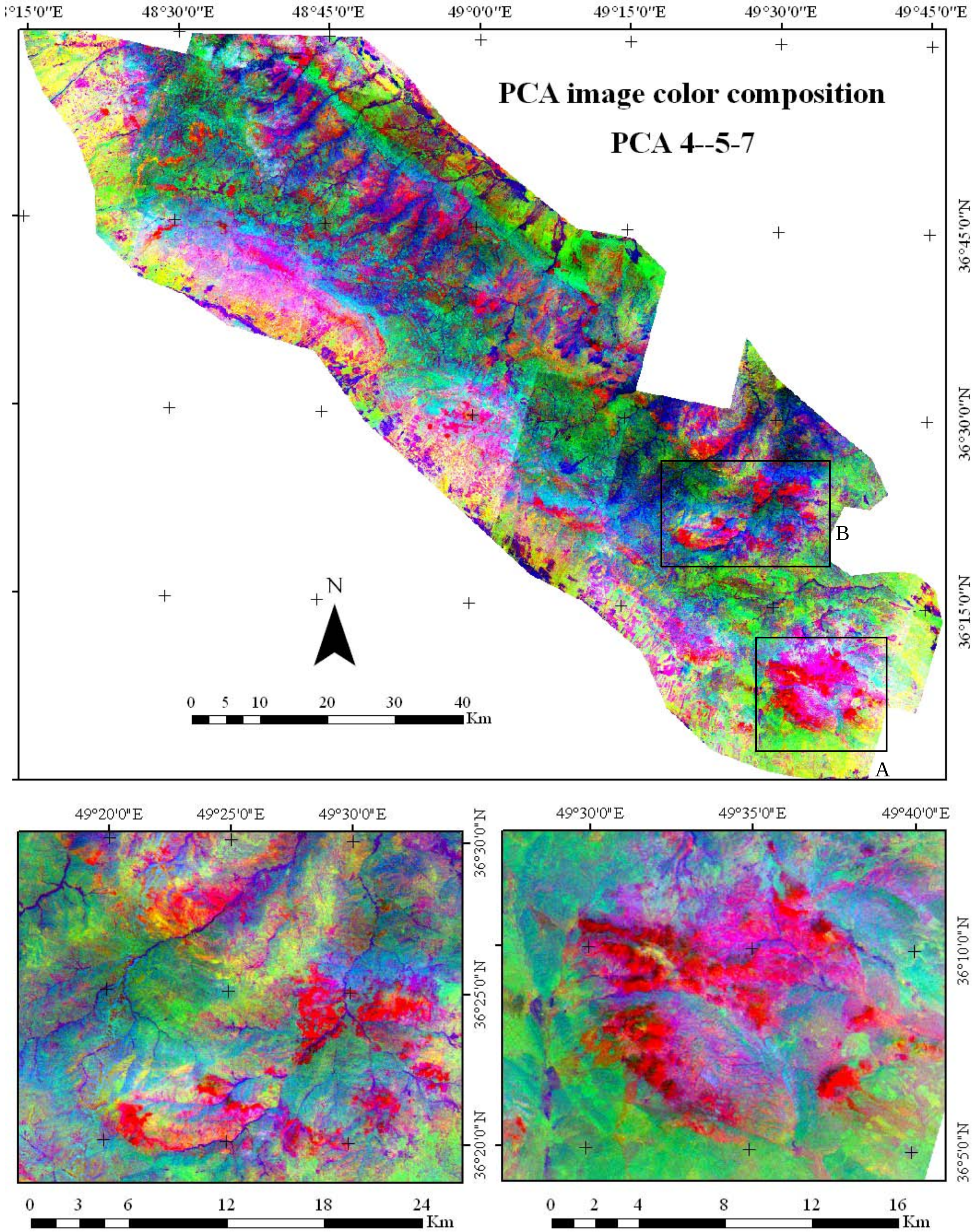

3-11 b: represent PCA for 3 selective bands (4-5-7), 2 alteration zones have been enlarged in the study area; zones A and B. red colour shows the area with silicic alteration. Light purple colour shows propylitic and sericitic alteration. Alunitic alterations can recognize by high purple colour.

3.3.2.4 Classification

After enhancement of geological feature we need to extract demanded data. Classification is one tool that remote sensing software offer to extract demanded data. There are two type classifications for multispectral imagery that consist of supervised and unsupervised classification. Sabine 1999 believe classification accuracies for lithological studies are mainly poor and cannot be compared by performance of experienced image interpreters. An expert can apply textural and contextual information with spectral information, and also with his/her geological knowledge. But a spectral classifier operates on pixel-by-pixel basis data and ignores contextual information. Sabine 1999 suggest neural net and fuzzy logic classification for improving of accuracy; these classifiers require too much training data from field measurements to be practical. For the study area there were not much training data hence fuzzy logic and neural net cannot be practical and accurate manner.

Various supervised classifications have been tried with different success, for the study area the Parallelepiped classifier results have more conformity with experimental interpretations. In figure 3-12 can see the results of Mahalanobis distance and Parallelepiped classification on PCA 4-5-7 on ASTER image. Figure 3-12a shows Mahalanobis Distance classification and figure 3-12b show Parallelepiped classification results. I have applied also neural net classification for the study area, but because of low accuracy in the training ROIs area, the result can only show silicic alteration area. In figure 3-12c, I have digitalized the alteration area manually by using geological information and comparing many data for interpretation. For digitalizing manually, I have considered to spectral classifications too. In classification have been distinguished 4 type alterations, that consist of silicic, alunitic, prophylitic-sericitic and iron oxide alteration.

There are similarities between quaternary sediments and phyllosilicates spectral reflectance in the images. That create mistakes to discriminate phyllosilicates from them, hence to eliminate them, geological maps are useful, quaternary sediments area have been eliminated in the classification processing or in digitalizing.

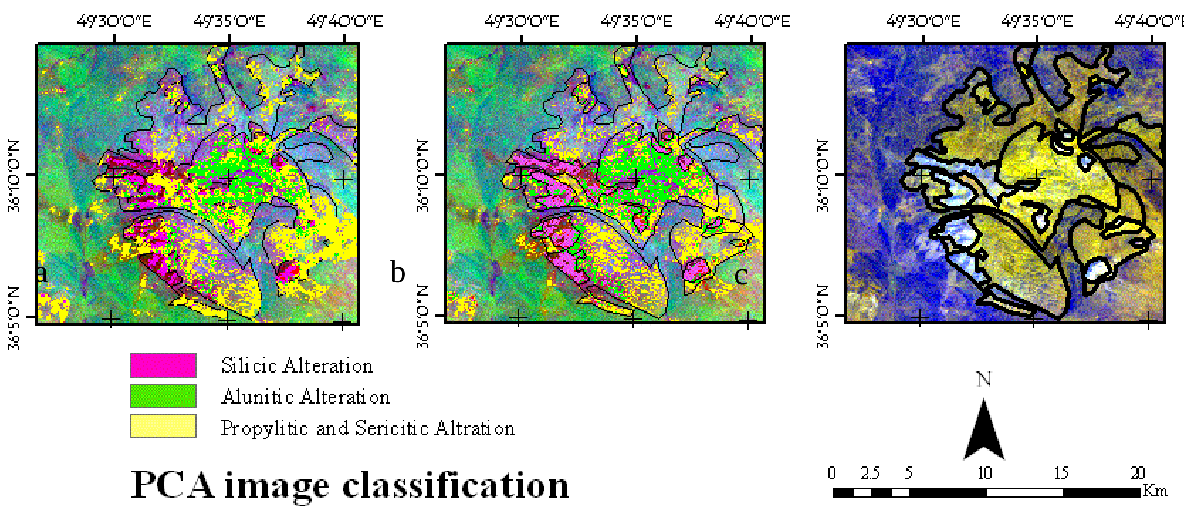

Figure 3-12: represent alteration classification in area A (figure 3-11). in a can see classification coming along Mahalanobis Distance and b show Parallelepiped classification results, in c alteration area have been digitalized by experimental interpretation with regards to classification results.

3.4 Geological maps

Already, chapter one has discussed about geological data as a basic data which can guide us for main strategy and treatment with data for mineral exploration. As mentioned in chapter one, the

study area cover 7 separate geological map sheets. Hence for making uniformity between them I have applied remote sensing data and geophysics data processing results.
With regards to geological maps of the study area main lithological units in the area contain basalts, andesite, tuff et cetera. In some place can see acidic to intermediate intrusive rocks table 1 in attachment indicate description of the units in 7 sheets and figure 1-4 show geological map, in this map all extrusive with pink colour to be indicated and intrusive rocks with red colour and quaternary sediments with yellow colour. Quaternary sediments occupy around of the igneous rocks and igneous rocks outcrop in southeast-northwest direction. In this direction, four great intrusive masses intrude in the volcanic rocks with similar compositions. The intrusive mass rocks that locate in southeast of the area, are associated by a big alteration zone. In this alteration zone there are silicic, propylitic, alunitic alteration beside phyllosilicates minerals. In right side of intrusive mass can see alteration minerals around and on the intrusive mass, but in left side the alteration minerals can see only on the intrusive masses, not the around.

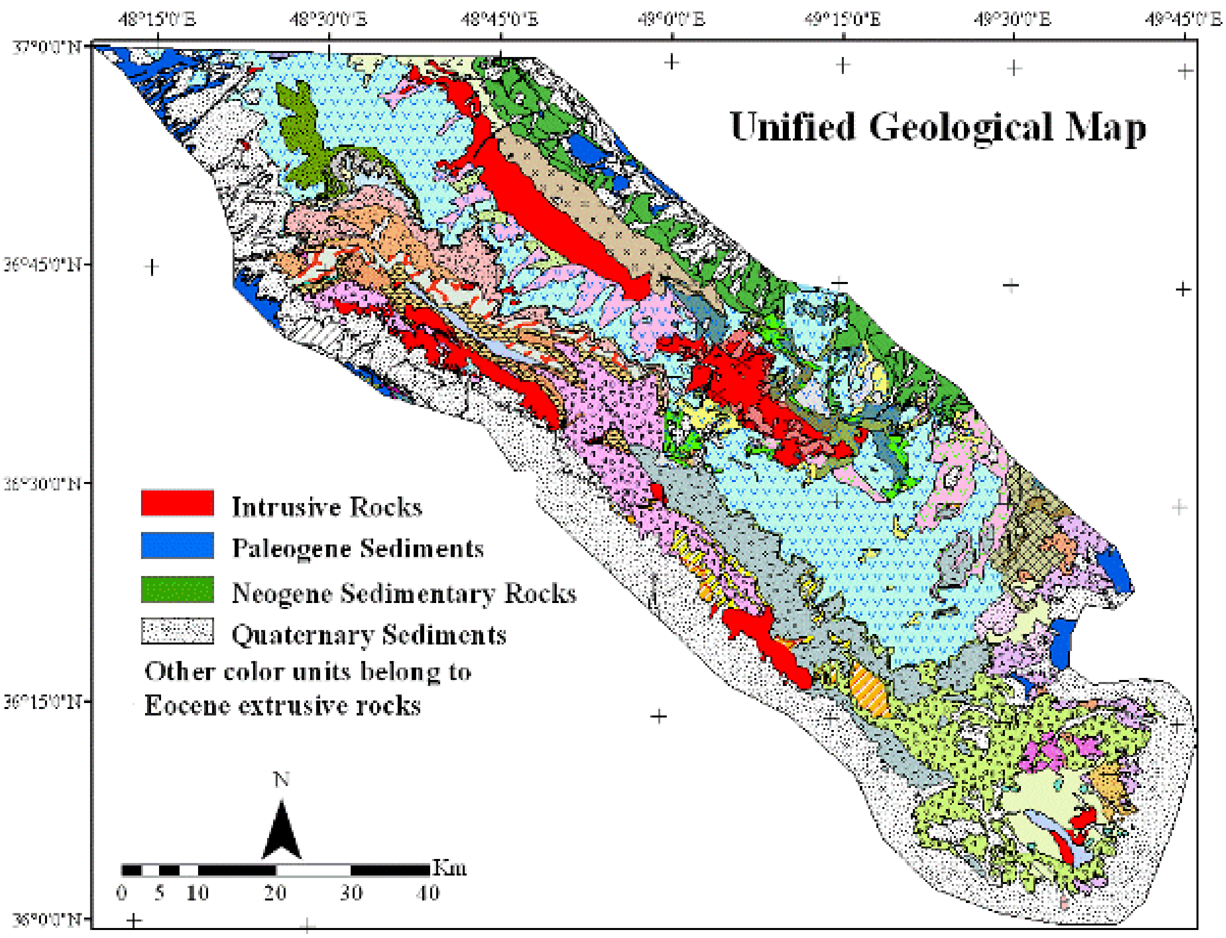

Figure 3-13: unified geological map, in this map can see have been distinguished colour units for intrusive rocks, quaternary, Paleogene, Neogene sedimentary rocks and other colour units belong to Eocene extrusive rocks.

ASTER images and some techniques that have been applied for enhancing of alteration area, in this case also can be used. False colour composition, band ratios, band ratios colour compositions, PCA technique etcetera also can help to enhance lithological feature to discrimination of them. Table 3-7 shows some additional band ratios to discriminate silicate rocks.

Feature	Band or Ratio	Comments
Quartz rich rocks	14/12	
Silica	(11x11)/10/12	
Basic degree index (gnt, cpx, epi, chl)	12/13	Exoskarn (gnt, px)
SiO2	13/12	Same as 14/12
SiO_2	12/13	
Siliceous rocks	(11x11)/(10x12)	
Silica	11/10	
Silica	11/12	
Silica	13/10	

Table 3-7: present some band ratio can help for recognition of lithological units and in this research have been applied. (Kalinowski 2004)

Already table 3-3 and 3-2 have mentioned band ratios and colour composition orders for alteration area and lithological discrimination. Figure 3-13 indicate unified lithological map of the area after digitalizing some units and removing some of them and editing of some boundaries with more conformity to ASTER images.

3.5 Index points

The area with this high potential for mineralization could be many historical mines and so can see many inactive mines in different places. The inactive mines contain copper, lead, zinc minerals majorly and sometimes iron and gold minerals. The mines Ab_barik and Zeh_Abad are two mines among them for extracting Cu ore deposits, these mines have been abandoned recently and they are inactive yet. Still there are some kaolinite and alunite mines that are active, beside their porcelain factories. Recently an Au ore deposit district in south east of the area has been detected by GIS studies.

In addition of mine points there are some samples that have been collected by geologists from the area with high amount of Au, Pb-Zn, and Cu minerals in different part of the area. This data have been reported in literatures like geological reports for maps, some student thesis, and different reports that have been provided by geological survey of Iran. In this research, I collected the information about this mines and samples from these literatures. The all collected data was ordered as point file with coordinates in UTM system. due to different reference for these data, in this layer can be seen some discordances in coordinates between points so have been tried to extract all points and then via comparing of them that were classified to mines and index points for samples with reliable and less reliable groups. The mines and index points have been acquired to do interpretation on geological, geophysical and RS data. These index points give view for an expert to choose favorable data to derivation and also give view to give weight scores to data units for integrations. For example if an expert see some indexes points outcrop in the special lithological unit this lithological unit can have more score in weighting, or there are more index points on structures with northwest-southeast direction so these structure can take more scores in weighting.

3.6 The Geophysics data

Among the geological data geophysics data has important place for prospecting. Geophysics studies are done either on the ground surface directly or like remote sensing image that are done by airborne remotely. The airborne geophysical data is accessible for the study area. The airborne geophysical data have been provided during two different surveys by GSI (1974-1977) and AEOI (Atomic Energy Organization of Iran 1977-1978). For the study area GSI have provided only magnetic data to achieve more information about regional tectonic and geology. This regional information has been applied in big scale to recognition of important favorable zone for deposits and Hydrocarbon fuel exploration. Figure 3-14 indicate the lineament

structure in big scale that provided by this regional surveying. Aero Service (Houston, Texas) have done the flights, flight lines are in N–S orient, Control flight lines are in E–W orient whiles mineralization zones have NW-SE trend and distance between flight lines are 7.5 Km and control lines are 40 Km. A twin engine airplane survey the area with a high-sensitivity cesium vapor magnetometer sensor that was installed on it with sensitivity of 0.02 nT (nanotesla). During flights, Barometric altimeters changed between 7000 foot in the mountains and flatlands in differential GPS navigation system.
Magnetic lineament in figure 3-14 based on results obtained from an aeromagnetic survey, magnetic lineaments are traced. Lineaments are interpreted using Werner disconsolation in conjunction with total magnetic intensity maps and existence of continuity or discontinuity of both magnetic anomalies and calculation of depth of magnetic sources. Most of the traced magnetic lineaments correlate well with previously mapped faults, and the continuation of those faults are traced where the surface is covered by the younger sediments, in addition, completely unrecognized lineaments are traced which they have contributed either in young sediments or deep basement, However the interpreted lineaments based on their contributions such as depth, displacement and other events are classified into the five groups Magnetic lineaments, possible fault. Sense of movement unknown, most of the lineaments, which are, interpreted in this group they might indicate the contact-between layers. Magnetic lineaments, which play an important role on regional geology or tectonics, but recognition the exact nature of the lineament requires, more detailed geological and geophysical investigations.
The area has been surveyed to achieve radiometry and magnetometery data by Rotary airborne

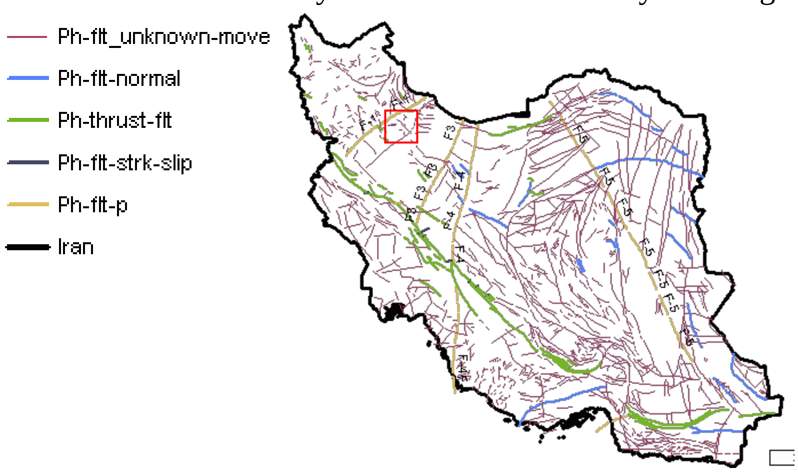

Figure 3-14: represent magnetic lineament of Iran and red rectangle show the study area with major NW-SE trend of magnetic lineaments.

and Fix Wing Aircraft during 1976 till end of 1978. The outcome data consist of magnetometric measurements and Gamma radiometric measurements. Gamma radiometric measurements provide distribution of the elements U, Th and K. Magnetometric and radiometric sensor record data digitally in different formats contain: raw, xyz; the data can be found on analogue chart and stacked profiles. Airborne data, as a huge data is the main part of Geo data. Nominal flight altitude is 120 m, line spacing 500 m and tie line spacing 10 times more than line spacing, spaced of 5,000 m. The altitude of the electromagnetometer was monitored by a PS100E laser platform.
Magnitudes of magnetic fields on the earth surface are affected by magnetism of earth core, material of crust and near crust of the earth. Even other planets' magnetism effects on the amount of magnetic fields' magnitude. In mineral exploration, crustal affects and near crustal materials affects are important so others should be eliminated. Hence that is necessary to do some correction on the initial geophysics data before processing and interpretations. IGRF correction (International Geomagnetic Reference Field) and other corrections are performed daily when the area surveyed. After these corrections remain magnetic fields that are related to

crustal and near crustal materials. Cosmic correction is the effect of cosmic radiation that is removed from each window by multiplying the cosmic channel by the cosmic stripping factor for each window and subtracting the result from the window data. Dead time is definite time that spectrometer don’t show reaction of gamma ray change to process each pulse from the detectors so Dead time correction remove that.
Emitted radon gas from the earth surface cause problem in detecting of emitted gamma ray from the earth so radon correction removes effect of this gas by upward-looking detectors. Sometimes emitted gamma ray from radioactive elements (potassium, thorium and uranium) are scattered and that is possible to be recorded interchangeably so Compton Effect correction remove this effects from the data. Another correction performs for increasing elevation effects, air between earth surface and magnetometer sensor absorb the gamma ray so absorption increase by increasing of elevation. This correction is used for removing elevation change effects. Measurement unit for gamma ray is cps (cycles per second) that convert to percentage for potassium and thorium and uranium to ppm.
Altitudes of flights are important in resolution of data. When the flight altitude becomes lesser, sensors can receive even small structures with high accuracy. With increasing of the altitude, sensors can receive bigger magnetic field sources and deeper. Flight line distance are also important, in low line distance sensors can record smaller anomalies too. Emitted gamma rays from potassium, thorium and uranium elements are related to near surface of the earth in maximum 35 cm deep. So this information is useful for lithology of surface rocks and alteration area.
For interpretation of magnetic data, filters have been used on Total Magnetic Intensity data (TMI). Filters include in vertical first derivation, analytic signal, reduce to the pole and upward continuation. In radiometric data; lineal composition and ratio of them can reach to some information about lithology and alteration area. Favorable area for mineral exploration can be extracted also by integration of radiometric data and magnetic data.

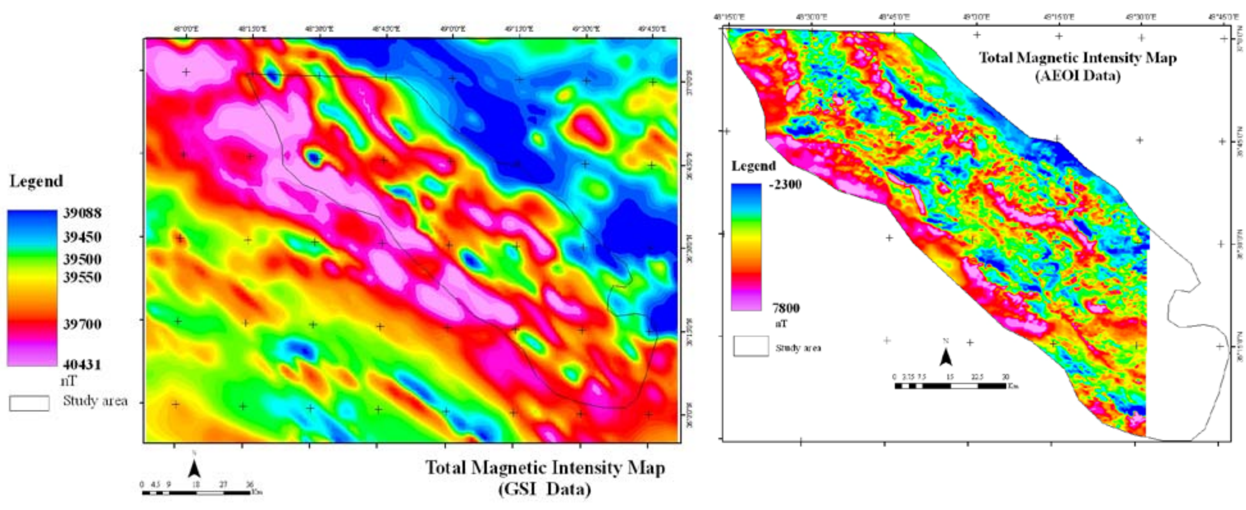

Figure 3-15: represent Total Magnetic Intensity, the main trend of magnetic sources are in NW_ES direction, left side data relate to GSI flights and right side relate to AEOI flights.

Magnetic and radiometric data from AEOI cover five geological map sheets in scale 1/100,000. There are'nt data from source AEOI to Takestan and Jirandeh sheets in east of the area. But magnetic data from GSI cover all the study area. Figure 3-15 represent magnetic data from GSI and AEOI flights, the main trend of magnetic sources are in NW_ES direction. Data are in grid formats and to be represented by false-colour images in maps, the false-colour layer ranges from pink to yellow and green to blue. Pink colour represent areas of the earth's crust which contain high anomaly of magnetic and radiometric range. The blue colour shows which areas that have very little magnetic and radiometric susceptibility. The grid file can be converted to database file, figure 3-16 represent an instance of grid file and its database with profile in the Geosoft software. Processes and filters have been done on both grid and database channels for enhancement of favorite data.

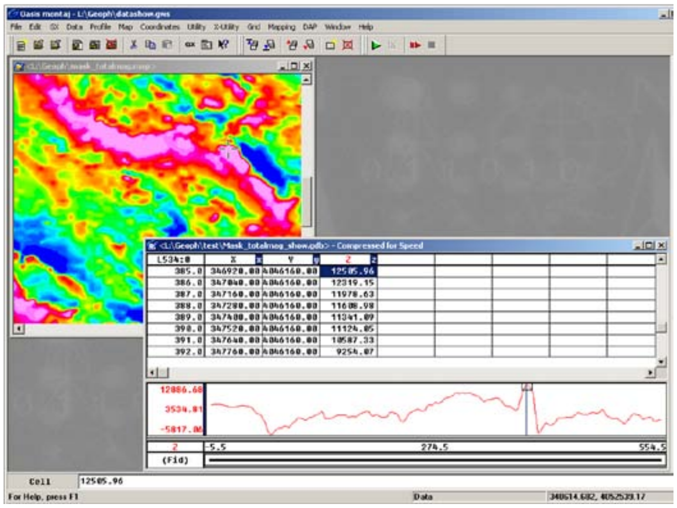

Figure 3-16: represent a part of Geosoft software and windows for grid and data. The grids can convert to data base. In data base can see pointer located on line 534 on cell 385 by coordinate of x and y. Channel z in this data base relate to amount of magnetic intensity.

3.6.1 Total Magnetic Intensity (TMI) data

Total Magnetic Intensity is abbreviated by TMI; TMI data show distribution of magnetic susceptible minerals in earth crust. Figure 3-15 represent Total Magnetic Intensity (TMI) grid map for the area, total magnetic intensity is the combined reading from all magnetically susceptible minerals within the earth's crust down to a depth of 10 km or the Curie Point, in Curie Point minerals lose their magnetic susceptibilities. Magnetic intensity is measured in nanoTeslas (nT) and the earth has a background magnetic susceptibility which varies in strength from about 25,000 nT in equatorial regions to about 70,000 nT at the poles. The strength of individual anomalies can range from a few tens nT over deep metamorphic bodies to several hundred nT over basic intrusions or even several thousand nT over magnetite ores (Kearey and Brooks, 1991). Figure 3-15 represent Total Magnetic Intensity for the study area and channel z in figure 3-16 represent the magnetic intensity's amounts. Geosoft software presents some tools to extract more special information to interpretation. There are methods that data can give an idea of magnetic mineral distribution at certain depths. These methods are called depth slicing or upward-downward continuation. A vertical derivative filter is used to enhance the geological feature which is close to the surface. Vertical derivative filter results detect the edges of magnetic bodies better than the TMI image. Reduce to the pole filter have been applied on this aeromagnetic data for next processes also. The next sections explain some of these methods that I use for enhancement of some features.

3.6.1.1 Reduce to the magnetic Pole (RTP) filter

The shape of any magnetic anomaly depends on the inclination and declination of the main magnetic field on the ground. Thus the same magnetic body will produce an anomaly with different shape depending on where it happens and its orientation. The reduce to the magnetic pole filter reconstruct the magnetic field of a data set how it located in the pole. This means that data can be viewed in map form with a vertical magnetic field inclination and a declination of zero (Macleod et al., 1993).

Since the Reduce To the magnetic Pole (RTP) filter works on the phase as well as the amplitude the power spectrum of the reduced field and the shape of the amplitude portion of the filter is not very useful .This type of filtering only works at magnetic data that its latitudes are greater than 30 degrees.

$$L(\theta)=\frac{1}{[\sin(I_\alpha)+i\cos(I).\cos(D-\theta)]^2}, \text{if}\,(|I_\alpha|<|I|), I_\alpha = I \qquad (3\text{-}1)$$

Where:

I: geomagnetic inclination, Iα: inclination for amplitude correction (never less I).

D: geomagnetic declination

Iα: Inclination to be used for the amplitude correction. Default is 20 degrees. If |Ia| is specified to be less then |I|, it is set to I.

Average declination and inclination are 2.365411, 53.61354 respectively, that have been calculated by IGRF 1975 model. Average magnitude for total magnetic is calculated 46290.16 nanoTesla (nT) by IGRF 1975 model.

Figure 3-17 show RTP anomalies which have been replaced toward the North Pole relative to TMI. Intensity position in some place changed and that is common but the general trend of the structure is the same and there aren't changing in the structures form of anomalies. Generally this grid files are applied as the base grid files for other filters processing. On figure 3-17 lineament and place of some outcropped intrusive rocks have been represented. Intrusive mass rocks in area A, B, C and D can see on the magnetic anomalies, left picture data relate to GSI flights and right picture data relate to AEOI flights. Anomalies in the area in this map also show main trend NW-SE that mentioned already in lithological units. TMI in the both outside of the area have been increased and that can be seen majority in blue and green colours (figure 3-17). In other words the area enclosed by low magnetic intensity, lithological units in both outside area include sedimentary rocks, in both side can see Quaternary sediments but in right side sedimentary rocks are more related to Neogene sedimentary rocks. There is another low intensity trend in the center of the area with direction NW-SE; this trend has conformity with

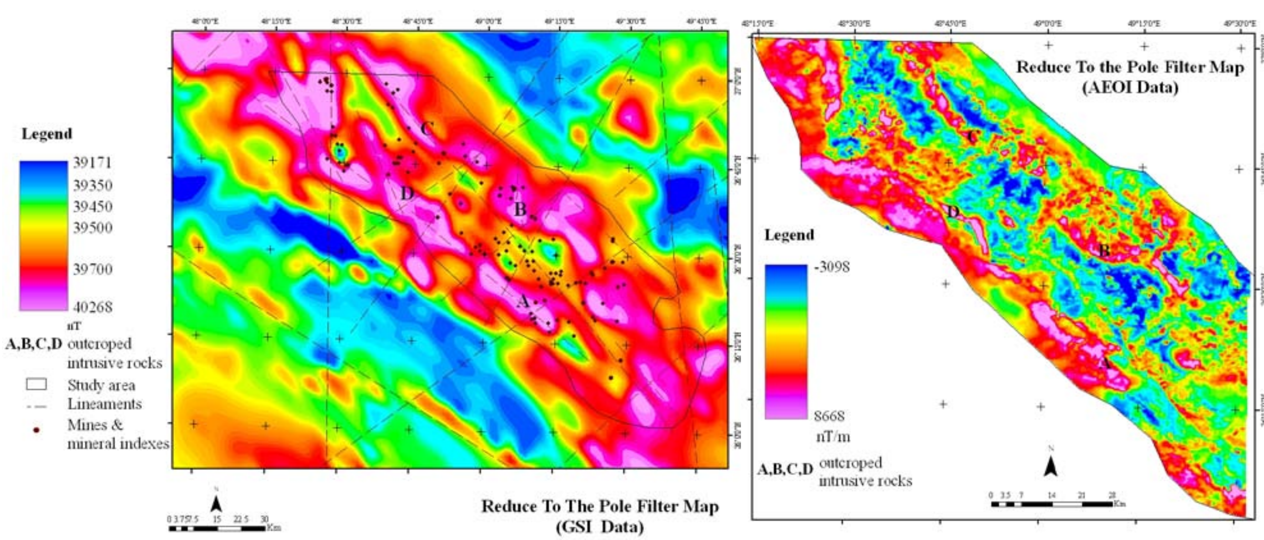

Figure 3-17: represent RTP grid map, left side data relate to GSI flights and right side relate to AEOI flights. Extracted lineament and Index point can be seen on the GSI data.

main trends. Majorly lithological units in this district (central area) are volcanic rocks that associated with tuff, pyroclastic and sedimentary rocks. In both side of the central district there are trends of high magnetic intensity; this districts associated with intrusive rocks. The main four intrusive mass A; B, C and D outcropped in these districts (figure 3-17). Whoever there are other small outcropped in these trends but in central trend only can see a small outcropped intrusive rocks on the small magnetic anomaly. Points on the map show old mine and mineral indices; those also have the same trend. Index points located more on the right side over high anomaly trend, and can see some of them on the central trend, on the left side anomaly trend there are index points but less than right side relatively.

3.6.1.2 Vertical Derivative (VD) filter

Spatial resolution can also be achieved by using the Vertical Derivative or Derivation in the z Direction filter. The vertical derivative filter calculates the vertical rate of change in the magnetic field. The VD filter applies z channel of total magnetic intensity data base and is common to enhance the shallowest geologic source in the data. That enhances the high-wave number components of the spectrums. In addition low-pass filter must be applied to remove high-wave number noise.

The following expression 3-2 computes channel z in this filter:

$$L(r) = r^n \qquad (3\text{-}2)$$

n: Order of differentiation,

r: Wave number (radians/unit), $r = 2\pi k$, where k is cycles/unit.

The results represented in new z channel in nT/m unit. Figure 3-18 shows grid result of this filter, in this grid trends are clearer and has been used for extraction of lineament. In addition outcropped intrusive rocks are superposed on the anomalies with more distinct boundary.

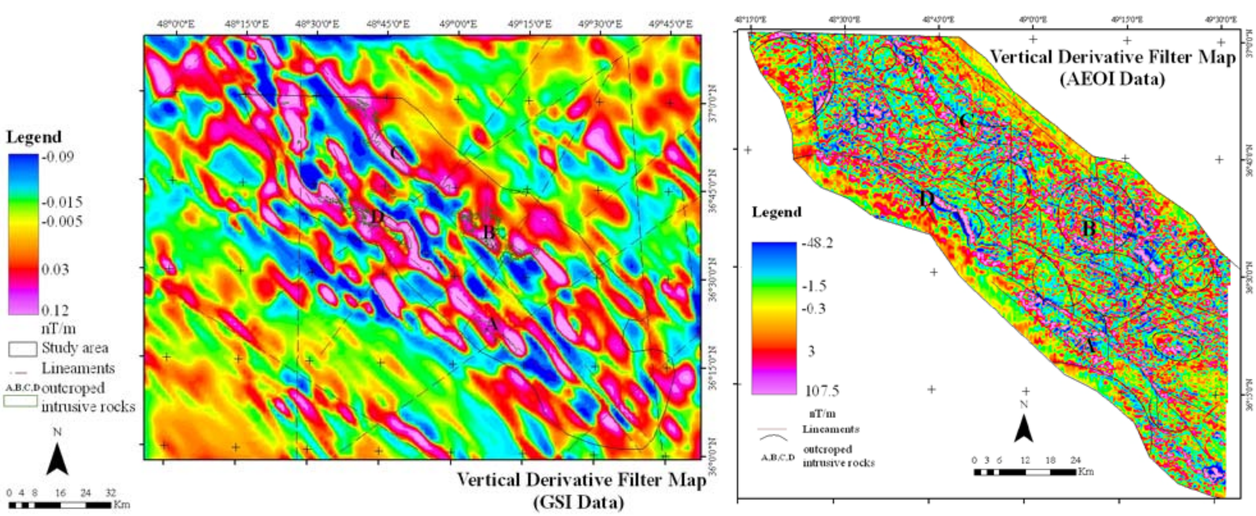

Figure 3-18: Show Vertical Derivative (VD) filter results in grid maps, left side data relate to GSI flights and right side relate to AEOI flights. VD grid data and RTP grid data have been used to draw lineaments.

3.6.1.3 Analytic Signal (AS) filter

This filter calculates the analytic signal of channel z in RTP data base. The analytic signal can be useful for locating the edges of remanent magnetized bodies and in area of low magnetic latitude (Macleod et al., 1993). Nabighan 1972 indicated that the analytic signal peaks occur over the edge of magnetic bodies. Peaks of the grids in great source magnetic bodies show edge of the bodies and boundary of them but in long linear sources peaks lie on center of the sources and show the trends.

The analytic signal (AS) is the square root of the sum of the squares of the derivatives in the x, y and z direction, analytic signal of a profile is defined as expression 3-3:

$$as = \sqrt{dz.dz + dx.dx + dy.dy} \qquad (3\text{-}3)$$

Where:

dz   is the vertical derivative

dx, dy   is the horizontal derivative

I apply AS filter on total magnetic intensity and Figure 3-19 represents grid map of analytic signal filter and can see changes in three directions. In the data from GSI; the distance of flight lines are great hence the information have low accuracy however some lineaments indicate the trends in center of the anomalies. AEOI data shows more details figure 3-19 right side map indicate grid map of AS filter on AEOI data. Lineaments extracted from this data and VD filter map in some locations they match to boundaries of intrusive rocks. This filter have been used often for define 3D information and extracting of depth to base. I applied AS filter results to interpretation and to extract shallow bodies too.

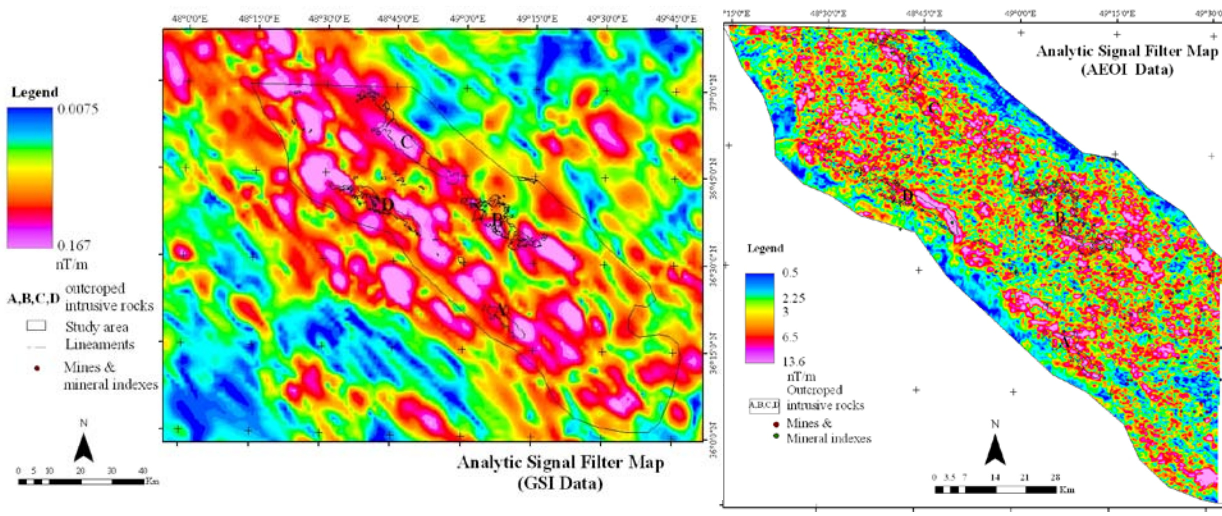

Figure 3-19: shows Analytic Signal (AS) filter results grids this data beside of UC filter results can help to pull out shallow bodies.

3.6.1.4 Upward Continuation filter

This filter applies RTP results, this filter is used often to remove or minimize the effect of shallow sources and noise, this technique to isolate deep against shallow sources. Upward Continuation filter cause low wave-number anomalies to be amplified against of high wave-number anomalies hence deeper anomaly sources can be enhanced by this filter. Following expression 3-4 applies in this filter:

$$L(r) = e^{-hr} \qquad (3\text{-}4)$$

h   the distance, in ground units, to continue up relative to the plane of observation.

r   wave-number (radians/ground_unit). r= 2πk, where k is cycle/ground_unit.

Continuation distance for GSI data 600 m and for AEOI data 200m have been applied and figure 3-20 result of the filter. In these maps can see two trend but anomalies expanded in periphery with halo that show the anomaly sources continued in deeper around of the high anomalies.

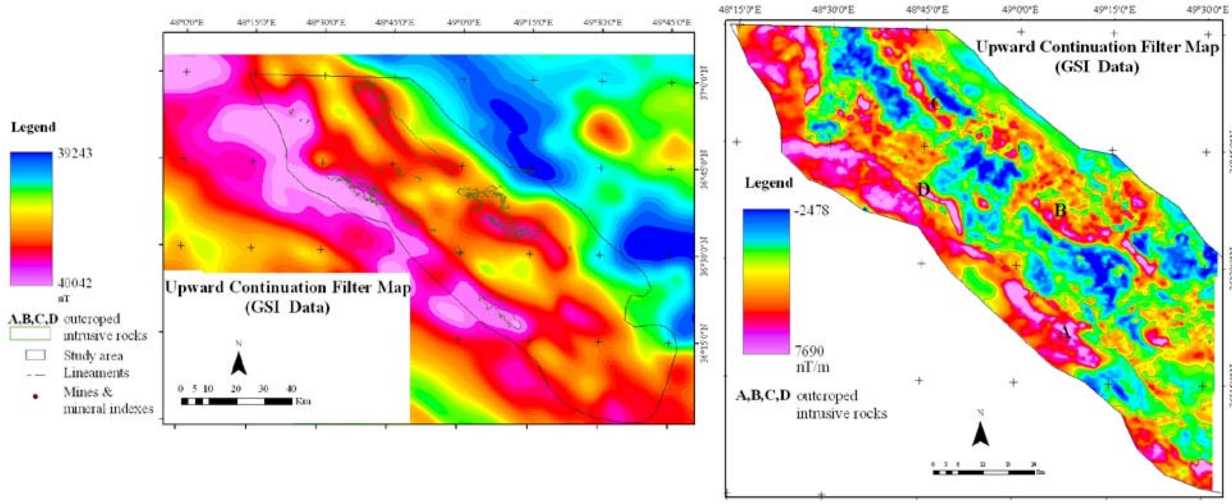

Figure 3-20: shows Upward Continuation filter results grid, this data beside of SA filter results and radiometric data have been applied to pull out of shallow bodies.

3.6.1.5 Structural analyses

Extracted structures from geophysics data include lineaments structures. Lineament in geophysics is defined by long narrow feature. These features in geology include faults, dikes, contact of lithological units and smashed zones. In some place, adjacent geological units drop dawn and rise up by faults like horst and graben structures these structures appear as lineaments on the earth surface. Due to considerable permeability in these phenomena, there are appropriate environments to pass fluids that include minerals. In such environments also there are free spaces between smashed rock pieces so minerals can deposit there.

On these phenomena, magnetic intensities change by settlement of some materials that come from fluids in addition of magma settlement. Hence these regions can be distinguished by the magnetic intensity changing.

Important lineament phenomena that can create appropriate locations for mineralization include: 1.fault structures with magnetic mineralization, 2. fault structures that has been lost magnetic minerals by leaching of hydrothermal liquids, 3. magnetic block edges that have displacements in perpendicular and horizontal direction, 4. smashed zone on the earth surface and 5. Ring structure lineaments can be appeared due to vertical displacement of magnetic sources. That should be considered; intersections of lineaments make more suitable conditions for mineral deposit and detection of intersections are helpful for prospecting too.

Figure 3-21 represent extracted lineament by interpretation of induced grids from total magnetic intensity data. More lineaments in the area have NW-SE trend according on the main trend of the area. In addition of straight oriented lineaments some ring structures and curved structures have been detected and presented in Figure 3-21. I have applied DEM data for extracting of faults and ring structure too. Figure 3-22 a, b, c illustrate some lineament and ring structure on outcropped intrusive rocks in south part of Rudbar map sheet, those indicate accordance between these structures on DEM map and ASTER image. Structural features in ASTER images, DEM data and geophysics data are match, figure 3-22 a, b and c show a part of the study area that can see this accordance too. Figure 3-21 and 3-22 represent index point also on the other grid data, here can see conformity between index point and structures.

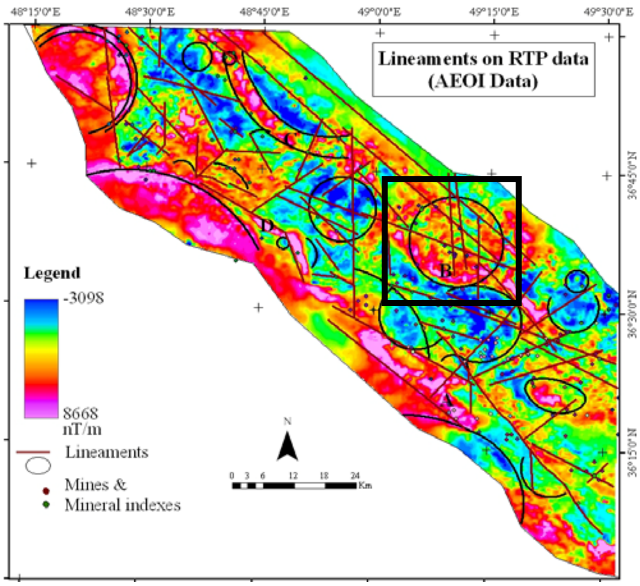

Figure 3-21: lineaments include straight lines, ring and curved structure on the RTP have been displayed.

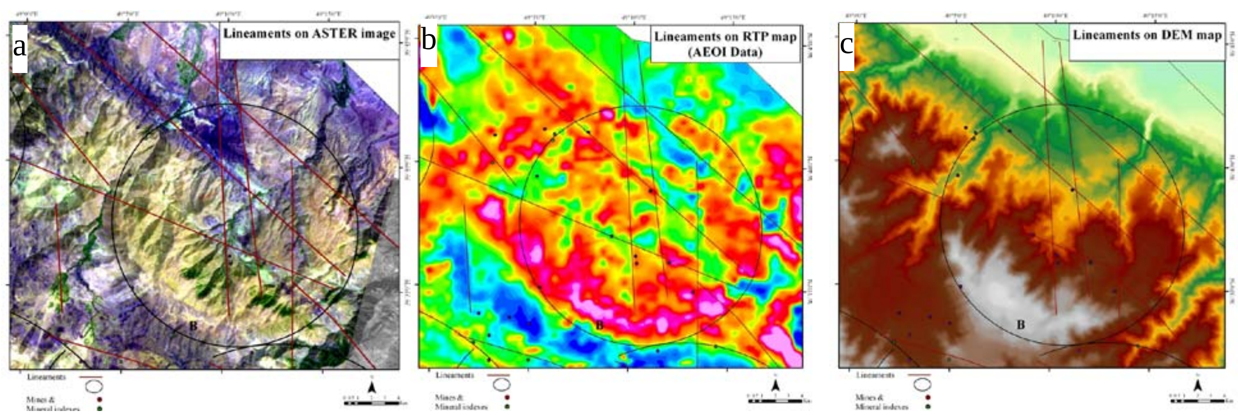

Figure 3-22 the quadrangle area on figure 2-21 have been enlarged to represent more details a show Magnetic lineament on ASTER image band c respectively display these lineament on the RTP and DEM map, apparently can see accordance between three data.

In more case, index points have been located on or outside of ring structures and curved structures that enclose high magnetic intensities but in the case of figure 3-22 can also see index points inside part of ring structure on the straight lineaments.

In the ring structures that have been enclosed by low magnetic intensity; index points can be seen more on the lineaments and inside part related to straight lines. Straight lines structures have been located on low magnetic and high magnetic anomalies but index points are situated more around of straight lines in high anomalies.

3.6.2 Radiometric data

These gamma radiations are emitted by three naturally occurring elements potassium (K), Thorium (Th) and Uranium (U). These three radioactive elements have the most abundance among other naturally occurring radioactive elements on the earth's surface. The data have been used for unifying of lithological units from geological map sheets in scale 1/100,000 and on the other hand for detection of alteration area. AEOI have provided these data for the area beside total magnetic intensity, by GSI flights gamma radiations data is not accessible. Figure 3-23 represent maps of distribution of radioactive elements K, Th and U, in a, b and c respectively. Natural gamma radiations come from the earth's surface depth about 30 cm. In the picture light pink indicate high potential K, Th and U; dark blue show low potential for K, Th and U. As we can see, the area with A, B, C and D title are intrusive rocks area, these area show high potential for radiometric elements. Low potential areas are more related to volcanic rocks.

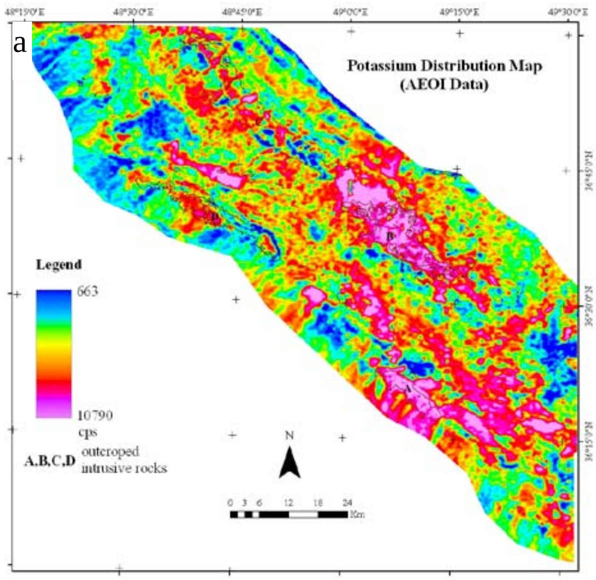

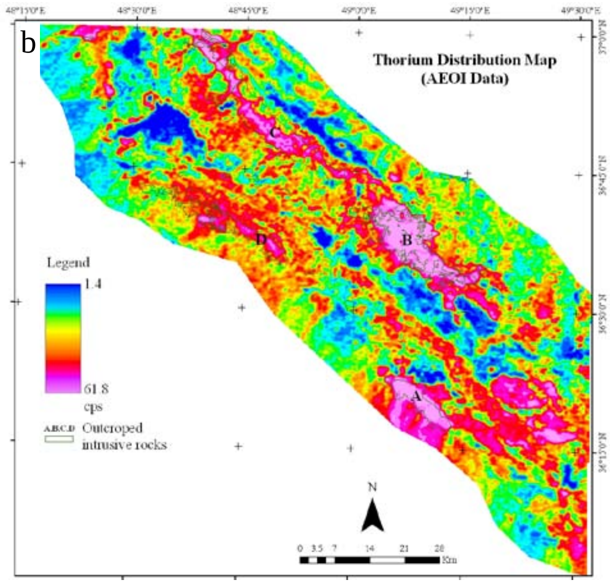

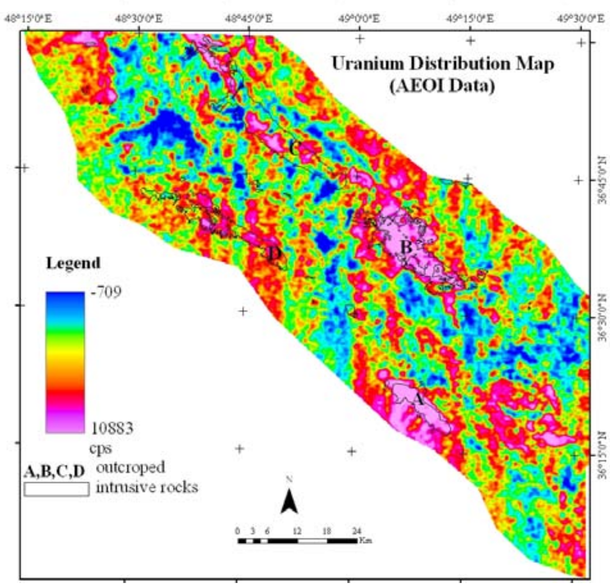

Figure 3-23: a, b, c show radiometric data K, Th and U respectively. In the picture Light pink indicate high potential for Th, U, and K; dark blue show low potential for Th, U, and K. As we can see, the area with A, B, C and D title are intrusive rocks area, these area show high potential for radiometric elements. Low potential areas are more related to volcanic rocks.

The varying concentrations and distribution of radiometric K, Th and U provide an indication of soil and rock characteristics. Potassium is a major constituent of most rocks and is a common alteration element in certain types of mineral deposits. Uranium and thorium are present in trace amounts, as mobile and relatively immobile elements, respectively. As the concentration of these different radioactive elements varies between different rock types, we can use the information provided by a gamma-ray spectrometer to map the rocks where the 'normal' radioactive element signature of a host rock is altered by a mineralizing system.

In figure 3-23b; Th distribution indicate good accordance to outcropped intrusive rocks especially in intrusive masses A and B, however C and D indicate relatively this conformity. Like this conformity can be seen in distribution maps of radiometric elements K and U in Figure

3-23a and c respectively. All three radiometric distribution grids represent relationship between these radiometric elements and lithology.

3.6.2.1 Applying of ratio techniques

Some geochemical elements can sit in place of the K-ion and that happens in rocks with hydrothermal alterations. The geochemical element K is very mobile element so by passing fluids in through the smashed rocks this element displaces quickly, in other words alteration processes discharge rocks from the element K. The element U is relatively mobile but less than K; the element K belongs to LFS group of elements and is incompatible element and very mobile ion. The element Th acts completely converse of elements K and U and it is an immobile element belongs to HFS group of elements. So when hydrothermal alteration effect on rocks by fluid phases, it is possible the element Th increase relative to the elements K and U. These reactions of elements, guide us to use some ratios to find alteration areas.

Ratios of the elements have been applied for subtle variation; in figure 3-24 can see of three ratio results of Th/K ratio in a, U/K in b and Th/U in c results. In figures 3-25 and 2-26 for representing more details ratios results in some parts have been enlarged. In these figures can see enrichment of immobile (Th) and relatively immobile (U) elements in comparison with mobile (K) element and can see conformity of the alteration zones with ratio of Th/K and U/K in volcanic rocks (figure 2-26 profiles). In figure 2-26 alteration area from remote sensing studies have been brought and can see alteration area on the grid maps too; in provided profile also there are correlations of the peak points with alteration area, Th/K show more correlations.

Figure 3-25c, d and e part has been enlarged to illustrating of alteration around and over the

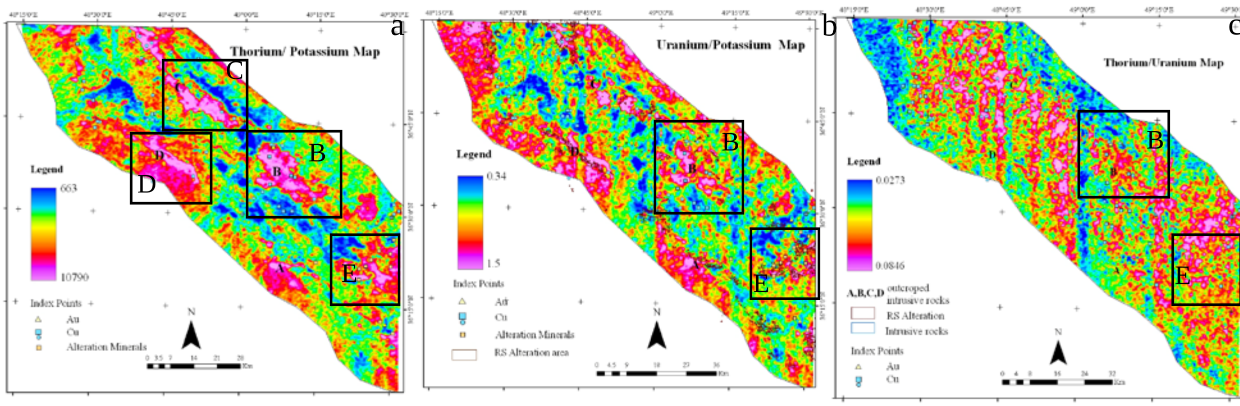

Figure 3-24: illustrate Th/K ratio in a, U/K in b and Th/U in c. in c can see there is a concentration of Th relative to K and this area is an alteration zone, in addition on the intrusive masses there are these concentration. b show also enrichment of U relative to K but not as Th. In c cannot see special concentration of Th relative to U on alteration zone E or on intrusive masses but there are conformity between index point and anomaly areas of this ratio.

intrusive mass B, in this case there are some inactive mine for Cu and two index point of polymetallic composition of Cu-Au (Ag-Sb-Bi-Ba). In this case Th/K has high rate on the intrusive rocks and around of that. According to the report of the geological map of Abhar sheet; this massive rocks has been composed of granite- monzonite, aplite with many diorite enclaves and surface of that has been intensively eroded, around of this mass can see alteration area and there are some inactive alunite mines too. On the intrusive rocks there aren’t remarkable alterations and high anomaly of Th/K; this can relate to leaching of K by weathering however that has been considered hydrothermal alteration in the area. In addition can see an interesting correspondence between Au-Cu index points and Th/U ratio grid map, in figure 3-25c because of abundance of index point in area B can see this relation obviously, this matter are clear in figure 3-26a too. In figure 3-25a and b, intrusive masses of C and D have been enlarged from grid image for ratio Th/K; in this data can see relation between these intrusive rocks, anomalies from ratio Th/K and RS alteration areas, there are conformity between them. With regard to conformity between index points and ratio grid of Th/U has applied independently as a radiometric potential for mineralization.

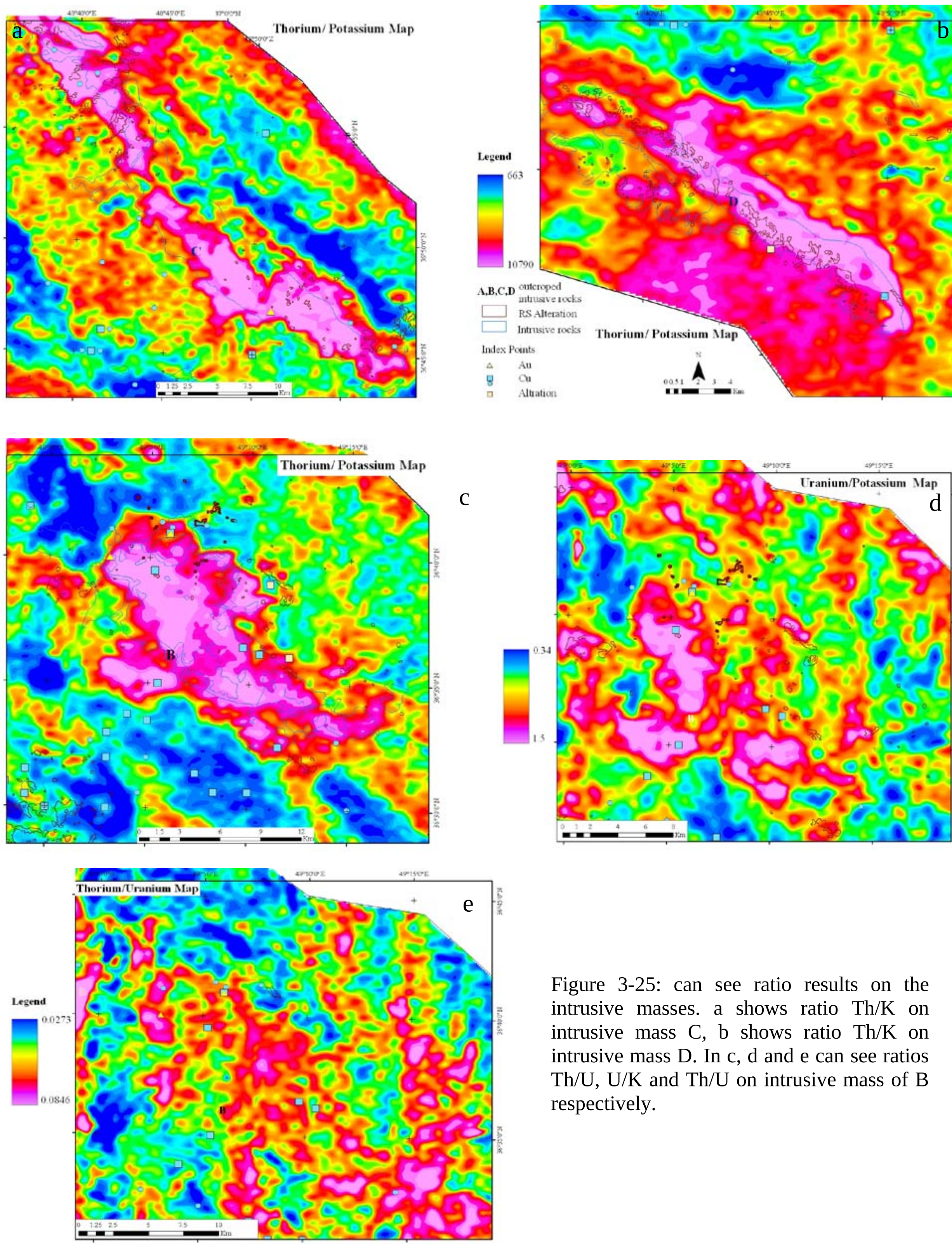

Figure 3-25: can see ratio results on the intrusive masses. a shows ratio Th/K on intrusive mass C, b shows ratio Th/K on intrusive mass D. In c, d and e can see ratios Th/U, U/K and Th/U on intrusive mass of B respectively.

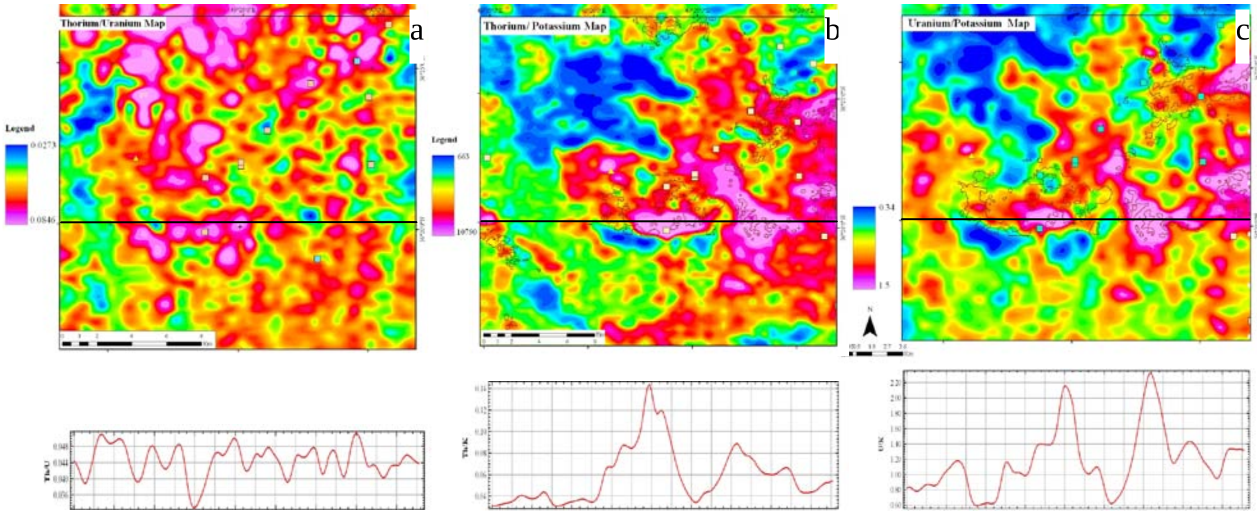

Figure 3-26: show enlarged part of alteration zone area E from figure 3-24 for ratios Th/U, Th/K and U/K in a, band c respectively relevant profile. profiles provide on the line in the grids a, b and c. those indicare the range numbers of ratios Th/K and U/K increase in the alteration district obviously.

Heier & Rogers, 1962 studies show the ratios of Th/K, U/K and Th/U are constant within one order of magnitude in a wide variety of rock types. The averages for basalts are: Th/K * 10^4 = 2.8, U/K * 10^4 = 0.60 and Th/U = 4.8. Some tendency exists, for increase in these ratios with igneous differentiation. The Th/U ratio is particularly low in tholeiites (1.6) from the orogenically active Japanese area and is also low in most basaltic rocks. Heier & Rogers, 1962 believe the process which leads to the formation of magma in orogenic areas causes removal of thorium, potassium and to a lesser extent, uranium from source materials before intrusion or eruption.

Often, depending on the complicate geological process; that are possible to detect the small difference in changing of the elements potassium, uranium and thorium but that couldn't detect easily. Hence the professional interpretations of gamma-ray spectrometry data require the instances of all the measurements and other relevant products in the area. Ratio calculations can enhance small differences in changing; this is important, especially when we study on alteration intensities associated with a special mineralizing process. Potassium alteration (enrichment) associated with certain types of mineral deposits, may occur in host rocks with normally low to moderate levels of K resulting in a high K signature. This would be easily recognized if this alteration occurred in isolation. However that may be normal, high K rock types in close proximity to the altered rocks. In this situation, the K associated with the alteration may not be distinguishable from other high K rock types. The ratio maps, in particular the Th/K ratio, can be a sensitive indicator of K alteration associated with mineralization and can be used as a direct indicator of mineralization. On a regional scale, subtle variations in the measured variables that are clearly reinforced on the ratio maps are shown by the U, Th and U/Th maps for southern Nova Scotia. Within the peraluminous granitic rocks of southern Nova Scotia, uranium concentrations generally increase and thorium concentrations decrease with increasing magmatic differentiation, resulting in abnormally high U/Th ratios associated with the most evolved parts of these granitic intrusions.

3.6.2.2 Ratio Th/U potential area

One of the rations is Th/U, which can see in figure 3-24c there are correlation between index point and anomaly area in grid image hence has been tried explaining of geochemical behavior of these elements. The average abundances of thorium and uranium in different igneous rocks which outcropped in the area have been presented in table 3-8. In table 3-8 rocks are divided into the following groups: silicic intrusive (quartzbearing rocks ranging from granite to tonalite plus syenite and monzonite); silicic extrusive rocks (same compositional range as silicic intrusive); basic extrusive (basalt and andesite) and alkaline (any feldspathoid rock). The concentrations of the elements have been presented in ppm and can compare them with geophysical gamma-ray spectrometry results for Th and U with cps unit.

For the outer few kilometers or so of the earth's continental crust, where granitic rocks predominate, the average thorium and uranium contents appear to be 10-15 ppm, and 3-4 ppm, with an average Th/U ratio of 3 to 4 respectively (Pliler, 1956; and Whrrfield, 1958). In deeper levels in the crust, where more and more basic rocks predominate, the thorium and uranium concentrations decline, in general the thorium and uranium contents of igneous rocks increase with increasing acidity or silica content. Thus, the average thorium and uranium contents of basic intrusive rocks are only about one quarter of those given above for granites.

Table 3-8: thorium and uranium in some igneous Rocks (Adams, Osmond and Rogers, 1959)

Rock	Thorium (in ppm)	Uranium (in ppm)	Th /U
Silicic intrusive	1-25	1-6	2-6
Silicic extrusive	9-25	2-7	4-7
Basic extrusive	0.5-10	0.2-4	3-7
Alkaline	variable	0.1-30	variable

The thorium and uranium are concentrated in normal accessory minerals such as zircon, apatite, and sphene. allanite appears to be one of the major radioactive minerals and in epidote, monazite and xenotime, uraninite and torbernite are also rare radioactive minerals in silicic intrusive igneous rocks, some of the thorium and uranium is contained in major constituents such as quartz and the feldspars. Several studies have shown that there is a general tendency for the radioactivity of a rock to increase with increasing silica content. In some cases, however, alkaline end-members of igneous sequences are particularly enriched in thorium and uranium.

The average abundances of thorium and uranium in silicic extrusive rocks are in the range of 10-20 ppm, and 3-6 ppm respectively, and the average Th/U ratio is 3-5 ppm. The abundances of thorium and uranium in basic extrusive rocks (basalts and andesites) are in the range of 0.5-10 ppm, and 0.2-4 ppm respectively, and the average of Th/U ratio is 3-7 ppm. The thorium and uranium in studied basic volcanic rocks is roughly uniformly distributed among the various constituents or concentrated into the glassy phase.

Most studies have shown that the average Th/U ratio in igneous rocks is about 3.5. This ratio is found in rocks which are greatly different in average thorium and uranium contents and is the characteristic ratio of the very low concentrations present in the major rock-forming minerals like quartz and the feldspars. During the crystallization of the normal minerals of basic rocks (pyroxene, calcic plagioclase, and apatite), may incorporate small amounts of thorium and uranium, no mineral crystallizes from a basic magma with a marked concentration of thorium and uranium.

In comparing of the Th/U ratio of gamma-ray spectrometry with the geochemical result in the area; high ratio has been distribute uniformly in all the area. In spite of grid images for Th/K and U/K, that doesn't show high anomaly on intrusive rocks (more with syenite and monzonite rocks) or alteration area. That confirms geochemical behavior of the Th and U and signifies

close ratio rate in intrusive and extrusive rocks. In the alteration area on southeast of the erea can see conformity of some high ratio with RS alterations. Interesting conclusion of Th/U grid is matching of index points with high ratio parts. In figure 3-27, the grid of Th/U has been classified; the total area show ratio between 0.02730-0.08461cps; class 3 is upper than 0.053580 cps; class 2 is upper than 0.04239 cps. Table 3-9 represents the area of every class and percentage of them. There are 114 index points which are more accurate, and in table 9-3 can see frequency of index points in every class. As mentioned before some index points have low accuracy and that should be consider too, in this research some of them have been eliminated for calculations. Index points with 34.21 percent have been appeared in 21.45 percent of the area in class 3; 7 Au index point with 77.78 percent occupy this class also. Approximately 90 percent of points take place on or around of the intrusive rocks with class 3.
Already figure 3-24c has been presented the index point on the grid of Th/U and now that can be seen in the figure 3-27 on the classified grid of Th/U.

Table 3-9: represents percentage of index points in 3 classes of Th/U ratio grid.

	Area (km^2)	Index points	Au index point	Percent of area	Percentage of index points	Percentage of Au
Class 1	1712.68519	37	1	40.31	32.46	11.11
Class 2	1624.23736	38	1	38.24	33.33	11.11
Class 3	911.66802	39	7	21.45	34.21	77.78
Total	4248.59057	114	9	100	100	100

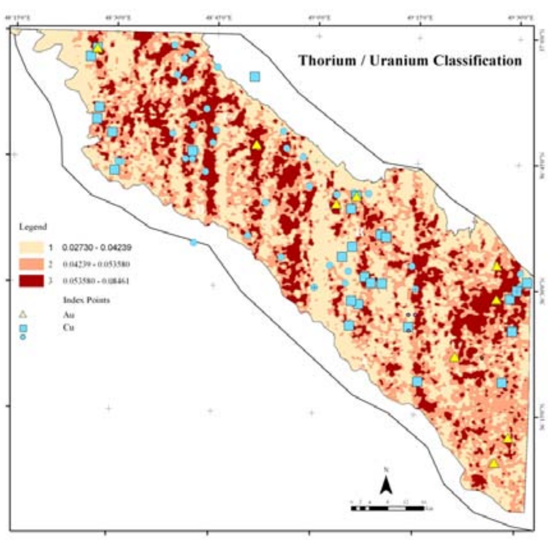

Figure 3-27: show Th/U ratio and classification of that, so indicate coherency between index points and anomaly area.

3.6.2.3 CMY ternary technique

Roberto et al, 2008 has proposed CMY ternary technique for potassium, thorium and uranium channels, this technique represents additional information relative to individual channel maps. In figure 3-28 can see CMY ternary technique results in grid maps for the area. In figure 3-28 a; contour lines delineate high anomaly of K, Th and U and in figure 3-28 b can see conformity between intrusive rocks and delineated anomaly areas in a. Intrusive masses A and B have dark colours how we can see red and purple colours dominate on intrusive masses areas in B and C.
In figure 3-28 can see part E in southeast of the area, in part E; there is no intrusive mass but that show concentration of the elements. With regard to geological maps there is hydrothermal alteration district in the part E. Considering figure 3-28 and lithological information; light colours show mainly low concentration of the three elements where lithologically have been

composed more volcanic rocks. Volcanic rocks include tuff, pyroclastics and sometimes include sandstones and sedimentary rocks accompany volcanic rocks in area by low concentration elements. Dark colours have been associated more by intrusive rocks as diorite, monzonite, syenite granite; this matter signifies enrichment of the three elements in this type of rocks. As mentioned in the E part there is enrichment of the three elements. Hydrothermal alteration minerals deposits in lithological units Ea6 and Ea5. These lithological units compose of more acidic lava, tuff and breccias (table in the attachment show composition of these units). However there isn’t like this concentration of three elements in the other place that have similar lithological units. That signify; enrichment have been done by fluids that passed in through smashed volcanic rocks and deposits the elements. On the other hand it is possible an intrusive mass source near the part E which supplies fluids.

In the area E (figure 3-28) there are some regions between volcanic rocks with concentration of the three elements and that represent dark colours like intrusive rocks. there are two possible reasons; with regard to near intrusive rocks that can be because of the origin of the both are unite and enrichment is primarily, other possibility can be related to moving of elements by fluids from deeper sources. According to geological reports and RS study in this district there isn’t remarkable alteration zone and by the way concentration of immobile Th element proves primary origin of the elements. In the upper part of the mentioned high anomaly E can see an area with low concentration of the Th, K, U.

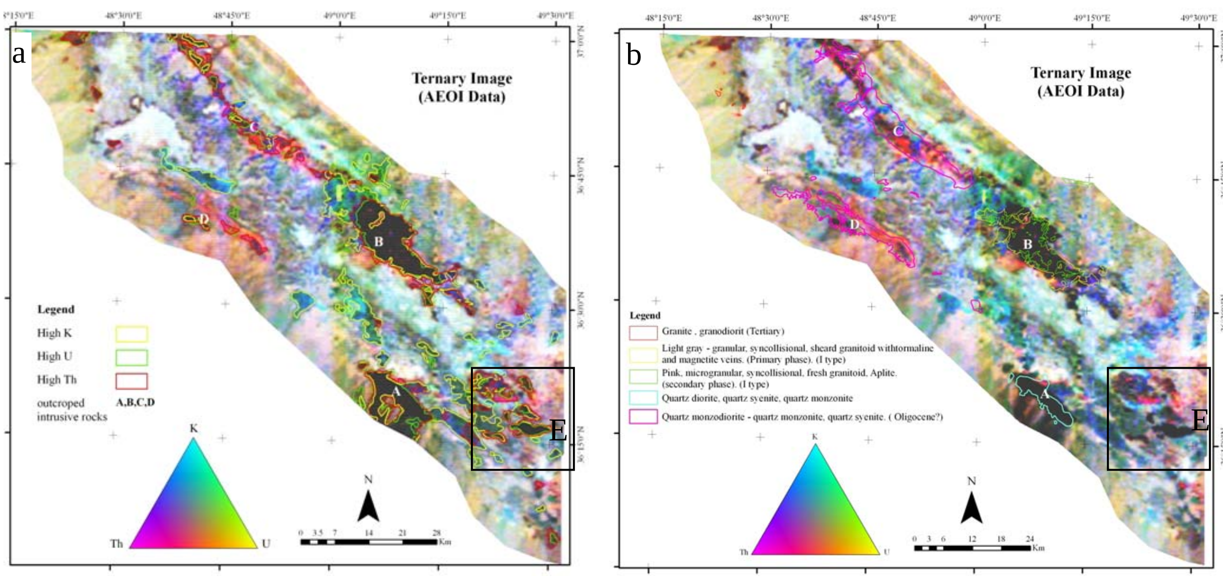

Figure 3-28: represents CMY ternary image for Th, K and U elements, a: have been illustrated contour line with high anomaly of Th, K and U. b: can see conformity between intrusive rocks with colours of the images, A and B bodies accompanied by dark colour and red tone dominate on B and C intrusive rocks. In E part there are no intrusive massive but that show concentration of the elements.

Figure 3-29 represent enlarged lithological units and CMY ternary image in the intrusive masses of B that indicate more details about this data. Figure 2-29a represents CMY ternary image in intrusive mass area B for elements K, Th and U. b is the part of geological map in the same area, obviously the maps show conformity between CMY ternary image in figure 2-30a and lithological units on figure 2-30b.

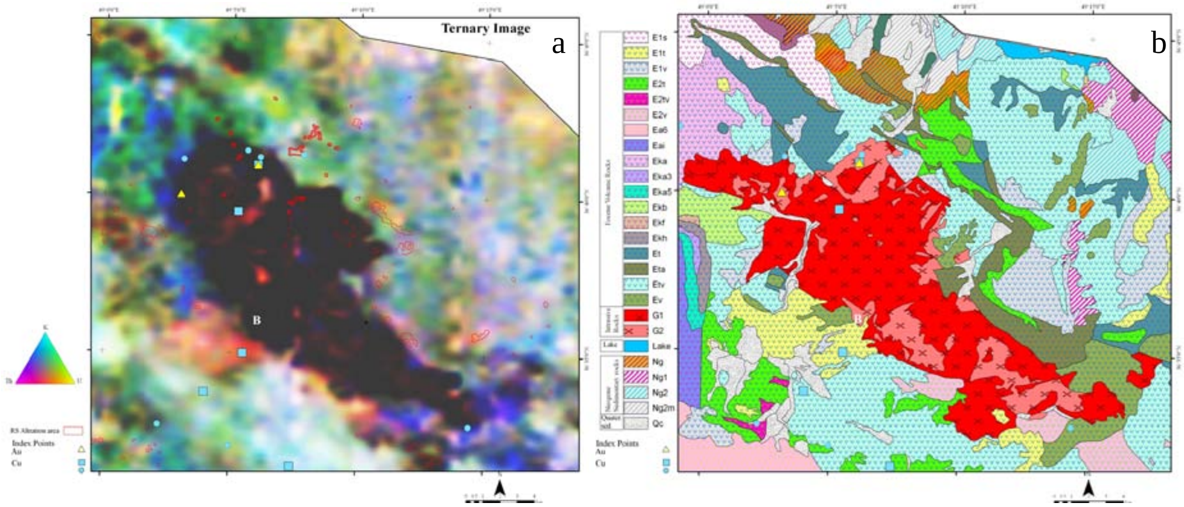

Figure 3-29: Intrusive mass B area have been enlarged for indicating more details, a represents CMY ternary image for K, Th and U elements in this district, b is the part of geological map in this district.

As mentioned the study area has been surrounded by quaternary sediments. In left and right side, border areas have been covered by quaternary sediments. These areas have mainly light colours except some place in continuous of intrusive rocks. Where can see the dark colours in quaternary sediments, there are intrusive masses in adjacent, here can see dark colored quaternary rocks beside mass A. That indicate the quaternary sediments are composed of intrusive masses' fractures. In the right board; quaternary sediments beside of masses B and C can see greenish colour that signify fracture compose more from U and K. In many place blue colour signify enrichment of K in rocks how red and purple colours, over masses D and C indicate more enrichment of Th relative to K and U in these masses.

3.6.3 Extraction of radiometric alteration area

For extracting of alteration area, with regards to previous explanation about radiometric data; all three ratios are helpful. In addition geological information can help to find and remove some lithological units which are impossible to deposited alteration minerals on them like quaternary sediments. These sediments can be seen in both sides of left and right; near the borders. Due to composition of fracture rocks in the quaternary sediments that come from adjacent volcanic and intrusive rocks, we can see high anomaly in these sediments though they are not appropriate place for prospecting in this case study. This place in ternary images (figure 3-28) mainly indicate lighter colours what show mixing of rock fractures from different composition except near intrusive mass of A.

During the late stages of crystallization, hydrothermal fluids may redistribute the thorium or uranium, or they may escape to form hydrothermal veins and pegmatites. Hydrothermal uranium veins are usually free from thorium. Also it is possible that the uranium to be transported as the simple or complex uranyl ion and fixed by reduction to the tetravalent state. Hydrothermal thorium veins exist also, but their mode of origin is unknown.

With respect to ratios, Th/K anomalies represents area which coordinate with RS and geological alteration wherever U/K results also confirm them, so this ratio classified with regard to geological and RS alteration area. In Th/K grid image (figure 24a) can see high range on the intrusive rocks but with respect to geochemical behavior of thorium and uranium elements that is normal high Th/K and U/K ratio on intrusive rocks with silicic composition. In according to geological map and RS alteration areas, there isn't remarkable alteration area on the intrusive masses A and B and high anomalies on these rocks can be caused by original characters of rocks not by hydrothermal processes. Hence for extraction of the radiometric alteration has been tried to increase some failures relate to some geochemical behaviour. The grid for ratio Th/K has been classified. I gave low weight score to intersection area between B and classified map. Figure 3-30 illustrate these steps for intrusive mass B, in a can see initial classified grid, in b intrusive mass of B and in c can see the classified grid after decreasing weights from intersection area. In intrusive masses C and D, there are many evidences for alteration so the weights in this area have not been changed, the result have been represented in figure 3-31. Class 3 show high probability and class 1 show low probability for occurring of alterations.

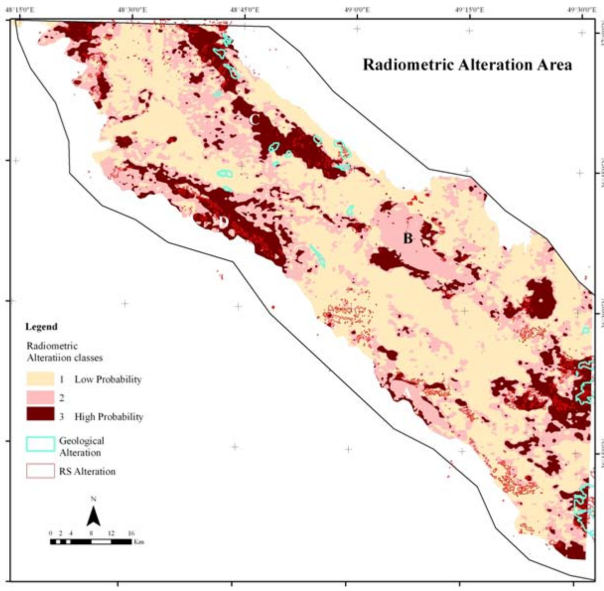

Figure 3-31: shows radiometric alteration area in three classes, class 3 indicate district with high probability and class 1 low probability for alterations.

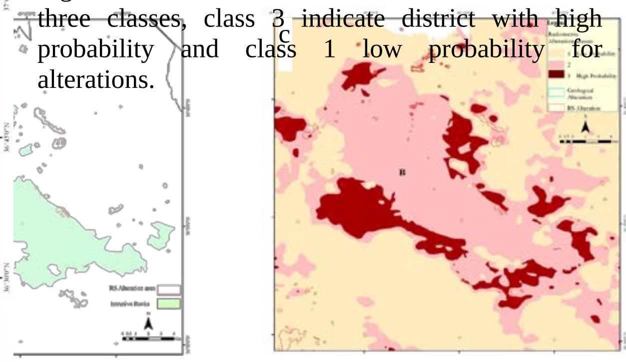

metric data processing results with geological intrusive usive mass of B and in c can see the classified grid after fied image.

3.6.4 Extracting of shallow bodies and intrusive rocks

With regard to metallogeny of the area with epithermal and porphyry mineralization, intrusive rocks play important roles in mineralization. Superposed volcanic rocks and associated sedimentary rocks over the shallow bodies can be as host rocks for minerals hence to locate shallow bodies would be helpful in the prospecting. The area indicate mainly high magnetic anomaly and that would be normal with respect to major lithology of area, where compose of intermediate volcanic rocks and relevant sediments more in central trend and with outcropped intrusive rocks in both lateral sides. On the earth's surface in some place of the area can see obviously relationship between outcropped intrusive rocks and magnetic anomalies. Hence high anomalies in other location can be caused by deeper sources so mainly the magnetic intensities data is applied to distinguishing the shallow bodies.

This research uses grid file from total magnetic intensity to interpretation and extracting of shallow bodies. Finally, that defines a ranked districts map with high probability and low probability for shallow bodies occurring in figure 3-32. Upward continuation filter results have been classified for deriving of high anomaly places for shallow bodies' locations. In figure 3-32a can see that high anomalies have been appeared over geological intrusive area and also in areas F, E, G, H.

With regard to geochemistry of Th, U, K elements, these elements especially Th and U appear in intrusive rocks with high amount while in extrusive rocks they have low amount and this matter can help to distinguish the area of intrusive rocks. In this case Th radiometric anomalies grids show more conformity with geological intrusive units relative to U grids data. Hence Th radiometric grid map has been classified with regard to outcropped intrusive rocks, threshold for that has been detected by boundary of the intrusive rocks with volcanic rocks. On the figure 3-32b can see result of classification of Th radiometric grid, U high anomaly also illustrated for indicating of conformity between two elements anomalies area. This map represents areas E, F, H in addition of geological intrusive rocks. H area in Zanjan map sheet has been mapped in small area but areas E and F have not been located in Abhar sheet and there isn't detailed geological map for this sheet.

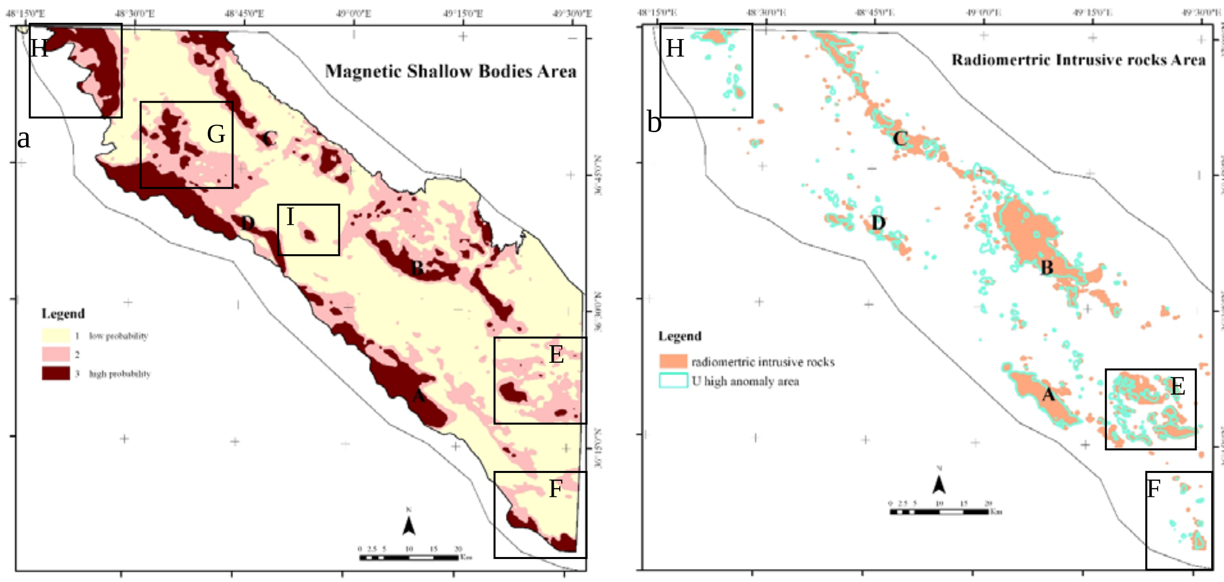

Figure 3-32: a show magnetic shallow body here in addition of the intrusive rocks area in F, E, G, H area can see high anomaly area. b in this map extracted intrusive rocks area from radiometric data has been presented. This data also confirm E, F, H area but cannot see remarkable anomaly in G area.

There are conformities between areas of magnetic shallow bodies and radiometric intrusive rocks except area G, this area indicate high magnetic intensity but low anomaly for three elements Th, K and U with regard to figure 3-28.

3.7 Geochemical data

Geochemical information for this area are very old and for some of map sheets there are no information hence applying this data don't give desirable results, conversely that can create

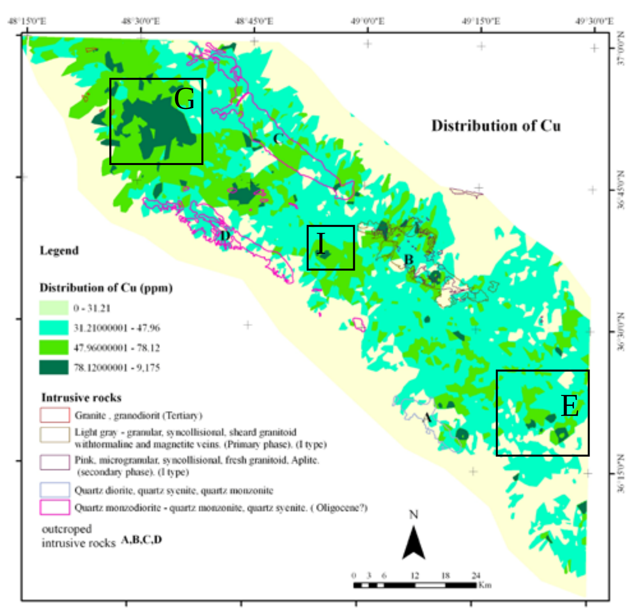

Figure 3-33: show geochemical study results for distribution of element Cu.

inaccurate results. I didn’t use this data as a data layer in the integration processing however I applied this data as information that can help for weighting the other layers with regard to integration model. Figure 3-33 show geochemical study results for distribution of element Cu. This data express concentration of Cu in northwest part of the area (G) and there are anomalies in area I and E where geophysics data show anomalies too. Around and on the intrusive mass B can see another concentration, but the other intrusive masses don’t show remarkable concentration for Cu.

3.8 Coordination of data and data formats

The evidence data for the area include vector data and raster data. Vector data is composed of lines, points and polygons and mainly their format are in shape or cad; geophysics grid data and remote sensing data are in raster formats. For processing of data in GIS software and programs that would be needed to make unity in format and coordinate systems. These data should be converted all to either vector or raster; I converted all data to raster formats and chose UTM coordinate system for them.

Processing in raster formats has more privilege relative to vector formats; in big area calculating of vector formats create very big tables and very big files this make software processing very slow, in addition can see many errors in calculation. Raster formats haven’t this problem but the error here can create when a vector file convert to raster file in this case in boundary place can see unconformity between vector lines and raster pixels but this replacement are in 1 or 2 pixels and that can be ignored.

Before converting vector data to raster it is better to do processing and making polygon files from points and lines for increasing of pixel replacement effects. In this research that is necessary buffering of faults and points so before converting of these shape form files, faults with 400 m distance and points with 200 m distance were buffered.

Geological units without essential changing only after weighting have been converted to raster formats, and about extracted vector data from RS images also have been turned to raster information, but geophysics data are in aster format and that can be applied without conversion. With regard to accuracy of the data; pixel size with 30*30 m^2 resolutions for this research has been chosen.

Chapter 4: Dempster-Shafer theory and relevant rules in mineral exploration data analysis

4.1 Introduction

This chapter submits the application of Dempster-Shafer theory and some relevant rules to determine uncertainties in mineral exploration data analysis. There are different degrees of uncertainties and mathematical methods presented that can help dealing with uncertainties for geological risk evaluation.
As mentioned in chapter two DST has capabilities for processing data of multiple sources. DST contains two parts. The first part presents methods to evaluate uncertainty on every data layer that comes from individual sources separately and the second part is related to the evaluation of data layer uncertainties from interactions of multiple sources which affect each other. For the first part DST's belief functions have been applied but for second part in addition of DST rules there are some combination rules which are compatible with weighted evidences by belief functions and can be used instead of DST's combination rules.
The main problems of this investigation are related to the second part of DST rules that means evaluation of uncertainties for the combination of data from different sources which has been already weighted by fist part of DST rules. Second problem to solve is the application of combination rules in spatial environments. A discussion of advantages and disadvantages of different rules follows in chapter 5.

4.2 Unifying of multiple source layers in geospatial case study

The last chapters explained mineral exploration processes and the potential of the area for specific ore reserves. Some geological data which can help to distinguish favorable area has been extracted like faults, lithological units, alteration areas and geochemical anomaly data. For obtaining some geological data, remote sensing data and geophysical data have been used. At the end there are about ten data layers as basic for mineral exploration. Some of these data are in vector format like information extracted from geological maps and geochemical data, some data are in raster format like alteration data that has been extracted from remote sensing images or information extracted from geophysical data.
According to basic data in chapter two DST's combining rules of datasets use a probability framework like Bayesian approach. Main concept in this method is the idea of prior and posterior probability. Every data has prior probability and with adding to each other we will have posterior probability. Hence for integration of this data that will be needed to bring all data in unit format, raster format has more advantage than vector formats in calculations. The raster can be represented as a rectangular matrix of numbers, and can be stored as a simple file structure with straightforward addressing of pixel in raster package files of GIS software. One advantage of the raster model is that spatial data of different types can be overlaid without the need for complex geometric calculations required for overlaying different maps in the vector model (Bonham-Carter 1994). Each layer of grid cells in a raster model records a separate attribute e.g. *.img grid format file used in ArcGIS. The cells are constant in size, and are generally square. The cells locations are addressed by row and column number. Spatial coordinates are not explicitly stored, information about the number of rows and columns, plus the geographic location of the origin are saved with each layer in a package raster file. The spatial resolution of a raster is the size of one pixel on the ground and for this area 30m resolution has been applied because of RS image data resolution; some information from Aster image has been extracted and major resolution in this images is 30*30 m^2 also.

Attributes of spatial objects are usually organized in lists or tables. Attributes for an integer grid (a type of raster file that can carry information in a attribute table) are stored in a value attribute table (vat). A vat has one record for each unique value in the grid. The record stores the unique value (value is an integer that represents a particular class or grouping of cells) and the number of cells (count) in the grid represented by that value. Figure 4-1 show lithological grid table of the area. All lithological data have been classified in five values in this table can see mass probabilities for every class that will be explained in next sections.

Attributes of Z_Tar_R_S_A_.img

OID	Value	Count	A13	B13	C13	D13	E13	F13	G13	Belief
0	1	185338	0.42	0.04	0.01	0.3	0.08	0.02	0.13	1
1	2	1668521	0.5	0.01	0.01	0.15	0.13	0.03	0.18	1
2	3	2530568	0.4	0.01	0.01	0.18	0.15	0.03	0.22	1
3	4	519163	0.3	0.03	0.03	0.14	0.19	0.06	0.25	1
4	5	391785	0.8	0.01	0.01	0.1	0.03	0.01	0.04	1

Record: 1 Show: All Selected Records (0

Figure 4-1: attribute table of lithology raster file.

As mentioned raster model are more suitable for overlaying of data and DST model uses overlaying. Processes are performed on attribute table of raster data so all data converted to the integer grid.

4.3 Weighting of spatial data evidence by belief functions

Geological investigations are characterized by particularly with geological maps, remote sensing images, geochemical data, geophysical data etc. But with regard to objects some layers are more helpful than others. With regard to this research requirement data layer have to be gathered. In last chapter, extracting data from raw information and preparing process for applying in GIS environment with DST rules have been indicated and discussed.

Dempster-Shafer theory assigns its masses to all of the subsets of the entities that, for this case there are three possible members: Rock, Cu, Au, that is three independent states and original set, if the original set is called S so that |S| = 3 and power set has 2^s subsets.

For providing this sets and a universal set the geological properties and mineral potential of the area should be considered. Regarding studies in the research area (chapter one) the area has potential for Au mineralization as Cu mineralization but according to outcropping of alteration area Au minerals are more possible. In the region there are also some intermediate to acidic intrusive rocks where Cu minerals can settle and appear, in this outcrops also alteration zone can be formed so Cu mineral beside of Au mineral in intrusive rocks to be seen. Some alteration area can be an alteration zone for intrusive rocks in deep how still hasn’t outcrop on the surface and to be covered in this condition sometimes Au minerals are associated with Cu minerals.

The universal set for mass has been shown in the following:

A = {Rock}
B = {Au}
C = {Cu}
D = {Rock, Au}
E = {Rock, Cu}
F = {Au, Cu}

G = {Rock, Au, Cu}
H = {Ø}

And the power set is L = {A, B, C, D, E, F, G, Ø}
For n data layers the power set can be assigned with:

L_1 = { A_1, B_1, C_1, D_1, E_1, F_1, G_1, Ø}
L_2 = { A_2, B_2, C_2, D_2, E_2, F_2, G_2, Ø}
.
.
.
L_n = { A_n, B_n, C_n, D_n, E_n, F_n, G_n, Ø }

This research has been concentrated on the second part of DST method or combination of basic probability assignment (bpa or m, mass function) from multisource data layers, but at first it is necessary to define mass function and then to calculate of belief and Plausibility functions(Bel, Pl). bpa can be defined by case study experts with regard to expression 2-3 Bel and Pl also can be calculated by expressions 2-6 and 2-7 respectively.

$$\sum_{A \in P(X)} m(A) = 1 \qquad (2\text{-}5)$$

$$Bel(A) = \sum_{B \mid B \subseteq A} m(B) \qquad (2\text{-}6)$$

$$Pl(A) = \sum_{B \mid B \cap A \neq \emptyset} m(B) \qquad (2\text{-}7)$$

Bel(A_n) is calculated by following statements:

Bel(A_n) = m(A_n)
Bel(B_n) = m(B_n)
Bel(C_n) = m(C_n)
Bel(D_n) = m(A_n) + m(B_n) + m(D_n)
Bel(E_n) = m(A_n) + m(C_n) + m(E_n)
Bel(F_n) = m(B_n) + m(C_n) + m(F_n)
Bel(G_n) = m(A_n) + m(B_n) + m(C_n) + m(D_n)+ m(E_n) + m(F_n)+ m(G_n)

These statements must be repeated for every pixel in raster file so that need much calculation. As mentioned Matlab programming can help to simplify calculations and for all calculation the codes are also indicated.
For applying of sets theories in programming software, codes in table 4-1 have been defined. In table 4-1, 1 show Ø, 2 indicates rock, 3 assigns Au and 4 show Cu, the first column has only 1 and is equal with set Ø, second column indicate both 1 and 2 so that present set A ({Rock}) next column has 1 and 3 so it presents set B ({Au}), set C ({Cu}) has codes 1 and 4 in fourth column. Fifth column has 1, 2 and 3 so that can be equal with set D ({Rock, Au}). Column 6 contain codes 1, 2 and 4 so that related to set E ({Rock, Cu}) and column 7 related to set F ({Au, Cu}) with codes 1, 3 and 4. Finally in column 8 there are all number 1, 2, 3, 4 and indicate set G ({Rock, Au, Cu}).

Ø	A	B	C	D	E	F	G
1	1	1	1	1	1	1	1
nan	2	3	4	2	2	3	2
nan	nan	nan	nan	3	4	4	3
nan	nan	nan	nan	nan	nan	nan	4

Table 4-1: codes for defining of sets in programming software.

In following Programming codes, lines 1 to 12 repeat in the first part of every DST integration methods. Lines 4 to 11 use codes in table 4-1 to define sets, for example line 4 define set Ø, line 5 define set A ({Rock}), … up to line 11 that assigns set ({Rock, Au, Cu}).

```
1       n  =n ;
2       n_n=n_n;
3       DST=zeros(n_n,8);
4       m(1,1)  =[1]      ;m(2:4,1)=nan;
5       m(1:2,2)=[1;2]    ;m(3:4,2)=nan;
6       m(1:2,3)=[1;3]    ;m(3:4,3)=nan;
7       m(1:2,4)=[1;4]    ;m(3:4,4)=nan;
8       m(1:3,5)=[1;2;3]  ;m(4  ,5)=nan;
9       m(1:3,6)=[1;2;4]  ;m(4  ,6)=nan;
10      m(1:3,7)=[1;3;4]  ;m(4  ,7)=nan;
11      m(1:4,8)=[1;2;3;4];
12      data1 = xlsread ('ExcelFile');
```

In the first line n is the number of extracted table attribute rows from raster file so the pixel number in the raster file; n_n indicates the number of data layers or sensors that is integrated in these manners.

Belief function can be calculated by expression 2-6. In code line 13 to 33 in the following program lines this is indicated. For that there are three loops. The first loop iterates the calculations in the number of data layers or sensors. The next loop iterates calculations in the number of pixels and third loop iterates the condition statement. Intersect syntax for defining conditional statements has been applied, line 25 and 27 present conditional statement of $B|B\subseteq A$ in expression 2-6.

```
13      for n1=1:n
14        for i1 =1:8
15          for i2 =1:8
16            s=intersect(m(:,i1),m(:,i2));
17            [s1,c1]=size(s);
18            if s1==1
19              s(2:4,1)=nan;
20           elseif s1==2
21              s(3:4,1)=nan;
22            elseif s1==3
23              s(4,1)=nan;
24            end
25            sm=isequalwithequalnans(s,m(:,i2));
26            if sm==1
27              bel(:,(n1-1).*8+i1)=bel(:,(n1-1).*8+i1)+data1(:,(n1-1)...
28                .*8+i2);
29              clear s
30            end
31          end
32        end
```

```
33      end
```

Line 27 indicates the calculation of expression 2-7.
Plausibility functions (Pl) can be calculated by following statements:

$Pl\ (A_n) = m(A_n) + m(D_n) + m(E_n) + m(G_n)$
$Pl\ (B_n) = m(B_n) + m(D_n) + m(F_n) + m(G_n)$
$Pl\ (C_n) = m(C_n) + m(E_n) + m(F_n) + m(G_n)$
$Pl\ (D_n) = m(A_n) + m(B_n) + m(D_n) + m(E_n) + m(F_n) + m(G_n)$
$Pl\ (E_n) = m(A_n) + m(C_n) + m(D_n) + m(E_n) + m(F_n) + m(G_n)$
$Pl\ (F_n) = m(B_n) + m(C_n) + m(D_n) + m(E_n) + m(F_n) + m(G_n)$
$Pl\ (G_n) = m(A_n) + m(B_n) + m(C_n) + m(D_n)+ m(E_n) + m(F_n)+ m(G_n)$

The language code is similar to belief function code except in the lines 25 to 27. Lines 25 and 26 choose $B|B\cap A\neq\emptyset$ condition in expression 2-5 and in line 27 this expression is been calculated.

```
13      for n1=1:n
14          for i1 =1:8
15              for i2 =1:8
16                  s=intersect(m(:,i1),m(:,i2));
17                  [s1,c1] = size(s);
18                  if s1== 1
19                      s(2:4,1)= nan;
20                  elseif s1==2
21                      s(3:4,1)=nan;
22                  elseif s1==3
23                      s(4,1)=nan;
24                  end
25                  sm=isequalwithequalnans(s,m(:,1));
26                  if sm==0
27                     pl(:,(n1-1).*8+i1)=pl(:,(n1-1).*8+i1)+data1(:,(n1-1).*8+i2);
28                     clear s
29                  end
30              end
31          end
32       end
```

This function has been calculated for lithological layer's m, all the time belief and plausibility function are 1in G set but generally this function to be obtained after fusion of layers in DST manners.

Table 4-2: show calculated belief and plausibility function for geological data layer.

Value	Bel-A13	Bel-B13	Bel-C13	Bel-D13	Bel-E13	Bel-F13	Bel-G13	Pl-A13	Pl-B13	Pl-C13	Pl-D13	Pl-E13	Pl-F13	Pl-G13
1	0.420	0.040	0.010	0.510	0.760	0.070	1.000	0.930	0.490	0.240	0.990	0.960	0.580	1.000
2	0.500	0.010	0.010	0.640	0.660	0.050	1.000	0.950	0.360	0.340	0.990	0.990	0.500	1.000
3	0.400	0.010	0.010	0.560	0.590	0.050	1.000	0.950	0.440	0.410	0.990	0.990	0.600	1.000
4	0.300	0.030	0.030	0.520	0.470	0.120	1.000	0.880	0.480	0.530	0.970	0.970	0.700	1.000
5	0.800	0.010	0.010	0.840	0.910	0.030	1.000	0.970	0.160	0.090	0.990	0.990	0.200	1.000

4.4 Applying of combination rules

Evaluation of uncertainty for every data layer alone in geological investigation for detection of risks is useful and can help us partly. But when there is more than one layer we can use these layers together, so again mathematic can help us to treat more accurate with uncertainty in data layer. As discussed in chapter two DST rules are mathematic methods that present proper ways to treat many data layers from different sources. This part applies DST rules and some additional rules. These rules have capability for combining of weighted data that already have been weighted by first part of DST rules in geospatial environments. Investigations results for applying of these rules come in the following sections.

4.4.1 Dempster-Shafer theory and Yager's modified combination rules

Before than this mathematical statement for two layers fusion in Dempster_Shafer rules has been mentioned.

$$m_1 \otimes m_2(A) = \frac{\sum_{B \cap C = A} m_1(B) m_2(C)}{1 - K} \qquad \text{When } A \neq \text{Ø} \qquad (2\text{-}12)$$

$$m_1 \otimes m_2(\text{Ø}) = 0 \qquad (2\text{-}13)$$

Where $K = \sum_{B \cap C = \text{Ø}} m_1(B) m_2(C)$ (2-14)

For calculation of $m_1 \oplus m_2(A)$ the numerator of this fraction, as mentioned in expression 4-2, can be calculated by the following statement:

$[(A_1)*(A_2)]+ [(A_1)*(D_2)]+ [(A_1)*(E_2)]+ [(A_1)*(G_2)]+ [(G_1)*(A_2)] +[(D_1)*(A_2)] +[(D_1)*(E_2)] +[(E_1)*(A_2)] +[(E_1)*(D_2)]/1-K$

The division statement in Dempster - Shafer theory has normalized by 1-K factor and in the division statement for calculation of K that must be used subsets without intersections, K represent bpa with conflicts, this is determined by summing the products of the bpa's of all subsets where there is not intersection.

K can be calculated by the following statement for two layers:

$K = [(A_1)*(B_2)]+ [(A_1)*(C_2)]+ [(A_1)*(F_2)]+ [(B_1)*(A_2)]+ [(B_1)*(C_2)]+ [(B_1)*(E_2)]+ [(C_1)*(A_2)]+ [(C_1)*(B_2)]+ [(C_1)*(D_2)]+ [(F_1)*(A_2)]+ [(E_1)*(B_2)]+ [(D_1)*(C_2)]$

This statement can be used when we have two data layers for integration; in this research there are more than two raster layers with more than two masses so this expression can change to:

$$\bigotimes_{i=1}^{n} m_i(A) = \frac{\sum_{L1 \cap \dots \cap Ln = A} m_1(L_1) \dots m_n(L_n)}{1 - (K_{1,\dots,n})} \qquad (4\text{-}1)$$

$$K_{1,\dots,n} = \sum_{L1 \cap \dots \cap Ln = \text{Ø}} m_1(L_1), \dots, m_n(L_n) \qquad (4\text{-}2)$$

With regarding to the possible subset products in this modeling procedure and Dempster-Shafer combining rules, with n layers can be seen in following expression. In this expression the possible products with intersection in A has been assigned for n layers combining.

$$([A_1]*[A2]*[A3]*\ldots*[A_n])+$$

$$([D_1]*[A_2]*[A_3]*[A_4]*\ldots*[A_n]) + ([A_1]*[D_2]*[A_3]*\ldots*[A_n]) + ([A_1]*[A_2]*[D_3]*[A_4]*\ldots*[A_n]) + ([A_1]*[A_2]*[A_3]*[A_4]*[D_5]*[A_6]*\ldots*[A_n]) +\ldots+([A_1]*[A_2]*\ldots*[A_{n-1}]*[D_n]) +$$

$$([E_1]*[A_2]*[A_3]*\ldots*[A_n]) + ([A_1]*[E_2]*[A_3]*[A_4]*\ldots*[A_n]) + ([A_1]*[A_2]*[E_3]*[A_4]*\ldots*[A_n]) +([A_1]*[A_2]*[A_3]*[E_4]*[A_5]*\ldots*[A_n]) + ([A_1]*[A_2]*[A_3]*[A_4]*[E_5]*[A_6]*\ldots*[A_n]) +\ldots+([A_1]*[A_2]*\ldots*[A_{n-1}]*[E_n]) +$$

$$([G_1]*[A_2]*[A_3]*[A_4]*\ldots*[A_n]) + ([A_1]*[G_2]*[A_3]*[A_4]*\ldots*[A_n]) + ([A_1]*[A_2]*[G_3]*[A_4]*\ldots*[A_n]) + ([A_1]*[A_2]*[A_3]*[G_4]*[A_5]*\ldots*[A_n]) + +\ldots+([A_1]*[A_2]*\ldots*[A_{n-1}]*[G_n])+$$

$$([D_1]*[E_2]*[A_3]*[A_4]*\ldots*[A_n]) + ([D_1]*[A_2]*[E_3]*[A_4]*\ldots*[A_n]) + ([D_1]*[A_2]*[A_3]*[E_4]*[A_5]\ldots*[A_n]) + \ldots + ([D_1]*[A_2]*[A_3]*\ldots*[A_{n-1}]*[E_n])$$

$$([E_1]*[D_2]*[A_3]*[A_4]*\ldots*[A_n]) + ([A_1]*[D_2]*[E_3]*[A_4]*\ldots*[A_n]) + ([A_1]*[D_2]*[A_3]*[E_4]*[A_5]*\ldots*[A_n]) + \ldots + ([A_1]*[D_2]*[A_3]*\ldots*[A_{n-1}]*[E_n])$$

$$([E_1]*[A_2]*[A_3]*[D_4]*\ldots*[A_n]) + ([A_1]*[E_2]*[A_3]*[D_4]*[A_5]*\ldots*[A_n]) + ([A_1]*[A_2]*[E_3]*[D_4]*[A_5]*\ldots*[A_n]) + \ldots + ([A_1]*[A_2]*[A_3]*[D_4]\ldots*[A_{n-1}]*[E_n])$$

.

.

.

$$([E_1]*[A_2]*[A_3]*[A_4]*\ldots*[A_{n-1}]*[D_n]) + ([A_1]*[E_2]*[A_3]\ldots*[A_{n-1}]*[D_n]) + ([A_1]*[A_2]*[E_3]*[A_4]*\ldots*[A_{n-1}]*[D_n]) + \ldots + ([A_1]*[A_2]*\ldots*[A_{n-2}]*[E_{n-1}]*[D_n]) /1 - K$$

In this case $m_{i,\ldots,n}$ (A) has been assigned with {Rock} set and according to condition of "$L_1 \cap \ldots \cap L_n = A$ " so can multiply with subsets that have also {Rock} set like m_n (D), m_n (E), m_n (G) and for calculating of $m_{i,\ldots,n}$ (B) the multiplication can be done with m_n (B), m_n (D), m_n (F), m_n (G), for $m_{i,\ldots,n}$ (C) with m_n (C), m_n (E), m_n (F), m_n (G) , for $m_{i,\ldots,n}$ (D) the multiplication should be done with m_n (G) and m_n (D) , for $m_{i,\ldots,n}$ (E) between m_n (E) and m_n (G) , for $m_{i,\ldots,n}$ (E). For calculation of K with n layer we confront with longer statement.

As can be seen there are huge statements for integration of n layers that produce mistakes in calculations and also make problem to submit an algorithm. With regard to Wilson 2004 study; combination can be calculated between two layers and then conclusion again can be used for combination with next layers. Hence we should n-1 times combine two layers according to expression 2-12, first $m_1 \otimes m_2$ and then $(m_1 \otimes m_2) \otimes m_3$, and so on, until calculating of $m_1 \otimes \ldots \otimes m_n$ as $(m_1 \otimes \ldots \otimes m_{n-1}) \otimes m_n$. This needs a big calculation expression for every mass of subset so that will be need using of some algorithms to make simple calculation. For calculation has used some calculation programs like MATLAB environment.

The following codes in Matlab indicate applied algorithms for integration of the layers.

```
for n1=1:n-1
if n1==1
```

```
15      a1(1:n_n,1:8) = data1(1:n_n,(n1-1)*8+1:(n1-1)*8+8);
16      end
17      a1(1:n_n,9:16) = data1(1:n_n,(n1)*8+1:(n1)*8+8);
18      for i1 =1:8
19         for i2 =9:16
20            gg=a1(:,i1).*a1(:,i2);
21            s=[1;2;3;4];
22            s=intersect(s,m(:,i1));
23            s=intersect(s,m(:,i2-8));
24            [s1,c1]=size(s);
25            if s1==1
26               s(2:4,1)=nan;
27            elseif s1==2
28               s(3:4,1)=nan;
29            elseif s1==3
30               s(4,1)=nan;
31            end
32            for nm=1:8
33               sm=isequalwithequalnans(s,m(:,nm));
34               if sm==1
35                  DST(:,nm)=DST(:,nm)+gg;
36                  break
37               end
38            end
39         end
40      end
41      for io=2:7
43          DST(:,io)=DST(:,io)./(1-DST(:,1));
44      end
45      DST(:,1)=zeros(n_n,1);
46      a1(:,1:8) =DST;
47      DST=zeros(n_n,8);
48      end
49      DST=a1(:,1:8);
```

In this algorithm line 1 to 12 repeat like last section in 4-1; n is the number of the layers that will be combined and n_n is the number of the rows in the matrix (pixel number in raster data layer), n_n numbers depend on original data in the geospatial environment.

In this algorithm first two layer integrate then the result make a new layer the new layer integrate with next layer this process repeats until the layer. The first loop from line 13 to 16 define the number of repetition of the integrate process and depended on number of data layers or sensor that change and can repeat n-1 time, in matrix a1 column 1 to 8 (set numbers) dedicated to the first layer or to new results of integration two layers and column 9 to 16 to be dedicated to next layer which should integrate with first layer or new results of integration.

There are three loops within each other from line 18 to 40 that define conditional statement in DST's expression while K calculate in the line 35, the first loop indicate sets in first layer and iterate in first layer second loop go to sets in second layer, s in line 21 are equal with 1,2,3,4; 1 means Ø set, 2 means A set, 3 means B set and 4 is equivalent with C set, line 22 and 23 use intersect condition between s and m.

According to expression 4-1 while intersect of the sets are Ø so $\overset{n}{\underset{i=1}{\otimes}} m_i(A) = K$ and line 35 calculate it, other loop from line 41 to 44 calculate DST's expression for every two layers. finally line 47 bring new result from DST integration in a1 column 1 to 8 the loop can repeat with next data layer matrix that to be replaced in a1 column 9 to 16 by line 17 in codes.

Figure (4-1) have been provide after DST calculations and importing of the extracted matrixes in attribute of raster files the matrixes are classified to show simplified maps**.** Natural breaks (Jenks) classification has been used for classifying in this manner classes are based on natural groupings inherent in the data. ArcMap identifies break points by picking the class breaks that best group similar values and maximize the differences between classes. The features are divided into classes whose boundaries are set where there are relatively big jumps in the data values.

In Figure 4-2a can be seen the second column in the matrix that show A set (Rock) and has been imported in raster file and classified, dark blue colour in this raster map signify the high value of mass function after integration of five layers by DST expression, light blue colour show the lowest mass function value for rock after integration this map has bring here only for showing of the results and this set related to rock which we don't need that in this research for mineral exploration but sometimes can help to know which place has lowest mass function for minerals.

Next map (figure 4-2b) related to third column of the matrix and B set which show only Au minerals. In this map dark blue colour show high value of mass function after integration of layers, mineral points (old mine and index points) have been bring on the map and signify an accordance between the points and the dark blue places.

Figure 4-2c indicate map with classification of the column of C set which show Cu mass functions. In this map also can see approximate accordance between dark blue colour what show high value of mass function and mineral points of Cu. figure 4-2d indicate F set classification where mass function has been calculated for Au and Cu in this raster map also this accordance can be seen.

After classifying for B and C set have been provided a table that show the frequency of Mineral points in every classes, this table signify increasing of mass value with raising of mineral points frequency while decreasing of pixel count in every classes. Table 4-3 and 4-4 have shown for B and C sets respectively mass classifying, pixel count for every classes and frequency of mineral points finally relation between frequency and area. With regard to pixel size the area of the every class has been provided in square Km (every pixel has 30*30 m^2 sizes). Figure 4-3 and 4-4 for B and C sets respectively design graphs that show relationship between mineral point frequency and mass functions value; with increasing of mineral points frequency increase mass function value and decrease every class area.

Table 4-3: the table presents number of Indices (mineral points) in every classes of m for set B. after calculations of m for the study area m has been classified class 1 shows low m function and class 6 show high values.

Class Value	Pixel Count	Area sq km	Au Indices number	Index number/Area
1	1885753	1697	1	0.0006
2	1305819	1175	4	0.0034
3	502390	452	2	0.0044
4	396557	356	3	0.0084
5	313422	282	3	0.0106
6	113404	102	3	0.0294

In C set graph there is a break which related to class four; in this part frequency increase relation to close classes, what can be caused by imprecise points and this matter also appear in other methods for integration, other reason can relate to some imprecise data layer, in this case look like the lineament layer create some anomaly however in some other integration method in next parts this break have been adjusted.

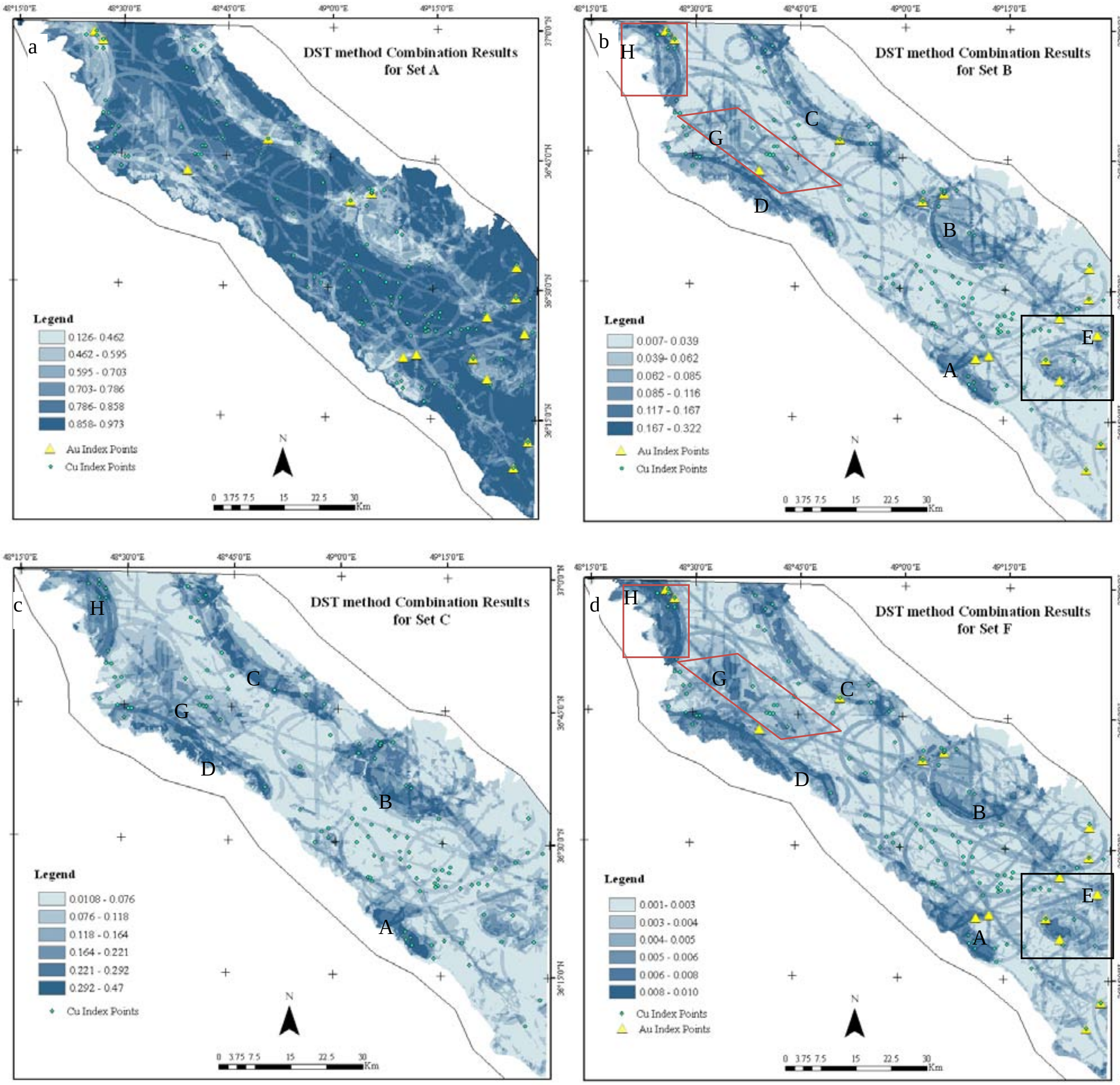

Figure 4-2: present DST integration results, in a bpa have been provided for A set that show the area with only rock outcrops so in this map where have low potential for minerals that have been shown by dark blue colours, b show classified DST for B set in this set there are only Au member and Au mineral point also have shown on the map, dark blue colour on this raster map signify high mass function value. c show the area that can have high mass function value for C set (only Cu), d show F set where can have favorability for occurrence of two paragenesis minerals of Au and Cu. In the figure A, B, C and D signify intrusive masses places, E indicate alteration zone in southeast of the area and G and H are the area that after integration of the all data show high anomaly for mineralization.

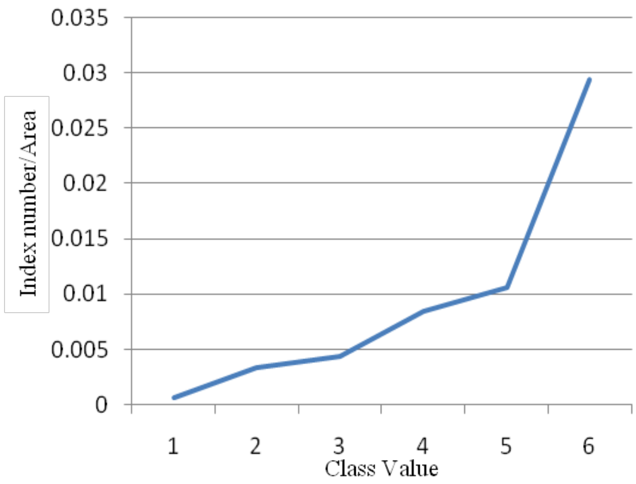

Figure 4-3: present graph for last column of table 4-3, y axis shows division of index number on area, x axis shows classes for set B, with increasing of m, Index number/Area increase too.

Table 4-4: the table shows number of Indices (mineral points) in every classes of m for set C. class 1 shows low values for m function and class 6 shows high values.

Class Value	Pixel Count	Area sq km	Cu Indices number	Index number/Area
1	1861156	1675	28	0.0168
2	1072864	966	32	0.0331
3	582003	524	20	0.0382
4	505105	455	13	0.0286
5	292518	263	14	0.0532
6	203699	183	11	0.0600

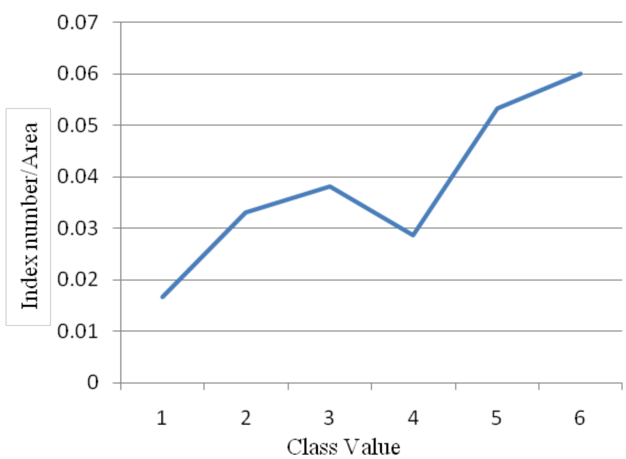

Figure 4-4: present graph for last column of table 4-4, with increasing of m value, Index number/Area increase too. On class four can see a break point.

4.4.2 Discount + combine method and Mixing or average method

These methods have been used for some layer with the same type like alteration. There are more than one data layer from different sources for alteration area. One comes from airborne geophysics data another comes from remote sensing data and other comes from geological map data, also lineaments structures come from three different sources. In some places they have overlaid, and some parts are absolute separate. It is normal that overlaid places have more importance. In Discount + combine method, Shafer has used the discounting function to each specified belief but in Mixing or average method that to be used basic probability assignment (m). Both related to reliability of the sources. By this method a unit basic probability assignment has been provided for alteration area and structures for integration in next methods in DST methods.

$$\mathrm{Bel}^{\alpha\, i}(\mathrm{A}) = (1-\alpha_i)\mathrm{Bel}(\mathrm{A}) \qquad (2\text{-}15)$$

$$\overline{Bel}(\ A) = \frac{1}{n}(Bel^{\alpha}1(A) + ... + Bel^{\alpha}n(A)) \qquad (2\text{-}16)$$

$$\mathrm{m}_{1\ldots n}(\mathrm{A}) = \frac{1}{\mathrm{n}}\sum_{\mathrm{i}=1}^{\mathrm{n}} \mathrm{w}_{\mathrm{i}}\mathrm{m}_{\mathrm{i}}(\mathrm{A}) \qquad (2\text{-}38)$$

As can be seen in expressions 2-14, 2-15 and 2-40, this integration method is similar to simple average and the calculation can be done in attribute calculation of ArcMap. The raster results are illustrated in Figure (4-5). In this maps high value of bpa (mass) to shown by dark blue colour and low value of bpa by light blue colour.

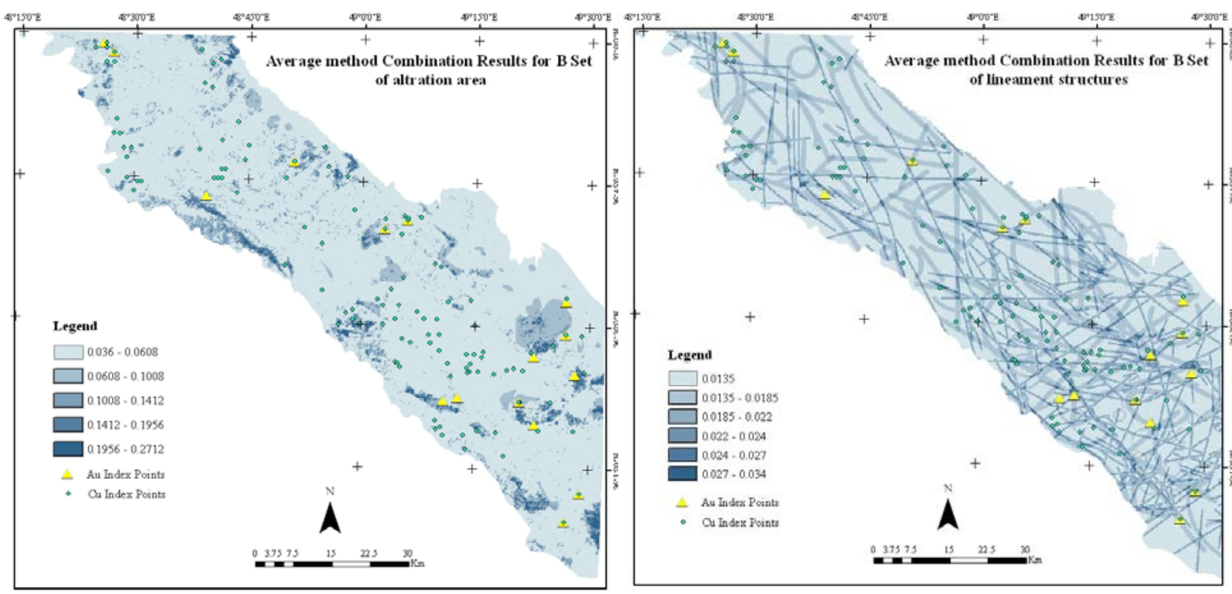

Figure 4-5: present integration results for B set on the raster map, in a alteration area from deferent sources to be combined and in b lineament structure data layer to be combined.

4.4.3 Yager's modified Dempster's rule

Yager's modified combination rules with regard to chapter 2 use expressions 2-18. That is the same denominator of Dempster-Shafer but in this method without normalization part. Figure 4-6 present grid result for mass function after combining data by Yager's modified rule. As mentioned in this rule there isn't normalization part. So when there are many numbers of sensors or data layers this calculation creates very small values and this matter make inaccuracy. In this case, the result of integration of five layers show some adjusting and modifying in table 4-5 and the figure 4-7, the related graph raise without decreasing and breaking in class four.

$$\mathrm{q}(\mathrm{A}) = \sum_{\bigcap_{\mathrm{i}=1}^{\mathrm{n}} \mathrm{A}_{\mathrm{i}} = \mathrm{A}} \mathrm{m}_1(\mathrm{A}_1)\mathrm{m}_2(\mathrm{A}_2)\ldots\mathrm{m}_{\mathrm{n}}(\mathrm{A}_{\mathrm{n}}) \qquad (2\text{-}18)$$

$$\mathrm{m}^{\mathrm{Y}}(\mathrm{X}) = \mathrm{q}(\mathrm{X}) + \mathrm{q}(\varnothing) \qquad (2\text{-}20)$$

The programming codes change from line 41 to 47; according to expression 2-18 only in universal set (G in column 8) there are calculation of K and normalizing by that how can see in line 43 that has been acquired and other column from 2 to 7 have been found out by line 45.

```
41        for io=2:8
42            if io== 8
43                DST(:,io)=DST_Yager(:,io)+ DST(:,1);
44            elseif io==2:7;
45                DST(:,io)=DST(:,io);
46            end
47        end
```

Table 4-6 and figure 4-8 present the result of this method combination in 6 classes and frequency of the indices in every class in these tables like last method; frequency raise by decreasing of area and increasing of mass value (bpa), there aren't considerable breakings in the graphs and last problem have been solve in this method.

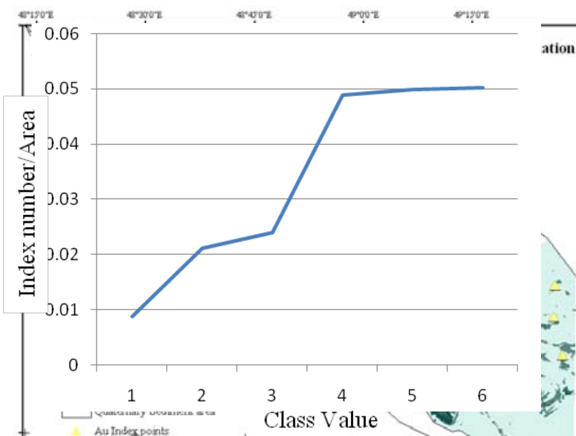

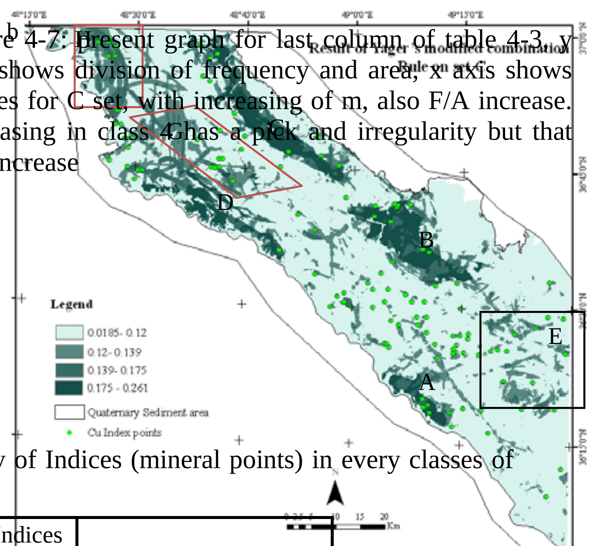

Figure 4-7: present graph for last column of table 4-3, y axis shows division of frequency and area, x axis shows classes for C set, with increasing of m, also F/A increase. Increasing in class 4 has a pick and irregularity but that still increase

Table 4-6: the table provided for showing of the frequency of Indices (mineral points) in every classes of classified set B.

Class Value	Pixel Count	Area sq km	Au Indices number	Index number /Area
1	1083609	973	1	0.00103
2	1171220	1054	1	0.00095
3	1026991	924	3	0.00325
4	647664	583	4	0.00686
5	348796	314	4	0.01274
6	241065	217	3	0.01388

Figure 4-6: represent grid result of mass function after applying Yager's modified rule for integration in this grid map a show mass function for set B (Au) and b show the integration result for set C (Cu). In both mass functions increase in alteration zone, and in intrusive rocks area in addition there are two area with increasing mass function in northwest of the study area due to geophysics anomalies.

Table 4-5: the table provided for showing of the frequency of Indices (mineral points) in every

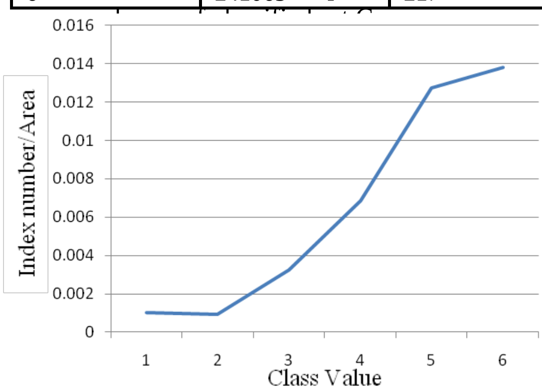

km	Cu Indices number	Index number/Area
	4	0.0088
	30	0.0212
	23	0.0240
	29	0.0488
	19	0.0498
	13	0.0502

Figure 4-8: present graph for last column of table 4-3, y axis shows division of frequency and area, x axis shows classes for B set, with increasing of m, also F/A increase.

4.4.4 Inagaki's unified combination rule

In this method, expressions 2-34 and 2-35 have been used for integration of data layers. As mentioned in last parts X is a universal set and equivalent with G set in this research. With regard to expression 2-34, C are all set that aren't equal with universal set and include set Ø, A, B, C, D, E, F.

$$m^{U}_{k_{ext}}(C) = \frac{1 - q(X)}{1 - q(X) - q(\varnothing)} q(C) \qquad \text{For } C \neq X, \qquad (2\text{-}34)$$

$$m^{U}_{k_{ext}}(X) = q(X) \qquad (2\text{-}35)$$

Following codes in Matlab have been provided for calculation of this expression; the loop calculates column 2 to 7 which are equivalent with A to F sets, column 1 is Ø.

```
for io=2:7
    if io==8
        DST(:,io)= DST(:,io);
    end
    DST(:,io)=((1-DST(:,8)).* DST(:,io))./(1-DST(:,8) - DST(:,1));
end
```

Figure 4-9 represent grid result for mass function after combining data by Inagaki's unified combination rule. The integration result show high mass function value on intrusive rocks and

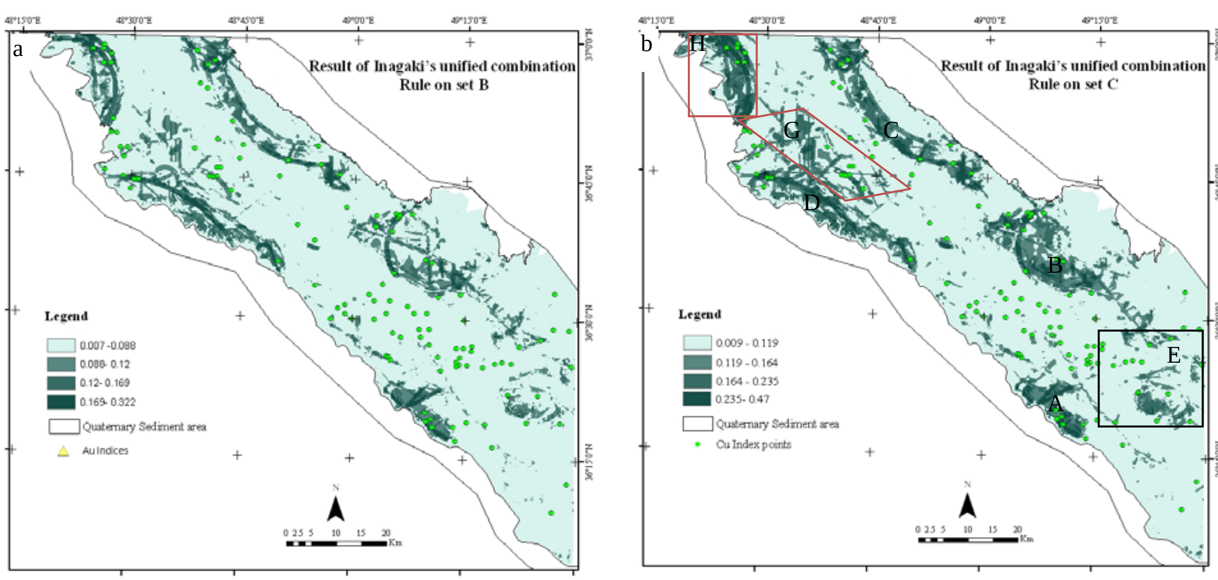

Figure 4-9: represent grid result of mass function after applying Inagaki's unified rule for integration of mass functions, in this grid map a show mass function for set B (Au) and b show the integration result for set C (Cu). In both grid map, mass functions increase over alteration zone, and intrusive rocks area. in addition there are two area with increasing mass function in northwest of the study area due to geophysics anomalies.

alteration area in addition of geophysics anomalies area.

The results about frequency of mine points in the area have been brought in Tables 4-8, 4-9 and figure 4-10, 4-11. this time graph in figure 4-8 show a breaking in class 5; faults generally in class five and four; in the south of the area create a false anomaly other way it is possible that imprecise points create this false anomaly, with regard to Au mineral points there are a few points but they are more precise and such problem cannot appear on the graphs and tables.

However that have been tried to consider them in mass functions (m) but still in some methods that create false anomaly.

Table 4-8: the table provided for showing of the frequency of Indices (mineral points) in every classes of classified set C.

Class Value For set C	Pixel Count	Area sq km	Cu Indices number	Indices number / Area
1	1666597	1410	26	0.0173
2	996961	897	19	0.0212
3	701158	631	28	0.0444
4	543566	489	19	0.0388
5	415925	374	8	0.0214
6	193138	174	18	0.1036

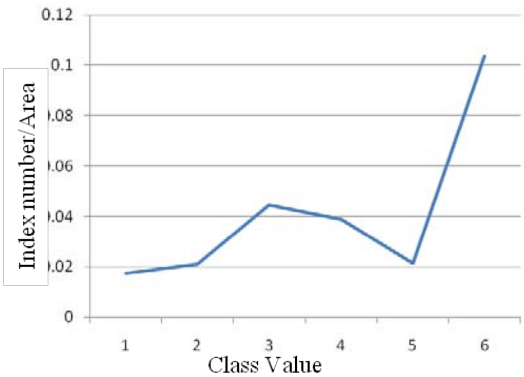

Figure 4-10: present graph for last column of table 4-3, y axis shows division of frequency and area, x axis shows classes for C set, with increasing of m, also F/A increase. in class 4 and 5 again there is irregularity but that increase in class 6.

Table 4-9: the table provided for showing of the frequency of Indices (mineral points) in every classes of classified B set. Area have been also calculated for every class in fourth column, in the last column can see division of the frequency by area (F/A), these can help to explain the area with high m after integrating have more capability to have mineral points.

Class Value For Set B	Pixel Count	Area sq km	Au Indices number	Indices number /Area
1	1885310	1697	1	0.0006
2	1331017	1198	4	0.0033
3	552622	497	2	0.0040
4	373337	336	3	0.0089
5	266491	240	3	0.0125
6	108568	98	3	0.0307

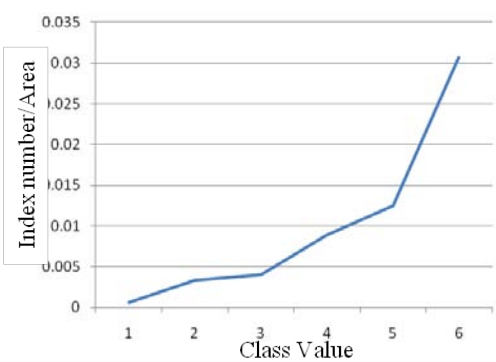

Figure 4-11: present graph for last column of table 4-3, y axis shows division of frequency and area, x axis shows classes for B set, with increasing of m, also F/A increase.

4.4.5 Dubois and Prade's disjunctive consensus rule

With regard to chapter two this method uses union of the bpa by extending the set-theoretic union:

$$m \cup (C) = \sum_{A \cup B = C} m_1(A) m_2(B) \qquad (2\text{-}36)$$

for two layers can be presented by the following expressions:

$m_1 U\ m_2 (A) = [m(A_1)*m(A_2)]$

$m_1 U\ m_2 (B) = [m(B_1)*m(B_2)]$

$m_1 U\ m_2 (C) = [m(C_1)*m(C_2)]$

$m_1 U\ m_2 (D) = [m(A_1)*m(B_2)] + [m(B_1)*m(A_2)] + [m(D_1)*m(D_2)] + [m(A_1)*m(D_2)] + [m(D_1)*m(A_2)] + [m(B_1)*m(D_2)] + [m(D_1)*m(B_2)]$

$m_1 U\ m_2 (E) = [m(A_1) * m(C_2)] + [m(C_1) * m(A_2)] + [m(E_1) * m(E_2)] + [m(A_1) * m(E_2)] + [m(E_1) * m(A_2)] + [m(C_1) * m(E_2)] + [m(E_1) * m(C_2)]$

$m_1 U\ m_2 (F) = [m\ (B_1) * m(C_2)] + [m(C_1) * m(B_2)] + [m(F_1) * m(F_2)] + [m(B_1) * m(F_2)] + [m(F_1) * m(B_2)] + [m(C_1) * m(F_2)] + [m(F_1) * m(C_2)]$

$m_1 U\ m_2 (G) = [m(A_1)*m(F_2)] + [m(A_1)*m(G_2)] + [m(F_1)*m(A_2)] + [m(G_1)*m(A_2)] + [m(B_1)*m(E_2)] + [m(B_1)*m(G_2)] + [m(E_1)*m(B_2)] + [m(G_1)*m(B_2)] + [m(C_1)*m(D_2)] + [m(C_1)*m(G_2)] + [m(D_1)*m(C_2)] + [m(G_1)*m(C_2)] + [m(D_1)*m(G_2)] + [m(G_1)*m(D_2)] + [m(E_1)*m(G_2)] + [m(G_1)*m(E_2)] + [m(F_1)*m(G_2)] + [m(G_1)*m(F_2)] + [m(G_1)*m(G_2)] + [m(D_1)*m(E_2)] + [m(E_1)*m(D_2)] + [m(D_1)*m(F_2)] + [m(F_1)*m(D_2)] + [m(E_1)*m(F_2)] + [m(F_1)*m(E_2)]$

In the Matlab codes in line instead of intersect syntax has been used union syntax and line 26 code calculates that.

```
18      for i1 =1:8
19          for i2 =9:16
20              gg=a1(:,i1).*a1(:,i2);
21              s=union(m(:,i1),m(:,i2-8));
22              s=s(1:4);
23              for nm=1:8
24                  sm=isequalwithequalnans(s,m(:,nm));
25                  if sm==1
26                      DST(:,nm)=DST(:,nm)+gg;
27                      clear s
28                      break
29                  end
30              end
31          end
32      end
33      for io=2:8
34      end
```

Table 4-10, 4-11 and figure 4-12, 4-13 signify the best result. The related graph to C set (figure 4-11); the same Cu, don't create breaking by abnormal high mass function value and with frequency increasing that so increase uninterruptedly. But problem is in very small mass value in B and C sets due to multiplying of many mass functions what are less than one by the way absence of normalizing part. When the data layers are more this small mass function value can create imprecise results.

Figure 4-14a and b show the raster map of Classified B and C set for Au and Cu respectively.

Table 4-10: the table provided for showing of the frequency of Indices (mineral points) in every classes of classified set C.

Class Value For Set C	Pixel Count	Area sq km	Cu Indices number	Indices number /Area
1	2372066	2135	43	0.020
2	1319771	1188	36	0.030
3	509745	458	17	0.037
4	208477	187	11	0.059
5	89617	80	9	0.112
6	17669	15	2	0.126

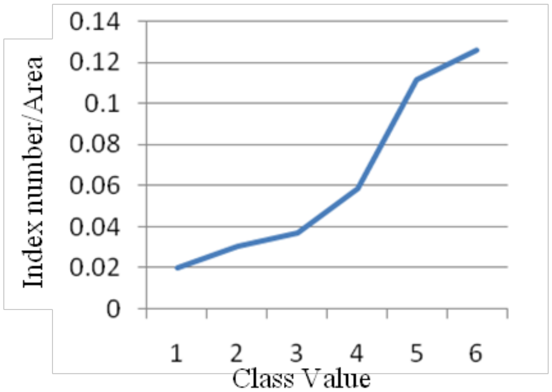

Figure 4-12: present graph for last column of table 4-3, y axis shows division of frequency and area, x axis shows classes for C set, with increasing of m, also F/A increase. This graph shows that previous problem have solved apparently.

Table 4-11: the table provided for showing of the frequency of Indices (mineral points) in every classes of classified set B.

Class Value For Set B	Pixel Count	Area sq km	Au Indices number	Indices number /Area
1	2552296	2297	3	0.0013
2	1168439	1052	4	0.0038
3	471027	424	2	0.0047
4	191253	172	3	0.0174
5	134330	121	5	0.0413
1	2552296	2297	3	0.0013

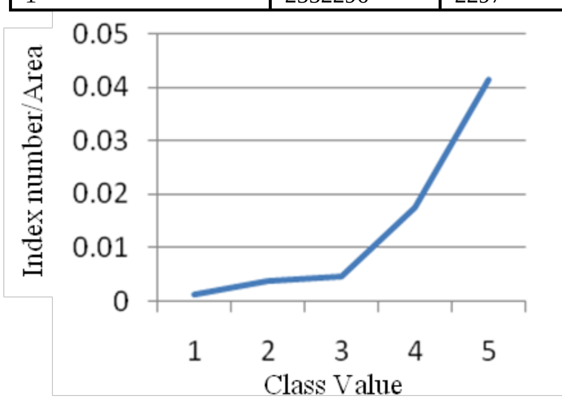

Figure 4-13: present graph for last column of table 4-3, y axis shows division of frequency and area, x axis shows classes for B set, with increasing of m, also F/A increase.

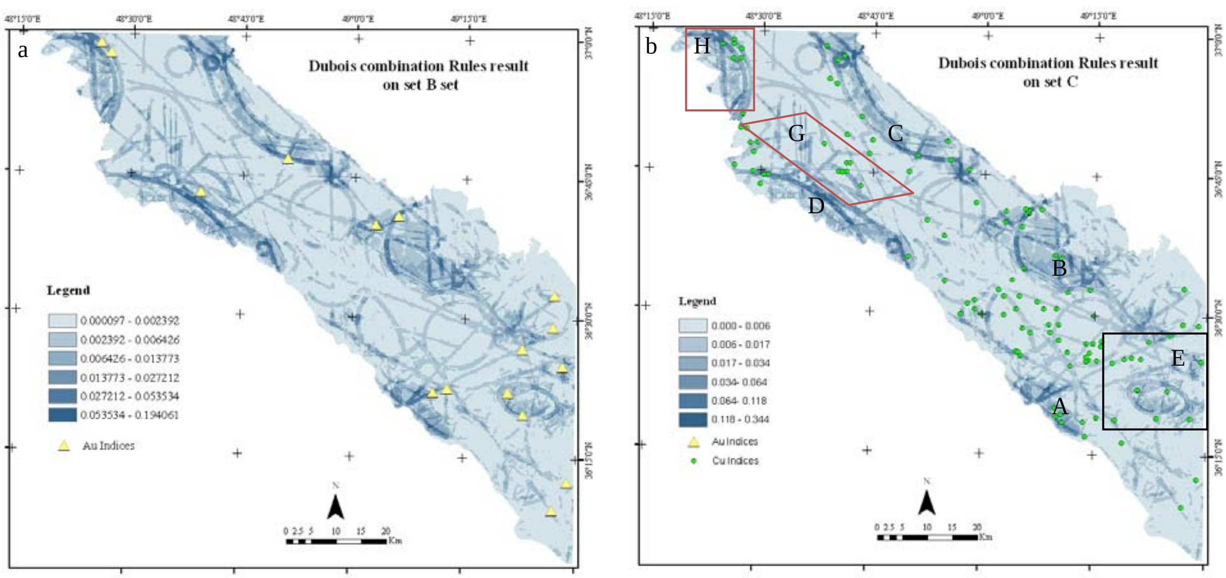

Figure 4-14: present integration results for B set and C set in a and b raster maps respectively, dark blue show high m while light blue show low m, in legend can see the number of results are very small.

4.4.6 Convolutive X-Average and Zhang’s center combination rule

As mentioned in chapter two convolution x-average is a generalization of average for scalar number and with regard to X set and sets in this research there isn’t ability in this project with geospatial background defining the sets with scalar numbers so this modified method wasn’t use in this case.

Chapter 5: Discussion and conclusion

5.1 Introduction

After all processing in last chapter we need to understand and evaluate which DST rules are more compatible to solve uncertainty in GIS environment and which rules give more desirable results to find mineral potential area. This chapter discusses results and tries to present a comparison between different modification rules results. The comparison is explained especially on combining parts and finally evaluates their results.

5.2 Comparison and evaluation

In this thesis I use 5 modified rules from DST rules to determine uncertainty in a GIS environment for mineral exploration. All 5 modified rules use the first part of DST rules (bpa or m, mass function) to assign a score to the data. However in the second part with the combination of data, every 5 DST modified rules are different from each other.

As mentioned in the last chapters Dempster-Shafer theory (DST) has three important functions. The basic probability assignment or mass function (bpa or m), the Belief function (Bel) and the Plausibility function (Pl) to weight data. In this research, the bpa is adequate for making weighted data and combining the data. Finally, after combining different layer using the DST combination rules, graphs show the comparison of results. This research applies Pl and Bel functions to provide the graphs but the results are near to from bpa function weighting.

Second part of the DST expression formed from a fraction with two terms: denominator and numerator. Main differences are in the denominator parts; numerators change less than in the DST rules expressions. The following sections present advantages and disadvantages for every DST modified rules in terms of expressing uncertainty.

5.2.1 Dempster-Shafer theory

Dempster-Shafer theory uses bpa function as well as other related rules for weighting. After weighting of different data layer from different sources are combined by applying expression 2-12. Expression 2-14 shows calculating of K in the denominator part of the ratio in the expression 2-12.

With regard to last chapter, I calculate DST in MATLAB and import the extracted matrices in the grid files then I classify the matrices to show simplified maps in figure 4-1. Natural breaks (Jenks) classification has been used for classifying, in this way; classes are based on natural groupings inherent in the data. ArcMap identifies break points by picking the class breaks that best group similar values and maximize the differences between classes. The features are divided into classes whose boundaries are set where there are relatively big jumps in the data values.

Figure (4-1) shows the attribute table of lithology data layer. For every data layer we have a grid file and for every grid file there is an attribute table like figure 4-1. The three first columns have been made by software program for five classes. I quantify the scores for mass value in the next seven columns for every class, for all data layer I quantify mass value like as figure 4-1. The seven columns A, B, C, D, E, F, G show sets {Rock}, {Au}, {Cu}, {Rock, Au}, {Rock, Cu}, {Au, Cu}, {Rock, Au, Cu} and {Ø} respectively. When all grid files combine with each other in the ArcGIS software it will provide an attribute table with grid file. I use the data of this attribute table to DST calculation in the other software. After DST calculations we have 7 columns for 7 sets again. These data can be imported in the attribute table of the final grid file. When you have the new attribute file for the final grid file you can reclassify the grid file.

Figure 4-2b represents the final grid file after reclassifying of DST calculation results for set B (set {Au}) which show the area with range of mass function for Au minerals. In these maps, dark blue colours show high value of bpa after integration of layers. Mineral points (old mine and index points) have been represented also on the map and signify correspondences between the index points and the dark blue places, most point lie on dark blue colour classes. Figure 4-2c shows the classification of mass value for set C which shows Cu mass functions. Also indicate approximate correspondence between dark blue colour (high value of mass function) and Cu mineral points. Figure 4-2d indicates set F classification where mass function has been calculated for set {Au, Cu} where both minerals can occur. The maps show correspondence between index point and dark blue clearly. In addition, some graphs in chapter 4 also show this correspondence between index points and high mass value classes.

In chapter four you can see for every combination method some table beside of graphs, like table 4-3 and figure 4-3. As explained in last chapter, I use the tables for providing graphs. I classified mass functions from DST calculations for B (which indicates Au) and set C (which indicates Cu) to make table (4-3). Table 4-3 shows ID of classes, the frequency of Mineral points in every class (index point number in the every class), the area for every class and ration of frequency on area. In this table can be seen increasing of mass value (Class ID) with increasing of mineral point frequency while area for every class decreases. The Tables 4-3 and 4-4 in last chapter show mass functions classifying for sets B (Au) and C (Cu) respectively. Figure 4-3 and 4-4 for sets B and C respectively show graphs, Figures show relationship between mineral point frequency and mass functions value; with increasing mineral point frequency, mass function value increase too, but area in every class decreases.

In set C graph (figure 4-4) that can be seen a break pint in class 4, in this part frequency increase between neighbour classes. That can be caused by imprecise data and that also appear in other DST integration methods. The other reason can be related to some inaccurate data layers, in this case, that look like the lineament layer create some anomaly however in some other integration method in next parts this break point has been adjusted. Table 4-3 shows the area with high m after integrating has more capability to have mineral points. Figure 4-3 presents graph for table 4-3, while m increases, F/A increases too. But a break point on class four can be noticed.

Table 4-4 shows the frequency of Indices (mineral points) in every classes of classified set B. Area have been also calculated for every class. In the last column you can see division of the frequency by area (F/A), these also show with high m after integrating have more capability to have mineral points. Figure 4-4 presents related graph for last column of table 4-3, y axis shows division of frequency and area, x axis shows classes for set B, with increasing of m, also F/A increase. There is not a clear break point on this graph.

The break point shows low accuracy in results and that can be related to the first step in bpa determine and on the other hand that can be related to accuracy in initial data. I try to apply accurate bpa and initial data but it is possible some low accurate data like lineaments or alteration area create incorrect results.

As in figure 4-2 can be seen the mass function integration show anomalies over the intrusive masses A, B, C and D; alteration zones special in area E and on geophysics anomalies. In area H and G there aren't remarkable alteration zone ore intrusive masses but index points and geophysics study and finally integration results of the data show a desirable area for prospecting.

5.2.2 Discount + combine method and Mixing or average method

Discount + combine methods of DST are suitable for layers with the same type like alteration or lineament structures data, as mentioned in last chapters. In these type layers, there are more than one data layer for alteration area from different sources. One alteration layer comes from airborne geophysics data another comes from remote sensing data and other come from geological map data. I extract lineaments structures from three different sources and submit them in tow layers. For Discount + combine method, has been used the discounting function to each specified belief. In Mixing or Average methods, basic probability assignment (bpa or m) has been used both are related to reliability of the sources.

By this method a unit basic probability assignment has been provided for alteration area and structures for integration in next methods in DST methods. As that can be seen in expression 2-15, 2-16 and 2-40, this integration method is so similar to simple average and the calculation can be done in attribute calculation of ArcMap, the grid results have been illustrated in Figure (4-5) in this maps high value of bpa (mass) to be shown by dark blue colour and low value of bpa to be shown by light blue colour. Figure 4-5 shows integration results for set B on the grid map, in a alteration area from deferent sources to be combined and in b lineament structure data layer to be combined.

In other method when there are many data layer that create a very small K and small numerator so result of the DST fraction will be very small value, therefore create imprecise result. After using this method for six alteration and lineament data layers; we have only two layers for alteration area lineament structures without remarkable decreasing in the m values. Thus this method help to decrease number of exchangeable data layers for applies in other DST methods.

5.2.3 Yager’s modified combination rules

Yager’s modified combination rules for combining of data layers use expressions 2-17 to 2-25. Dempster’s rule is an example of an associative combination operation and the order of the information does not impact the resulting fused structure. Yager points out that in many cases a non-associative operator is necessary for combination. However, the arithmetic average can be updated by adding the new data point to the sum of the pre-existing data points and dividing by the total number of data points. This is the concept of a quasi-associative operator that Yager introduced in.

Yager starts with an important distinction between the basic probability mass assignment (m) and what he refers to as the ground probability mass assignment (designated by q). With regard to expression 2-17, the Yager's rule of combination is not associative, the combined structure q(A) can be used to include any number of pieces of evidence. As mentioned for 2-16 Through the quasi-associativity that Yager describes, the combined structure q(A) can be updated based on new evidence.

Instead of normalizing out the conflict, as that find in the case of the Dempster rule, Yager, at the end attributes conflict to the universal set X through the conversion of the ground probability assignment to the basic probability assignments. The interpretation of the mass of the universal set (X) is the degree of ignorance.

Dempster’s rule has the effect of changing the evidence through the normalization and the allocation of conflicting mass to the set null. Yager’s rule can be considered as an epistemologically honest interpretation of the evidence as it does not change the evidence by normalizing out the conflict. In Yager’s rule, the mass associated with conflict is attributed to the universal set and thus enlarges this degree of ignorance.

Figure 4-6 represent the mass function integration results for set C and B, here can see anomalies lie on the intrusive masses A, B, C and D; alteration zones special in area E and on geophysics anomalies. In area H and G there aren't remarkable alteration zone or intrusive masses but index points and geophysics study and finally integration results of the data submit two desirable areas for prospecting.

In this case study with integration of five layers the result show some adjusting and modifying. With regard to chapter 4, table 4-5 and the figure 4-7 show some results for set C. the table shows frequency of Indices (mineral points) in every classes of classified. Area have been also calculated for every class in fourth column, in the last column can see division of the frequency by area (F/A), these can help to explain the area with high m after integrating have more capability to have mineral points. With increasing of F/A m also rise. Figure 4-7 present graph for last column of table 4-3, y axis shows division of frequency and area, x axis shows classes for set C, with increasing of m, also F/A increase. Increasing in class 4 has a pick and irregularity but that still increase. The combination results classified to six classes and tables show indices frequency in every class. Frequency rise by decreasing of area and increasing of final mass value (m). In the related graph; F/A rise without decreasing but still there are small breakings in class three and four. Table 4-6 and figure 4-8 present the result of this method combination for set B. Here also, the graph show rising of F/A by rising classes, while there is break point on class four.

In DST method can see remarkable F/A increasing and breaking for both sets but there aren't considerable breakings in the graphs in Yager’s method. Last problem have been solved somewhat in this method.

5.2.4 Inagaki’s unified combination rule

This combination rule takes advantage of the ground probability assignment function (q) (As mentioned in chapter 2, expressions 2-26 to 2-35). Inagaki’s rule applies only to the situations where there is no information regarding the credibility or reliability of the sources.

The parameter k is used for normalization. The determination of k is an important step in the implementation of this rule, however, a developed well-justified procedure for determining k is lacking. In (Inagaki, 1991), Inagaki poses the optimization problem for the selection of k to be an open and critical research question. The value of k directly affects the value of the combined basic probability assignments and will collapse to either Dempster’s rule or Yager’s rule under certain circumstances. The parameter k gives rise to an entire parametrized class of possible combination rules that interpolate or extrapolate Dempster’s rule. With regard to figure 2-11 k in yager’s rule are 0 and in the inagaki’s rule is bigger than Dempster’s rule. So Inagaki’s Unified rule of combination use Yager’s ground functions to develop a parametrized class of combination rules that subsumes both Dempster’s rule and Yager’s rule. Inagaki compares and orders three combination rules: Dempster’s rule, Yager’s rule, and the Inagaki extra rule.

The grid for integration of mass functions in figure 4-9 represents results similar DST, and Yager’s modified combination rules there are in area G and H high value mass function results.

In chapter 4 shows applying of this rule to combination of m. The results about frequency of mine points can see in tables 4-8, 4-9 and figure 4-10, 4-11. The graph in figure 4-10 shows a breaking in class 5. Table 4-8 provided for showing of the frequency of Indices (mineral points) in every class of the basic probability assignments results for set C (Cu). Figure 4-10 presents graph for table 4-8, you can see with increasing of m, also F/A increase. In class 4 and 5, there is irregularity but that increase in class 6 again.

The table 4-9 indicates the frequency of Indices (mineral points) in every class of the basic probability assignments results for set B (Au). The Related figure 4-11 presents graph for table 4-9, with increasing of m, can see increasing F/A without break point.

Interruption and break points appear mainly in class five or four. That can be related to data layer that extracted from different source, because the precise of this information was low. On the other hand it is possible that interruption and break points appear due to imprecise index points. About Au mineral points; There are a few Au mineral points and they are more precise so such problem didn't appear on the graphs and tables. However that have been tried to consider them in first step of mass functions (m) determining but still in some methods that create false anomaly.

5.2.5 Dubois and Prade's disjunctive consensus rule

Dubois and Prade's disjunctive consensus rule define the union of the basic probability assignments $m_1 \cup m_2$ by extending the set-theoretic union with expressions 2-36 and 2-37.
As mentioned in last chapter, the union does not generate any conflict and does not reject any of the information asserted by the sources. But the disadvantage of this method is that it may yield a more imprecise result than desirable. The union can be more easily performed via the belief measure also. The disjunctive pooling operation is commutative, associative, but not idempotent. In interval-data type the upper and lower bounds for the disjunctive consensus are defined by the minimum of the lower bounds and the maximum of the upper bounds. The calculations for the joint of the basic probability assignments are the product of the marginal. This is also known as a convex hull of all unions.
Result of the union can see in tables 4-10, 4-11 and figures 4-12, 4-13. The table 4-10 shows frequency of Indices (mineral points) in every class of the basic probability assignments results for set C (Cu). With regard to Figure 4-12 that it show The related graph to table 4-10, with increasing of m, F/A increase also. Here can see, the basic probability assignments doesn't create breaking by abnormal high mass function value and low frequency; that increase without interruption. Table 4-11 shows the frequency of Indices (mineral points) in every class of the basic probability assignments results for set B (Au). In figure 4-13, related graph to table 4-11 can see increasing of m by increasing F/A without interruption and break point. Figure 4-14 present integration results for set B and set C in a and b grid maps respectively, dark blue show high m while light blue show low m, in legend can see the number of results are very small. In this grid map also can see high mass value on intrusive masses and alteration zone in addition of two areas H and G.
Main problem is mass value in sets B and C. This combining rule creates very small mass value, due to lacking of normalizing part. On the other hand in DST expressions on the numerator parts, there is multiplying of many mass functions that they are less than 1, so that create very small value m and consequently imprecise final m. When there are more than five data layers, this small mass function value can create imprecise results.
I use Disjunctive consensus pooling combine method and Mixing or average methods for avoiding of many data layers multiplication. As mentioned last parts Mixing or Average methods can be used when we have a type data from different sources. So that decrease number of data layers and the number of data layers for this combining reached to five. The result for both sets C and B (Cu, Au) in graph show increasing of m by increasing F/A without interrupting and break points especially in class four.

5.3 Final issue and suggestion

Dempster's rules for defining uncertainty confront with two issues; algebraic rules and their applications. Chapter 2 discuss the algebraic rules for solving the integration of uncertainty and chapter 4 shows how to apply the rules in GIS environment for finding mineral potential areas. Table 5-1 shows comparison of algebraic rules properties and results of combining data by these rules in GIS environment for mineral exploration.

Table 5-1- shows comparison between combination rules and their results for set C and B in mineral exploration. In this table can see algebraic properties also those come from table 2-14. Idem., Com., Asso. And Quasi-Asso show abbreviated form of Idempotent, Commutative, Associative and Quasi- Associative respectively.

Combination Rules	Integration results Correspondence with index points in graphs		Algebraic Properties			
	Set C	Set B	Idem.	Com.	Asso.	Quasi- Asso.
Dempster's Rule	decreasing in class 5	Continuously, break point in class 5	No	Yes	Yes	
Yager's Rule	Continuously, break point in class 5	Continuously, break point class 5	No	Yes	No	Yes
Inagaki's Rule	decreasing in class 5	Continuously	No	Yes	Depends on value of *k*	Depends on value of *k*
Disjunctive Consensus Pooling	continuously	continuously	No	Yes	Yes	

The table shows the results for set C and set B, in the all results you can see a break point in class 5 except (figure 5-1) for Disjunctive's rule results. As mentioned in last parts that can be relate to some imprecise data layers. With regard to chapter 3, the lineament layers have low accuracy and for some part of the area, there is imprecise lithological information like Abhare sheet. Also on the other hand with regard to discussions in chapter 2; Disjunctive's rule is the most imprecise of the combination method in DST's rules. However this method's results, show more imprecise results than others. That looks, these results are more correct because in graphs we can see correspondence between index points and results. But with regard to theory discussions (chapter 2); that can be related to low accuracy in the rule for the combination of data so the results in this method cannot be relied on.

With regard to processing in chapter 4, all DST's integration rules show almost similar results with a little difference; Dubois and Prade's rules show more conformity between index points and integration result in graph (figure 4-12 and 4-13). In the three other rules (Dempster's Rule, Inagaki's Rule, Yager's Rule), there are a break point in the near classes, therefore they can be used interchangeably.

As we see in algebraic theory for Yager's rule and Inagaki's rule, there is no conflict in mass functions (chapter 2) like Dempster's rule and in algebraic results also. They are similar but Yager's rule has preference in algebraic discussions. On the other hand with regard to Yager's rule results (chapter 4). It looks that integration results show more correspondence with index points. There is a break point in class 4 but not much increase or decrease. Already I explain some anomaly in class 5 related to low accuracy in primitive data. Consequently, I suggest Yager's rule before Dempster's rule and Inagaki's rule to define uncertainty for geological data in GIS environments.

Figure 5-2 proposes intrusive masses areas and delineated areas by red colour in Tarom zone for prospecting and detailed studies by more accurate data and more accurate methods like neural network or fuzzy logic.

The high mass function areas consist of areas H, G1 and G2 in northwest of zone and intrusive masses and some small areas. In areas H, G1 and G2, high mass values are due to geophysical anomalies, in area E is due to existence of alteration zone, and in areas I, J, and K are because of anomalies in different data.

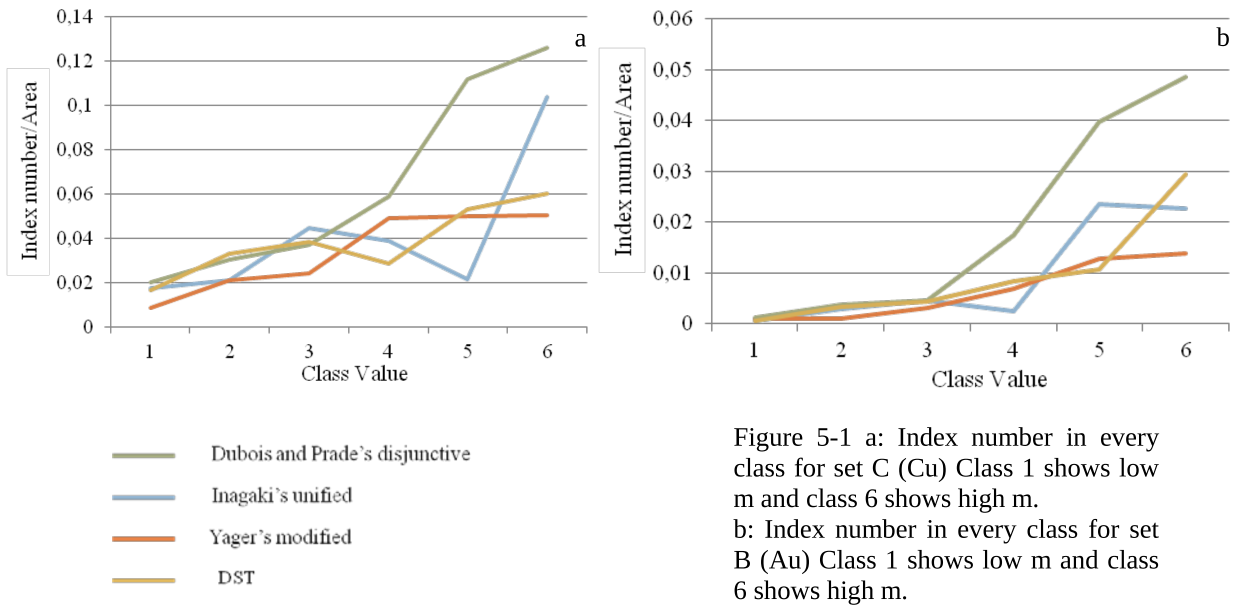

Figure 5-1 a: Index number in every class for set C (Cu) Class 1 shows low m and class 6 shows high m.
b: Index number in every class for set B (Au) Class 1 shows low m and class 6 shows high m.

Figure 5-2: represent mass functions for set F ({Au, Cu}) by Yager's modified combination.

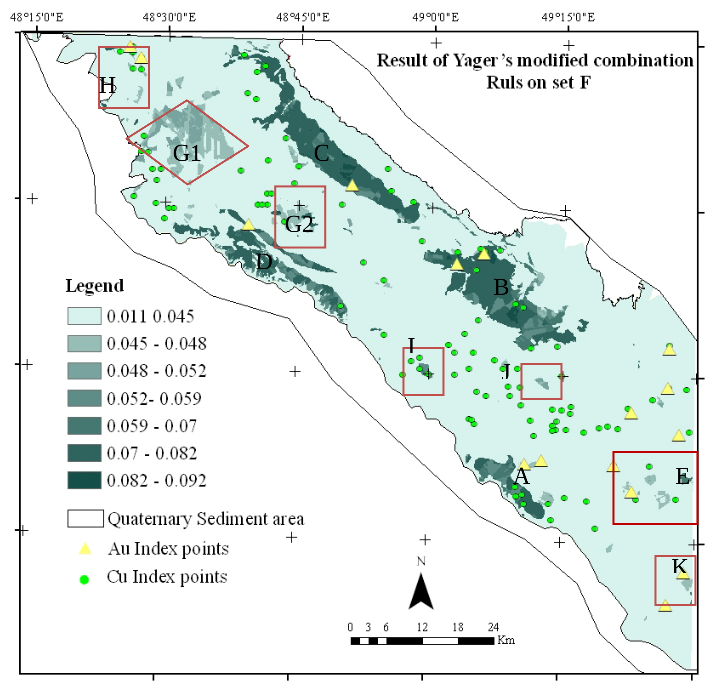

Appendix

Table 1: This table represents rock type of the area in 7 geological map sheets (1/100,000 scale) and age of them with range. This range has been defined by using models; number 1 show high probabilities and 5 low probabilities for mineralization.

LABLE	Rock type	Age	Range
Zanjan			
EA2	Fine to medium - grained bedded sandstone with black unstratified mudstone	Eocene	5
EA3	Plale green - lapilli tuff and tuff breccia with yellowish green nummulitic sandstone	Eocene	3
EA4	Sandstone and mudstone	Eocene	5
EA5	Thin bedded light pink tuff and lapilli tuff	Eocene	3
EA6	Porphyrite , andesitic tuff, welded tuff and sandstone	Eocene	2
EA7	Tuff breccia and lapili tuff, purple grey coloured	Eocene	3
EA8	Reddish purple andesite , tuff breccia, sandstone and mudstone	Eocene	2
EK1	Alternation of sandstone and mudstone with some intercalations of porphyritic andesit lava	Eocene	2
EK2	Sandstone coarse - grained, grey or light green coloured with grey to black porphyritic lavas	Eocene	2
EK3	Alternation of andesitic lava and sandy tuff	Eocene	2
EK4	Sedimentary tuff and tuffaceous, sandstone , green - dark blue coloured	Eocene	3
EK5	Pumice tuff, lapilli tuff and fine grained tuff, white to palegreen coloured	Eocene	3
EK6	Porphyritie andesite and sandstone plale yellow to grey coloured	Eocene	2
EK7	Black unstratified mudstone and grey sandstone	Eocene	5
g	Granite , granodiorit (Tertiary)		5
PLc	Conglomerate siltstone and sandstone with minor marl	Pliocene	5
Qf1	High level: old alluvial fans	Quaternary	5
Qf2	Low level: Young alluvial fans (gravel, silt, sand)	Quaternary	5
Qt1	High level: unconsolidated, variable texture , old clasitic deposits	Quaternary	5
Qt2	Low level unconsolidated young clastic deposits: (silt, sand, clay)	Quaternary	5
Soltanieh			
Er	Rhyolite	Eocene	1
Ks	Phillitic shale and volcanic rocks	Mesozoic	4
Qal	Recent alluvium	Quaternary	5
Qt	terraces ,gravel fans	Quaternary	5
Tarom			
Eai	Andesitic lava with tuff breccia, green tuff, sandstone and mudstone	Eocene	2
Eb	Dark greenish gray andesite basaltic lava flows, splitic lava	Eocene	2
Eka	Greenish gray tuffaceous sandstone, tuff, mudstone	Eocene	4
Eka1	Andesitic lava flows	Eocene	2
Eka3	Greenish gray tuffaceous sandestone, tuff, mudstone, siltstone partly with andesitic lava flows	Eocene	3
Eka4	Light green ash tuff, lapilli tuff, localy with pumice tuff	Eocene	4
Eka5	Porphyrite, andesite with sandstone and green tuff at the base	Eocene	2
Eka6	Light green tuff breccia, lapilli tuff	Eocene	4
Eka7	White - pink tuff, pumice tuff	Eocene	4
Eka8	Andesitic lava with tuff breccia, green tuff, sandstone and mudstone	Eocene	2
Ekab	Greenish gray tuffaceous sandstone, tuff, mudstonef	Eocene	4
Ekb	Tuff, tuffaceous sandstone, siltstone, mudstone with intercalations of tuff	Eocene	4
Ekb	Tuff, tuffaceous sandstone, siltstone, mudstone with intercalations of tuff	Eocene	4
Ekc	Gray - greenish gray tuffaceous sandstone, mudstone with minor porphyrite and andesite	Eocene	3
Ekd	Porphyrite, andesite with sandstone and intercalated tuff breccia	Eocene	2
Eke	Green to gray tuff and tuffite with intercalated tuffaceous sandstone and andesitic lava	Eocene	3
Ekf	Light green to pink tuff breccia, lapilli tuff, pumice tuff, welded tuff, crystal lithic tuff	Eocene	4
Ekg	Alternation of reddish gray to green ferrugineous tuff, sandy tuff with porphyrite and andesite	Eocene	3
Ekh	Gray alternation of sandstone and mudstone	Eocene	2
Et	Green to gray crystal - lithick tuff, vitric tuff, ash tuff with tuffaceous sandstone, siltstone and shale	Eocene	4
Ev	Greenish gray andesitic lava flows an lava breccia with intercalations of tuff and tuffite	Eocene	2
Evp	Greenish gray to pink porphyritic quartz, andesite - trachyandesite	Eocene	2
gd	Quartz monzodiorite - quartz monzonite, quartz syenite. (Oligocene?)		5
Ngb2	Dark gray basalt	Neogene	5
Ngc1	Red conglomerate	Neogene	5
Ngc2	Red to green conglomerate	Neogene	5

Ngm2	Alternation of light green gypsiferous marl, gypsum with reddish gray clay, sandstone and conglomerate	Neogene	5
P	Micro quartzdiorite porphyry		3
Pl-Qc	gray unconsolidated, moderate rounded and poorly sorted conglomerate	Neogene	5
Qal	Young terraces	Quaternary	5
Qf	Young terraces	Quaternary	5
Qt1	Old terraces	Quaternary	5
Qt2	Young terraces	Quaternary	5
Takestan			
A	Argillic - alunitic zone	Poste Eocene	1
E5vbt	Green well - bedded tuffaceous limestone and limy crystal to green sandy crystal tuff and black grey shale	Cretaceous	4
E6an	Brown dark andesitic basaltic trachyandesitic - andesitic and quartz andesitic lavas	Eocene	2
E6b	Grey - dark grey basaltic lavas	Eocene	4
E6dtbr	Red ferrogenous rhyodacitic, dacite lithic, vitric crystal tuff.	Eocene	2
E6gt	Olive green to green andesitic - dacitic crystal - lithic vitric tuff	Eocene	2
E6ig	Olive green partially red - blue rhyolitic - dacitic ignimbrite and tuff	Eocene	2
E6mp	Grey - dark megaporphyric and green porphyritic quartz andesitic , dacitic lavas	Eocene	2
E6tr-an	Dark and grey to red - brown amygdaloidal trachy - andesitic lavas	Eocene	2
E6v	Brown to dark olivine basaltic , trachybasaltic , trachyandesitic , andesite - basaltic and quartz andesitic lavas and intercalation of dark to dark brown tuffs	Eocene	2
E6vt	White grey to red colored rhyolitic - dacitic , lithic crystal vitric tuff	Eocene	2
g	Granite - microgranite	Poste Eocene	5
P	Partially epidotized , chloritized and silicified zone (propylitic zone)	Poste Eocene	1
PLQc	Cream consolidated conglomerate	Pliocene	5
Q	agriculture	Quaternary	5
Q1	Old and high level terrace	Quaternary	5
Q2	Young terrace	Quaternary	5
Qal	Recent alluvium	Quaternary	5
Qsc	Mud and salt flat	Quaternary	5
Qv	Dark vesicular basaltic lavas	Quaternary	5
Si	Silicified zone	Poste Eocene	1
Rudbar			
E1s	brown to red well - bedded medium to thick - bedded tuffaceous silty sandstone	Eocene	4
E1t	Intermediate andesitic - tuff, pyroclastic rocks	Eocene	2
E1v	Mainly intermediate lava.	Eocene	2
E2t	Violet crystaline partly devitrified, hyalo andesitic, tuff, tuffite and tuff micro sandstone	Eocene	2
E2tv	Undivided intermediate to acid volcanic rocks. (Middle volcanics) mainly post lutetian age	Eocene	2
E2v	Intermediate to acidic lava. (Vitrophyre, quartz, latite andesite, andesitic basalt)	Eocene	2
E3tv	Undivided intermediate to basic volcanic rocks, (upper volcanics) of Late Eocene age	Eocene	3
Et	Undifferentiated, texturally variable, pyroclastic rocks	Eocene	4
Eta	White, silicic, devitrified altered hyalo lithic tuff, volcaniclastic and acid volcanic rocks	Eocene	1
Etv	Undivided, alternating pyroclastic rocks and lava	Eocene	4
Ev	Undivided, texturally variable, lava	Eocene	4
G1	Light gray - granular, syncollisional, sheard granitoid withtormaline and magnetite veins. (Primary phase). (I type)	Paleogene	4
G2	Pink, microgranular, syncollisional, fresh granitoid, Aplite. (secondary phase). (I type)	Paleogene	4
Mv	Black andesite with slightly shearing, Conjugated joint and altration	Neogene	1
Ng	Piggyback basin deposits	Neogene	5
Ng1	Red to brownish tuffaceous claystone, siltstone with basal conglomeratic mudstone and gypsiferous red beds	Neogene	5
Ng2	Gypsiferous red beds with locally basal conglomerate in upper part	Neogene	5
Ng2cs	Brownish polygenetic conglomerate with silty Matrix	Neogene	5
Ng2m	Alternating yellow to brownish limy silt, gypsum localy with marl	Neogene	5
Ng2ssl	Alternating gray to green clay, marl, red limy, silicic claystone and sandstone with layers of gypsum and locally conglomerate unit in upper part	Neogene	5
PDs	Red to gray arkosic sandstone, paraquartzite and shale. (Dorud Formation)	Devonian	5
Plc	Gray to buff up ward coarsening, poly genetic, well - bedded conglomerate and coarse grain	Neogene	4

	sandstone		
Qal	Aluvium in major stream, channels sand	Quaternary	5
Qc	Cultivated land	Quaternary	5
Qt1	High level, unconsolidated, texturally variable, recent clastic deposits	Quaternary	5
Qt2	Low level, unconsolidated, Texturully variable, recent clastic deposits	Quaternary	5
Jirandeh			
Es	Dark grey and brown alternation sandstone and conglomerate with intercalations of tuff.	Paleogene	4
Ev2	Dark grey trachyandesitic-basaltic lava .	Paleogene	3
Et	Et: Grey, light green rhyo-dacitic tuff (ash-lapilli tuff), thin bedded , locally with intercalation of limestone.	Paleogene	2
Evt	Red ,pink and green dacitic shile and berccia tuff,as vitric-crystal tuff and lithic-crystal tuff.	Paleogene	3
Qt1	Old terraces and higher gravel fans .	Quaternary	5
Qal	Recent alluvium and river deposit.	Quaternary	5
Abhar			
Ea4	dacite, rhyolite and andesite lava	Eocene	2
Ea5	acidic lava, Tuff, breccias	Eocene	3
Ea6	lava, Tuff, breccias	Eocene	3
g	Quartz diorite, quartz syenite, quartz monzonite	Poste Eocene	4
Qt		Quaternary	5

References

Abrams M. & Hook S., 2001, ASTER user handbook, Jet Propulsion Laboratory; California Institute of Technology.

Adams J.A.S & Osmond J.K & Rogers J.J.W , 1959, The geochemistry of thorium and uranium, Phys. Chem. Earth 3, pp. 298–348.

Ahmadzadeh M. R. & Petrou M., 2003, Use of Dempster-Shafer theory to combine classifiers which use different class boundaries, Pattern Analysis & Applications Volume 6, Number 1, pp. 41-46.

An P., 1992. Spatial reasoning techniques and integration of geophysical and geological information for resource exploration. Ph.D. dissertation, The University of Manitoba.

An P., Moon, W.M., and Bonham-Carter, G.F., 1994b. Uncertainty management integration of exploration data using the belief function. Nonrenewable Resources, pp. 60-71.

An P., Moon, W.M., and Bonham-Carter, G.F., 1994a. An object-oriented knowledge representation structure for exploration data integration. Nonrenewable Resources, 3: pp. 132-145.

Aven, TT. & pörrn, K., 1998. Expressing and interpreting the results of quantitative risk analyses. Review and discussion. Reliability Engineering and System Safety 61, pp. 3-10.

Ayyub, B. M., 2001. Elicitation of Expert Opinions for Uncertainty and Risks, CRC Press.

B´ardossy G. & Fodor, J., 2001, Traditional and New Ways to Handle Uncertainty in Geology, Natural Resources Research, Vol. 10, No. 3, pp.179-186.

Bardossy, G. et al., 2003, A new method of resource estimation for bauxite and other solid mineral deposits, Journal of Hungarian Geomathematics, Volume 1, pp. 14-26

Bonham-Carter G.F., 1994, Geographic information systems for geoscientist, modeling with GIS, Computer Methods in the geosciences V.13, published by Pergamon 1994, pp. 267-333.

Bazin, D., and Hubner, H., 1969. Copper deposits of Iran, Geological Survey of Iran, report No. 13.

Berger B.R. & Bethke P.M., 1986. Editors; Reviews in Economic Geology Volume 2; Geology and geochemistry of epithermal systems; R.W. Henley: The geothermal framework for epithermal deposits , society of economic geologists, pp. 1-24.

Bogler, P. L., 1987. “Shafer-Dempster Reasoning with Applications to Multisensor Target Systems.” IEEE Transactions on Systems, Man, and Cybernetics, pp. 968-977.

Broome, J. & Carson, J.M. & Grant, J.A. & Ford, K.L., 1987. Modified Ternary Radioelement Mapping Technique and its Application to the South Coast of Newfoundland; Geological Survey of Canada, pp. 87-14.

Bourne, J. A. & O'Driscoll, E.S.T., Twidale, C. R., 2007. Crustal structures and mineral deposits: E.S.T. O'Driscoll's contribution to mineral exploration, Rosenberg Publishing Pty Ltd.

Carranza, E. J. M., 2002, PhD thesis: Geologically constrained mineral potential mapping , International Institute for Aerospace Survey and Earth Sciences (ITC), ITC Publication N. 86, pp. 252-260.

Chen Qi & Aickelin U., 2006, Dempster-Shafer for Anomaly detection, In: Proceedings of the International Conference on Data Mining (DMIN 2006), Las Vegas, USA.

Chokr, B & Kreinovich, V., 1994. How far are we from complete knowledge? Complexity of knowledge acquisition in the Dempster-Shafer approach. Advances in the Dempster-Shafer Theory of Evidence. R. R. Yager, J. Kacprzyk and M. Fedrizzi. New York, John Wiley & Sons, pp. 555-576.

Dantas, E. L. et al., 2003, Old geophysical data applied to modern geological mapping problems: A case study in the Sedrido Belt, Ne Brazil, Revista Brasileira de Geociencias; volume 33, pp.65-71.

Dempster, A.P., 1968. A generalization of Bayesian inference. Journal of the Royal Statistical Society, Series B (1968), pp. 205-247.

Dubois, D. & Prade H. , 2000., Fundamentals of Fuzzy Sets (The Handbook of Fuzzy Sets Series 7, Kluwer Academic Publishers, Boston/London/Dordrecht, pp. 647.

Dennis, P. & Cox & Singer & Donald, A., 1992. Mineral Deposits models, USGS, Bulltin N 1693.

Dubois, D. and Prade, H., 1992. "On the combination of evidence in various mathematical frameworks." Reliability Data Collection and Analysis. J. Flamm and T. Luisi. Brussels, ECSC, EEC, EAFC: pp. 213-241.

Ellis A.J., 1979. Explored geothermal system, in Barnes, H.L., Ed., Geochemistry of hydrothermal ore deposits (2nd ed.): New York, john wiely and Sons, pp. 632-683.

Explanatory text of the Zanjan quadrangle map 1:250,000 (Geological Survey of Iran. Geological quadrangle no. D4)

Explanatory text of the Qazvin and Rasht quadrangle map 1:250,000 (Geological Survey of Iran. Geological quadrangle no. E3, E4)

Ferson, S. & Kreinovich, V., 2002, "Representation, Propagation, and Aggregation of Uncertainty." SAND Report .

Ferson S. et al., 2003, Constructing Probability Boxes and Dempster-Shafer Structures, prepared by Sandia National Laboratories.

Haenni R., 1996, Propositional Argumentation Systems and Symbolic evidence Theory, Mathematisch-Naturwissenschaftlichen Fakültät der Universität in der Schweiz

Hall David L., McMullen Sonya A. H., 2004. Mathematical techniques in multisensor data fusion, Artech House Inc., pp. 220-229.

Hegarat-Mascle S Le et al., 2003, Multi-scale data fusion using Dempster-Shafer evidenc theory, Integrated ComputerAided Engineering (2003) Volume 10, Issue 1, pp. 9-22

Heier Knut S. & Rogers John J.W., 1962. Radiometric determination of thorium, uranium and potassium in basalts and in two magmatic differentiation series

Höhl Michael, September 1998, Dempster-Shafer-Theorie, Ausarbeitung für das Seminar Entscheidungskalküle.

Jian Guo Liu, Philippa J. Mason, 2009. Essential Image Processing and GIS for Remote Sensing, Imperial College London, UK , pp. 77-90.

Kalacheva E.G., & Rychagov S.N. & Belousov V.I., 2005. Hydrogeology and hydrodynamic of North-Paramushir geothermal area (Kuril Islands , Russia)

Kalinowski, A. and Oliver, Simon (compilers), ASTER Mineral Index Processing Manual, Remote Sensing Applications Geoscience Australia October 2004, pp.22-23.

Kearey, Phillip and Brooks, Michael, 1991, An introduction to Geophysical Exploration: Second Edition, Blackwell Scientific Publications.

Klir, G. J. & Wierman, M. J., 1998. Uncertainty-Based Information: Elements of Generalized Information Theory. Heidelberg, Physica-Verlag.

Kramosil, I., 2001. Probabilistic Analysis of Belief Functions. New York, Kluwer Academic/Plenum Publishers.

Macleod, I. N., Vierra, S., Chaves, A. C., 1993, Analytic signal and reduction-to-the-pole in the interpretation of total magnetic field data at low magnetic latitudes, Proceedings of the third international congress of the Brazilian society of geophysicists.

Malekzadeh Shafaroudi A. et al, 2009. Hydrothermal Alteration Mapping in SW Birjand, Iran, Using the Advanced Spaceborne Thermal Emission and Reflection Radiometer (ASTER) Image Processing, Journal of Applied Sciences, Volume: 9, pp. 829-842

Matheron, G., 1971. The theory of regionalized variables and its applications: Cah. Centre Morph. Math. Fontainebleau, V. 5, pp. 211.

McCauledy S. M., 2006, Integrating Multiple Information Sources with Dempster-Shafer Evidence Theory for Improved Forest Mapping, The graduate School of Geography, Clark University.

Moor A., 2005, Model-based cartographic generalization with uncertainty, the 17th Annual Colloquium of the Spatial Information Research Center University of Otago.

Musavy, S.R., Ashrafianfar N., 2004, Copper and Lead-Zinc favorability with GIS-based integration model in Abhar sheet, 8th Symposium of geological society of Iran, Shahrood University, 2004

Musavy, S.R., Giahchy p., ashrafianfar N.,2005, Exploration of mineral area in Tarom zone with applying GIS techniques, GIS and spatial Analysis IAMG 2005.Toronto Canada.

Nilsen T. & Aven T., 2003. Models and model uncertainty in the context of risk analysis, Reliability Engineering and system safety79, pp.309-317.

Nyborg M. et al., 2007, Detection of lineament using airborn laser scanning technology: Laxemar-Simpevarp; Sweden, Hydrothermal Journal 30, pp. 29-32.

Pavlovic, R., & Nikic, Z. & Trivic, B., 2003. The role of ground and underground waters in evolution of the ring structure of Jastrebac Mt., RMZ - Materials and Geoenvironment, Vol. 50, No. 1, pp. 293-296.

Roberto, C. et al., 2003, Infrared Spectroscopy and ASTER Imagery Analysis of Hydrothermal Alteration Zones at the Qaellaveco Porphyry-Copper Deposit, Southern Peru, ASPRS Annual Conference, Anchorage Alaska.

Roberto C & et al., 2008, Spatial Analysis of Airborne Geophysical Data Applied to Geological Mapping and Mineral Prospecting in the Serra Leste Region, Carajás Mineral Province, Brazil, Surveys in Geophysics, volume 28, Numbers 5-6, pp. 377-405.

Rockwell B. W.& Hofstra A. H., 2008, Identification of quartz and carbonat minerals across northern Nevada using ASTER thermal infrared emissivity data Implications for geologic mapping and mineral resource investigation in well-studies and frontier area, Geosphere February 2008; volume 4; No.1; pp.218-246

Rogers C. M, 2002, Application of Dempster-Shafer Theory to a Track association problem, University College London and QnnetiQ Malvern

Sabine, C., 1999. Remote sensing strategies for mineral exploration; Manual of Remote Sensing third edition volume 3: Remote Sensing for the Earth Sciences, pp. 375-426.

Sarkar, A. et al., 2005, Landcover Classification in MRF context Using Dempster-Shafer Fusion for Multisensor Imagery, IEEE Transactions on Image Processing, Volume 14, No. 5, pp.634-644.

Schuenemeyer, J., & Power, H. C., 2000, Uncertainty estimation for resouce assessment – an application to coal: Math. Geology, v. 32, no. 5, pp. 521–541.

Shafer G., 1982, belief function and parametric models, pp.223-250

Shafer, G., 1990. Perspectives on the theory and practice of belief functions. International Journal of Approximate Reasoning, pp. 1-40.

Shafer, G., & Judea Pearl, 1990. Readings in Uncertain Reasoning. Morgan Kaufmann, eds.

Shafer, G., 1976. A Mathematical Theory of Evidence. Princeton University Press.

Shafer G., 1992. The Dempster-Shafer theory of Encyclopedia of Artificial Intelligence, Second Edition by Stuart C. Shapiro, editor. Wiley, Pp. 330-331

Shaun, C., 2005, 'BELIEF' in the past: Dempster-Shafer theory, GIS and archaeological predictive modeling, Australian Archaeology, N. 60, pp.6-15.

Sentz, K. 2002. Combination of Evidence in Dempster-Shafer Theory, Thomas J. Watson School of Engineering and Applied Science Binghamton University, SAND 2002-0835.

Smithson, M., 1989. Ignorance and Uncertainty, Emerging Paradigms (Springer-Verlag, New York), pp. 367.

Stamoulis V. & Rogers P., 2003, Geological mapping for mineral exploration using ASTER data, MESA Journal 30, pp.16-19.

Tangestani, M. H. & Moore, F., 2001. The use of dempster-shafer model and GIS in integration of geoscientific data for porphyry copper potential mapping, north of Shahr-e-Babak, Iran, International Journal of Applied Earth Observation and Geoinformation, Volume 4, Issue 1, August 2002, P. 65-74

Using Geochemical Data: Evaluation, Presentation, Interpretation (Longman Geochemistry)

USGS EROS data center 2004, workshop on ASTER and MODIS data.

Volkov A. V. & et al., 2006. Tectonic Position of the Alshar Au–As–Sb–Tl Deposit, Macedonia, Doklady Earth Sciences, Vol. 407, No. 2, pp. 175–178.

Volkov A. V., & et al., 2008. Formation Conditions of Copper Porphyry Mineralization in the Kadica–Bukovik Ore District, Eastern Macedonia, Doklady Earth Sciences, Vol. 421, No. 5, pp. 769–773.

Wilson Nic, 2000, Algorithms for Dempster-Shafer Theory, School Computing and Mathematical Science Oxford Brookes University.

Yager, R., 1986. “Arithmetic and other operations on Dempster Shafer structures.” International Journal of Man-Machine Studies, 1986, pp. 357-366.

Yager, R., 1987. “On the Dempster-Shafer Framework and New Combination Rules.” Information Sciences, 1987a, pp. 93-137.

Zadeh, L. A., 1986. A Simple View of the Dempster-Shafer Theory of Evidence and its Implication for the Rule of Combination. The AI Magazine, p.p. 85-90.

Zadeh, L. A., 1984. “Review of Books: A Mathematical Theory of Evidence.” The AI Magazine, pp. 81-83.

Zimmermann, H.J., 2000. An application- oriented view of modeling uncertainty. European Journal of Operational Research, pp. 190-198.